Syntheses, Structures and Spectroscopic Properties of Mononuclear and Homodinuclear Lanthanoid(III) Dithiocarbamato Complexes

2020, March

Yakubu Abdallah

Graduate School of Natural Science and Technology

(Doctor's Course)

OKAYAMA UNIVERSITY

Content **Page**

Chapter Three

Syntheses, structures and spectroscopic properties of (*E*)-*N*-benzylidenepicolinohydrazonate-bridged homodinuclear lanthanoid(III) dithiocarbamato complexes

General Introduction

Dithiocarbamates are organosulfur compounds that belong to the class of 1,1-dithiolates [1, 2]. There is a growing interest in dithiocarbamates and their metal complexes because of their interesting physical and chemical properties [3, 4], biological activities [5, 6], structural features [7], optical and electrochemical properties [8] and a broad spectrum of applications in diverse fields such as inorganic analyses, agriculture, rubber industry [9], nanotechnology [10], and catalysis [11].

The dithiocarbamates (Scheme 1) are monoanionic chelating ligands with the ability to stabilize metal ions with low or unusually high oxidation states. The sulfur atoms possess strong σ-bonding and π-donating characteristics of the same order of magnitude, and the additional π-electron flow from the nitrogen atom to the sulfur atoms via a planar delocalized π-orbital system make the dithiocarbamate ligands behave as highly π-electron donating groups (i.e. thioureide) capable of bonding with metal ions at higher oxidation states. Dithiocarbamates form complexes with the main group metals, transition metals and lanthanoids as monodentate or bidentate chelating ligands [4, 12, 13].

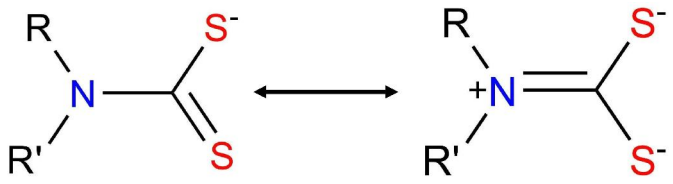

Dithiocarbamate Thioureide

Scheme 1. Dithiocarbamate and Thioureide structures.

The synthetic procedures of dithiocarbamates have been described in many reports [9, 14- 16]. The kinetics and mechanism of the formation of dithiocarbamates have also been studied [3]. They are generally prepared from the nucleophilic addition reaction of primary or secondary amines with carbon disulfide in the presence of a base such as sodium hydroxide, sodium hydride or excess of the amine (Scheme 2). The reactions are carried out in water, ethanol, methanol and other suitable solvents at lower temperatures. The dithiocarbamate salts depending upon the nature of the cation, can show good solubility in water or some organic solvents [17].

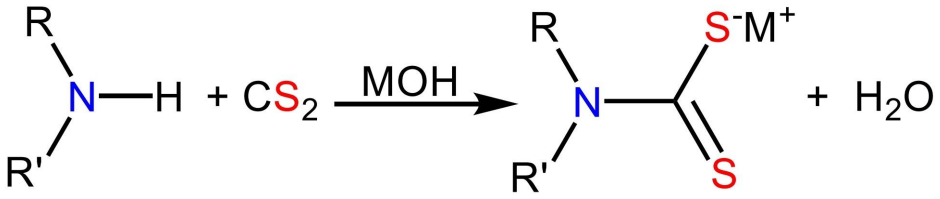

R = H, alkyl or aryl; R' = alkyl or aryl; $M^+ = Na^+$, K^+ or NH_4^+.

Scheme 2. Synthesis of dithiocarbamate salt.

Lanthanoids (Ln) are members of the *f*-block inner transition metals characterized by the gradual filling of electrons into the 4*f* orbitals. These elements mostly form stable trivalent (+3) oxidation states, with some exhibiting divalent (+2) and tetravalent (+4) oxidation states due to the presence of an empty, half-filled or fully filled 4*f* shell. The 4*f* electrons are spatially buried in the 5*s* and 5*p* orbitals and, as a result, it is suggested that they do not directly participate in chemical bonding and have no significant stereochemical influence. It is believed that the mixing of ligand and metal orbitals is not significant, and bonding between the ligand and Ln^{III} ion is largely electrostatic in nature. The coordination geometry of lanthanoid complexes are mainly determined by ligand steric effects with a broad variety of possible coordination spheres. Their coordination numbers are determined by the non-directional

bonding character and ionic size and vary between six (6) and twelve (12). The chemical, spectroscopic and magnetic properties of lanthanoid complexes are mostly independent of the ligand environment [18-22].

Lanthanoid coordination chemistry is a well-researched field in which many different complexes are continuously being studied and explored for various applications in many areas such as optical probes, medicine, agriculture, nanotechnology, magnetic materials and supramolecular assemblies [23, 24]. These complexes have been prepared from a wide array of ligands predominantly bearing O- and/or N-donor groups such as β-diketonates, Schiff bases, carboxylic acids, nitrates, amino acids and macrocyclic ligands [19]. Lanthanoid complexes bearing S-donor ligands such as dithiocarbamates, xanthates and dithiophosphates are rare in the literature because of the unfavorable bond formation between the 'hard acid' lanthanoid ions and 'soft base' S-donor atoms and instability of the complexes towards moisture [2, 9, 25]. Lanthanoid dithiocarbamato complexes were first described by Jørgensen in the 1960s [26]. Recently, interest in these complexes has resurfaced for many reasons including being studied for catalytic activities, luminescence properties and as single source precursors for lanthanoid sulfide nanomaterials (e.g. europium chalcogenides) [27, 28].

The general objective of this thesis is to describe the syntheses, structural features and spectroscopic properties of mononuclear and homodinuclear lanthanoid(III) dithiocarbamato complexes. Magnetic circular dichroism (MCD) was used as the special spectroscopic technique to study the magneto-optical properties of the complexes. This thesis comprises three thematic chapters, each describing a specific research activity undertaken to achieve the overall objective of the thesis. Chapter 1 describes the syntheses, crystal structures and the natural circular dichroism (CD) and magnetic circular dichroism (MCD) properties of a series of mononuclear Ln^{III} (Ln = Nd or Eu) adducts bearing achiral or chiral dithiocarbamato (dtc) ligands and 1,10-phenanthroline or 2,2'-bipyridine. Chapter 2 focuses on the preparation and

characterization of four new novel homodinuclear Ln^{III}_2 (Ln = Nd or Eu) dithiocarbamato complexes using 2,2'-bipyrimidine (bpm) as the bridging unit. The structural and spectral comparison of the dithiocarbamato complexes with corresponding β-diketonato analogues is also described. Chapter 3 describes the syntheses, crystal structures and spectroscopic properties of a series of new novel homodinuclear Ln^{III}_2 (Ln = La, Pr, Nd, Sm or Eu) dithiocarbamato complexes using (*E*)-*N*-benzylidenepicolinohydrazide (Hbphz) as a precursor of the bridging ligand.

Chapter 1

Coordinatively unsaturated lanthanoid complexes with tris(monoanionic bidentate chelate ligands), complete their coordination sphere by forming adducts with Lewis bases. The most commonly used Lewis bases are the 1,10-phenanthroline (phen) and 2,2'-bipyridine (bpy) [20]. These are bidentate neutral ligands that strongly coordinate with Ln^{III} ions. The concomitant use of these ligands leads to mononuclear neutral lanthanoid complexes with increased stability and interesting properties [29].

In this Chapter, 1,10-phenanthroline (phen) and 2,2'-bipyridine (bpy) were used to prepare a series of mononuclear lanthanoid complexes bearing achiral or chiral dithiocarbamato (dtc) ligands. Except for the achiral dithiocarbamato ligands (i.e. dimethyldithiocarbamato, Me_2dtc^- and pyrrolidinedithiocarbamato, $pyrdtc^-$), the chiral (*S*)-prolinoldithiocarbamato ligand (*S*-proOHdtc$^-$) was prepared and used. The crystal structures of the complexes were determined by X-ray diffraction method. The spectroscopic properties of the complexes were investigated by Infrared (IR), UV-visible absorption, natural circular dichroism (CD) and magnetic circular dichroism (MCD) measurements. The molecular structures in the crystals were revealed as an 8-coordinate geometry around the Ln^{III}

centers with three bidentate *S,S*-donating dithiocarbamato ligands and a bidentate *N,N*-donating phen or bpy. The complexes exhibited similar spectral patterns in their IR, UV-visible absorption, natural CD and MCD spectra. Although, the structures and properties of some of the complexes have been previously reported [10, 11, 30, 31], this study reported the first structure of a mononuclear lanthanoid complex bearing a chiral (*S*)-prolinol dithiocarbamato (*S*-proOHdtc^{-}) ligand as well as the magneto-optical properties of lanthanoid dithiocarbamato complexes measured by MCD spectroscopic technique.

Chapter 2

The use of polyazine ligands such as 2,2'-bipyrimidine (bpm: Scheme 3) to bridge transition metals is a well-established area of coordination chemistry [24]. The ligand, bpm is a planar heterocycle characterized by strong σ-donor and π-acceptor bonding characteristics and has a symmetric shape. It is capable of coordinating as a terminal or bridging ligand to metal centers to form stable complexes through its equivalent nitrogen atoms [32]. It is only recently that the coordination ability of 2,2'-bipyrimidine to form complexes with lanthanoids have been explored [29]. Although, some 2,2'-bipyrimidine-bridged dinuclear Ln^{III}_2 complexes bearing β-diketonates have been reported [33-35], its corresponding analogues of lanthanoid complexes bearing dithiocarbamates are yet to be studied.

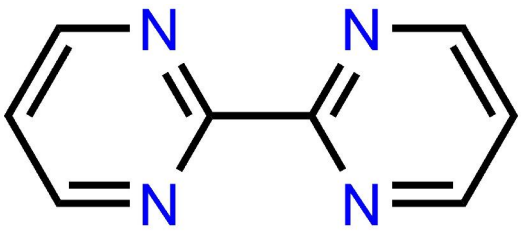

Scheme 3. 2,2'-bipyrimidine (bpm).

This chapter extends the coordination ability of the 2,2'-bipyrimidine to form dinuclear lanthanoid dithiocarbamato complexes. It describes the preparation and characterization of four new novel homodinuclear Ln^{III}_2 (Ln = Nd or Eu) dithiocarbamato complexes using bpm as the bridging unit. Two β-diketonato analogues were also prepared and characterized for structural and spectral comparisons. The crystal structures were determined by X-ray diffraction analysis, while the spectroscopic properties were measured by FT-IR, UV-visible absorption and MCD techniques. The synthetic method and results of the structural and spectroscopic characterization are presented and discussed.

Chapter 3

The coordination chemistry of hydrazones is an active research area in view of their general interests and application of hydrazone complexes [22, 36]. Hydrazones and their metal complexes have interesting magnetic, electronic, optical and biological properties and are involved in the design of supramolecular assemblies, single molecule magnets (SMMs), drug development and heterocyclic synthesis [37-40].

Hydrazones are a class of organic compounds in the Schiff base family characterized by the azomethine moiety (i.e. $–NH–N=CR_2$) in their molecule illustrated in Scheme 4 [41]. The azomethine moiety features an N-N bond and a C=N double bond that is conjugated with a lone electron pair on the nitrogen atom. Both nitrogen atoms are nucleophilic although the amino nitrogen is less nucleophilic, but acidic. The imine carbon atom has both nucleophilic and electrophilic character. The imine moiety (–N=CH–) contributes to the formation of geometrical *Z* and *E* isomers of hydrazones [42]. These structural motifs are mainly responsible for the physical and chemical properties of hydrazones [38, 43]. Aroylhydrazone (i.e. $Ar-CO-NH-N=CR_2$) are known to have a combination of amide oxygen and imine nitrogen as donor

atoms. The electron density of the amide oxygen and imine nitrogen involved in chelation can be controlled by protonation-deprotonation of the amide nitrogen [41, 44]. The coordination ability of hydrazones is influenced by many factors including changing the configuration and conformation, tautomerism, reaction conditions, stability of the complex and nature of the substituents on the hydrazone moiety [42]. Other methods of hydrazone synthesis have been described by [38] and in many reports.

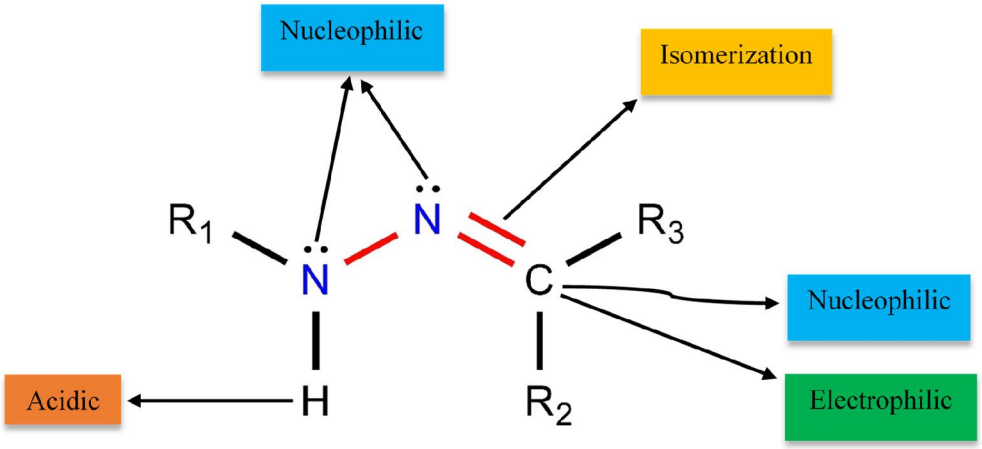

R_1, R_3 = aliphatic or aromatic; R_2 = H or alkyl.

Scheme 4. Structure and active features of hydrazones.

This chapter describes the syntheses, crystal structures and spectroscopic properties of a series of new novel homodinuclear Ln^{III}_2 (Ln = La, Pr, Nd, Sm and Eu) dithiocarbamato complexes using (*E*)-*N*-benzylidenepicolinohydrazide (Hbphz: Scheme 5) as a precursor of the bridging deprotonated hydrazonato ligand. The crystal structures were determined by X-ray diffraction method, while the spectroscopic properties were measured by FT-IR, ^{1}H NMR, UV-visible absorption and MCD techniques. The method of preparation, structural features and spectroscopic properties of these hydrazonato-bridged homodinuclear lanthanoid dithiocarbamato complexes are presented and fully discussed.

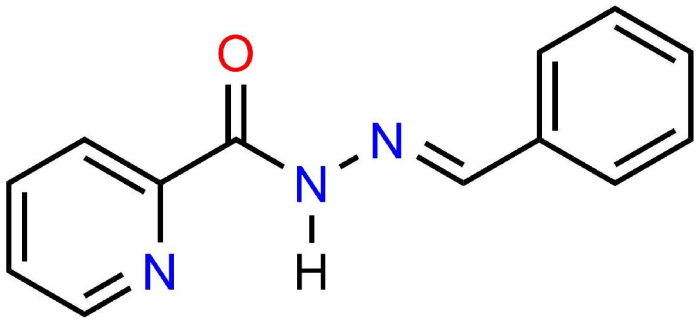

Scheme 5. (*E*)-*N*-Benzylidenepicolinohydrazide (Hbphz).

References

1. A. K. Sharma. *Thermochimica Acta,* **104** (1986) 339.
2. S. V. Larionov, Y. A. Bryleva. *Russian J. Coord. Chem.* **42** (2016) 293.
3. D. J. Halls. *Mikroehimica Acta [Wien]* (1969) 62.
4. M. Castillo, J. J. Criado, B. Macfas, M. V. Vaquero. *Transition Met. Chem.* **11** (1986) 476.
5. A. Z. Halimehjani, K. Marjani, A. Ashouri. *Green Chem.* **12** (2010) 1306.
6. P. M. Madalageri, O. Kotresh. *Int. J. Chem. Sci.,* **10** (2012) 983.
7. I. Raya, I. Baba, B. M. Yamin. *Malaysia J. Analy. Sci.,* **10** (2006) 93.
8. P. D. Beer, N. Berry, M. G. B. Drew, O. D. Fox, M. E. Padilla-Tostaa, S. Patella. *Chem. Commun.*, (2001) 199.
9. C. Su, M. Tan, N. Tang, X. Gan, W. Liu, X. Wang, *J. Coord. Chem.,* **38** (1996) 207.
10. M. D. Regulacio, N. Tomson, S. L. Stoll. *Chem. Mater.,* **17** (2005) 3114.
11. P. Pitchaimani, K. M. Lo, K. P. Elango. *Polyhedron,* **93** (2015) 8.
12. M. Chunggaze, M. A. Malik, P. O'Brien, A. J. P. White, D. J. Williams. *J. Chem. Soc., Dalton Trans.*, (1998) 3839.
13. H. Nabipour, S. Ghammamy, S. Ashuri, Z. S. Aghbolagh. *Org. Chem. J. ,* **2** (2010) 75.
14. B. Macias, M. V. Villa, M. R. Rodriguez-Gallego. *Transition Met. Chem.,* **20** (1995) 347.
15. G. M. de Lima. *J. Molecular Struct.,* **988** (2011) 1.
16. A. Z. Halimehjani, A. Dadras, M. Ramezani, E. V. Shamiri, S. E. Hooshmanda, M. M. Hashemib. *J. Braz. Chem. Soc.,* **26** (2015) 1500.
17. S. Kanchi, P. Singh, K. Bisetty.. *Arabian J. Chem.,* **7** (2014) 11.
18. D. F. Shriver, P. W. Atkins. (1999). *Inorganic Chemistry.* UK: Oxford University Press.

19. T. Akasaka, et al. (2010). *Rare Earth Coordination*: *Fundamentals and Application*. (C. Huang, Ed.) Singapore: John Wiley & Sons (Asia) Pte Ltd.

20. S. Cotton. (2006). *Lanthanide and Actinide Chemistry.* John Wiley & Sons, Ltd.

21. G. A. Lawrance. (2010). *Introduction to Coordination Chemistry.* UK: John Wiley and Sons, Ltd.

22. B. Moksharagni, K. H. Reddy. *Eur. J. Biomed. Pharm. Sci.,* **5** (2018) 810.

23. G. Zucchi, O. Maury, P. Thuery, M. Ephritikhine. *Inorg. Chem.,* **47** (2008) 10398.

24. S. Swavey, R. Swavey. *Coord. Chem. Rev. ,* **253** (2009) 2627.

25. M. Mahato, P. P. Jana, K. Harms, H. P. Nayek. *RSC Adv.,* **5** (2015) 62167.

26. C. K. Jørgensen. *Mol. Phys.,* **5** (1962) 271.

27. R. S. Selinsky, J. H. Han, E. A. Morales Perez, I. A. Guzei, S. Jin. *J. Am. Chem. Soc.,* **132** (2010) 15997.

28. W. M. Faustino, O. L. Malta, E. E. S. Teotonio, H. F. Brito, A. M. Simas, G. F. de Sa´. *J. Phys. Chem. A,* **110** (2006) 2510.

29. G. Zucchi. *Intern. J. Inorg. Chem.*, (2011) 1.

30. J. A. Vale, W. M. Faustino, P. H. Menezes, G. F. de Sá. *J. Braz. Chem. Soc.,* **17** (2006) 829.

31. V. Kubat, G. Demo, L. Jeremias, J. Novosad. *Z. Kristallogr.,* **228** (2013) 369.

32. A. Fratini, G. Richards, E. Larder, S. Swavey. *Inorg. Chem.,* **47** (2008) 1030.

33. N. M. Shavaleev, G. Accorsi, D.Virgili, Z. R. Bell, T. Lazarides, G.Calogero, N. Armaroli, M. D. Ward. Centers. *Inorg. Chem.,* **44** (2005) 61.

34. O. Sun, T. Gao, J. Sun, G. Li, H. Li, H. Xu, C. Wang, P. Yan. *CrystEngComm.,* **16** (2104) 10460.

35. W. Yu, F. Schramm, E. M. Pineda, Y. Lan, O. Fuhr, J. Chen, H. Isshiki, W. Wernsdorfer, W. Wulfhekel, M. Ruben,. *Beilstein J. Nanotechnol.,* **7** (2016) 126.

36. R. S. Baligar, V. K. Revankar. *J. Serb. Chem. Soc.,* **71** (2006) 1301.

37. A. M. Wu, P. D. Senter. *Nature Biotechology,* **23** (2005) 1137.

38. N. P. Belskaya, W. Dehaen, V. A. Bakulev. *ARKIVOC (i),* (2010) 275.

39. A. Gusev, R. Herchel, I. Nemec, V. Shul'gin, L. I. Eremenko, K. Lyssenko, W. Linert, Z. Travńícek. *Inorg. Chem.,* **55** (2016) 12470.

40. V. Vrdoljak, G. Pavlovic, T. Hrenar, M. Rubci, P. Siega, R. Dreos, M. Cindri. *RSC Adv.,* **5** (2015) 104870.

41. A. Kajal, S. Bala, N. Sharma, S. Kamboj, V. Saini. *Intern. J. Medicinal Chemistry* (2014) 1.

42. M. V. Angelusiua, S.-F. Barbuceanu, C. Draghici, G. L. Almajan. *Eur. J. Medicinal Chem.,* **45** (2010) 2055.

43. G. Verma, A. Marella, M. Shaquiquzzaman, M. Akhtar, M. R. Ali, M. M. Alam. *Journal of Pharmacy and Bioallied Sciences,* **6** (2014) 69.

44. M. Chang, H. Horiki, K. Nakajima, A. Kobayashi, H. -C. Chang, M. Kato. *Bull. Chem. Soc. Jpn.* **83** (2010) 905.

Chapter 1

Syntheses, structures and spectroscopic properties of mononuclear lanthanoid(III) dithiocarbamato complexes

Abstract

A series of Nd^{III} and Eu^{III} complexes containing achiral or chiral dithiocarbamato (dtc) ligands, [Ln(*RR*'dtc)$_3$(NN)] {Ln = Nd or Eu; *RR*' = dimethyl- (Me_2), pyrrolidine- (pyr), or (*S*)-prolinol- (*S*-proOH); NN = 1,10-phenanthroline (phen) or 2,2'-bipyridine (bpy)}, were prepared and their crystal structures and spectroscopic properties, in particular the natural circular dichroism (CD) and magnetic circular dichroism (MCD), were investigated. The crystal structures of the complexes analyzed by X-ray diffraction method showed an 8-coordinate geometry around the Ln^{III} center with comparable structural parameters to one another and to related complexes previously reported. These complexes exhibited similar spectral patterns in their absorption, natural CD and MCD spectra in solution. Weak but characteristic sharp f–f transition bands were observed in the absorption and MCD spectra, but no CD signals associated with these transitions were observed even in the *S*-proOHdtc complexes. The MCD spectral pattern of the Eu^{III} complexes revealed a local C_{2v} symmetry around the Ln^{III} center in solution, in contrast to the aqua and analogous β-diketonato Eu^{III} complexes.

1.1 Introduction

Lanthanoid complexes are currently being investigated extensively for a variety of their functionalities and applications, such as optical probes, medicine, microelectronics, and others [1,2]. Among the complexes widely studied, those of sulfur-donating ligands are still limited to report, owing to the unfavorable bond formation between the 'hard acid' lanthanoid ions and 'soft base' sulfur-donor ligands [3]. However, it has been well-studied in transition-metal complexes that dithiocarbamates ($RR'dtc^-$) stabilize a wide range of oxidation states of the metal ion, even for hard metal centers at higher oxidation states [4]. In fact, the synthesis and crystallographic studies of several lanthanoid dithiocarbamato complexes have been reported in the last decades [5]. Regulacio et al. described a series of lanthanoid dithiocarbamato complexes as precursors for lanthanoid sulfide materials and nanoparticles [6]. Boncher et al. [7] and Jin et al. [8] also prepared polycrystalline lanthanoid sulfide materials by the thermal decomposition of single source lanthanoid dithiocarbamato complexes. Lanthanoid complexes of piperidine and pyrrolidine dithiocarbamates have been investigated for their luminescence properties and catalytic activities in cyanohydrin syntheses [9]. Room temperature photoluminescence of Eu^{III} diethyldithiocarbamato and diphenyldithiocarbamato complexes was reported by Faustino et al [1]. Mahato et al. have reported a series of Ln^{III} morpholine 4-dithiocarbamate complexes with their interesting extended structure in the crystals and the spectroscopic properties in solution [2]. Notwithstanding these studies, the chiroptical and magneto-optical properties of lanthanoid dithiocarbamato complexes by means of natural circular dichroism (CD) and magnetic circular dichroism (MCD) measurements are rarely investigated. For instance, CD spectroscopic studies for lanthanoid(III) β-diketonato complexes have been reported; Berry et al. observed the solid-state CD spectra of the f–f transitions in $Na_3[Eu(ODA)_3]\bullet 2NaClO_4\bullet 6H_2O$ (ODA^- = oxydiacetate) [10]. Shirotani et al. reported a solution CD spectrum of the f–f transitions in $Na[Pr\{(+)\text{-}hfbc\}_4]\bullet CH_3CN$ ($hfbc^-$ =

3-heptafluorobutylrylcamphorate) [11]. Circularly polarized luminescence spectra of Ln^{III} complexes with chiral ligands have also been studied [12].

In this study, a series of neodymium(III) and europium(III) complexes with achiral or chiral dithiocarbamato ligands were prepared. (*S*)-prolinol dithiocarbamato (*S*-proOHdtc^{-}) complexes are newly synthesized. The crystallographic studies of the complexes as well as their CD and MCD properties were investigated.

1.2 Experimental section

Materials

Sodium dimethyldithiocarbamate dihydrate and ammonium pyrrolidinedithiocarbamate were purchased from Tokyo Chemical Industry Co., Ltd. Hydrated salts of neodymium(III) and europium(III) chloride and 2,2'-bipyridine were obtained from Kanto Chemical Co., Inc., while 1,10-phenanthroline monohydrate was purchased from Nacalai Tesque Inc. (*S*)-Prolinol and carbon disulfide were purchased from Wako Chemical Ltd. All chemicals were of high purity grade and used as received.

Physical Measurements

The C, H, N and S elemental analysis of the complexes was carried out with a Perkin Elmer Series II CHNS/O Analyzer 2400 at Advanced Science Research Center, Okayama University. FT-IR spectra were recorded on a JASCO FT-001 FT-IR Spectrometer in KBr disk in the range 4000 – 400 cm^{-1}. The absorption spectra were obtained on a JASCO V-550 UV/VIS spectrophotometer. The natural CD and MCD spectra were measured on a JASCO J-1500 CD spectrometer. The magnetic field apparatus used for the MCD measurements was developed in this laboratory and reported previously [13]. All the spectra were recorded at room temperature.

Synthesis of K(*S*-proOHdtc)

The potassium salt of *S*-prolinol dithiocarbamate, K(*S*-proOHdtc), was prepared, according to the method described previously [14] with some modifications. An aqueous (3 mL) solution of KOH (0.030 mol) was cooled in an ice bath and diluted with 50 mL of ethanol. The mixture was stirred for 5 min, and (*S*)-prolinol (0.030 mol) was added slowly with stirring, followed by dropwise addition of an excess amount of CS_2. The mixture was stirred for further

2 h in an ice bath, and the solvents were removed under reduced pressure. The residue was dried in vacuo over P_2O_5. A yellow solid product was formed, and the crude product was dissolved in a minimum amount of ethanol. The filtered solution was layered with diethyl ether to precipitate the dithiocarbamate salt. Yield: 50%. Anal. Calcd.: C, 33.46; H, 4.68; N, 6.50; S, 29.78%. Found: C, 33.07; H, 4.63; N, 6.44; S, 28.56%. FT-IR (cm^{-1}): ν(C─N) = 1399, ν(C─S) = 966.

Syntheses of Ln^{III} complexes with achiral dithiocarbamates

The Ln^{III} (Ln = Nd or Eu) complexes were prepared according to the procedure described previously [5] with some modifications. A methanolic solution (10 mL) of $LnCl_3$•$6H_2O$ (1.00 mmol) was slowly added to a methanolic solution (10 mL) of Na(Me_2dtc) or NH_4(pyrdtc) (3.00 mmol), followed by the addition of a methanolic solution (10 mL) of bpy or phen (1.00 mmol). The mixture was stirred for 1 h, and the resulting precipitate was collected by filtration, washed with portions of methanol and dried in air. The crude product was purified by recrystallization from a chloroform solution by vapor diffusion of diethyl ether. The analytical and FT-IR spectral data are given below.

[Nd(Me_2dtc)$_3$(phen)] (1a)

Pale blue crystals. Yield: 47.5%. Calcd for $C_{21}H_{26}N_5NdS_6$: C, 36.82; H, 3.83; N, 10.22; S, 28.08%. Found: C, 36.35; H, 3.74; N, 10.10; S, 27.55%. FT-IR (cm^{-1}): ν(C─N) = 1374, ν(C─S) = 984.

[Nd(pyrdtc)$_3$(phen)] (1b)

Pale blue crystals. Yield: 78.5%. Calcd for $C_{27}H_{32}N_5NdS_6$: C, 42.49; H, 4.23; N, 9.18; S, 25.21%. Found: C, 41.73; H, 4.24; N, 9.00; S, 24.64%. FT-IR (cm^{-1}): ν(C─N) = 1424, ν(C─S) = 1008.

[Nd(Me$_2$dtc)$_3$(bpy)] (1c)

Pale blue crystals. Yield: 20 %. Calcd for $C_{19}H_{26}N_5NdS_6$•$CHCl_3$: C, 30.98; H, 3.49; N, 8.97; S, 24.65%. Found: C, 31.20; H, 3.87; N, 9.67; S, 27.45%. FT-IR (cm^{-1}): ν(C─N) = 1374, ν(C─S) = 982.

[Nd(pyrdtc)$_3$(bpy)] (1d)

Pale blue crystals. Yield: 66%. Calcd for $C_{25}H_{32}N_5NdS_6$: C, 40.62; H, 4.36; N, 9.47; S, 26.03%. Found: C, 40.12; H, 4.32; N, 9.46; S, 25.15%. FT-IR (cm^{-1}): ν(C─N) = 1425, ν(C─S) = 1009.

[Eu(Me$_2$dtc)$_3$(phen)] (2a)

Brick-red crystals. Yield: 29%. Calcd for $C_{21}H_{26}N_5EuS_6$: C, 36.40; H, 3.78; N, 10.11; S, 27.77%. Found: C, 36.12; H, 3.66; N, 9.97; S, 27.01%. FT-IR (cm^{-1}): ν(C─N) = 1374, ν(C─S) = 987.

[Eu(pyrdtc)$_3$(phen)] (2b)

Brick-red crystals. Yield: 70%. Calcd for $C_{27}H_{32}N_5EuS_6$: C, 42.06; H, 4.18; N, 9.09; S, 24.96%. Found: C, 41.75; H, 4.21; N, 8.96; S, 24.74%. FT-IR (cm^{-1}): ν(C─N) = 1424, ν(C─S) = 1010.

[Eu(Me$_2$dtc)$_3$(bpy)] (2c)

Brick-red crystals. Yield: 20%. Calcd for $C_{19}H_{26}N_5EuS_6$•$CHCl_3$: C, 30.48; H, 3.45; N, 8.89; S, 24.41%. Found: C, 29.65; H, 3.71; N, 9.17; S, 25.12%. FT-IR (cm^{-1}): ν(C─N) = 1374, ν(C─S) = 984.

[Eu(pyrdtc)$_3$(bpy)] (2d)

Brick-red crystals. Yield 50%. Calcd for $C_{25}H_{32}N_5EuS_6$•$CHCl_3$: C, 36.05; H, 3.84; N, 8.08; S, 22.21%. Found: C, 36.18; H, 4.16; N, 8.37 S, 23.13%. FT-IR (cm^{-1}): ν(C─N) = 1428, ν(C─S) = 1011.

Syntheses of Ln^{III} complexes with a chiral dithiocarbamate

A methanolic solution (10 mL) of $LnCl_3$•$6H_2O$ (1.00 mmol) was added to a methanolic solution (10 mL) of K(*S*-proOHdtc) (3.00 mmol) with stirring. A white precipitate (KCl) which appeared immediately was filtered off, and a methanolic solution (10 mL) of bpy or phen (1.00 mmol) was added to the filtrate. The mixture was stirred for 1 h, and the solution was concentrated (to ca. 10 mL) under reduced pressure and filtered to remove the precipitated impurity. The filtrate was layered with diethyl ether to afford crystalline products, which were collected by filtration, washed with portions of Et_2O and dried in air. The analytical and FT-IR spectral data are given below.

[Nd(*S*-proOHdtc)$_3$(phen)] (1e)

Pale blue crystals. Yield: 49%. Calcd for $C_{30}H_{38}N_5O_3NdS_6$•$3H_2O$: C, 39.71; H, 4.89; N, 7.72; S, 21.20%. Found: C, 39.25; H, 4.57; N, 7.74; S, 20.79%. FT-IR (cm^{-1}): ν(C─N) = 1423, ν(C─S) = 972.

[Eu(*S*-proOHdtc)$_3$(phen)] (2e)

Orange crystals. Yield 52%. Calcd for $C_{30}H_{38}N_5O_3EuS_6$•$3H_2O$: C, 39.38; H, 4.85; N, 7.65; S, 21.03%. Found: C, 39.86; H, 4.53; N, 7.60; S, 20.53%. FT-IR (cm^{-1}): ν(C─N) = 1421, ν(C─S) = 972.

[Eu(*S*-proOHdtc)$_3$(bpy)] (2f)

Yellow powder. Yield 52%. Calcd for $C_{28}H_{38}N_5O_3EuS_6$•$C_4H_{10}O$: C, 42.18; H, 5.31; N, 7.69; S, 21.12%. Found: C, 42.03; H, 4.64; N, 7.74; S, 21.03%. FT-IR (cm^{-1}): ν(C─N) = 1419, ν(C─S) = 969.

X-ray diffraction analysis

Single crystals of complexes **1a**, **1b** and **2a**–**c** were obtained from a mixture of chloroform and diethyl ether, while those of complexes **1c** and **2e** were from dichloromethane/diethyl ether and methanol/diethyl ether, respectively, using a vapor diffusion method. X-ray diffraction intensity data were collected on a Rigaku R-AXIS RAPID diffractometer using graphite monochromated Mo-Kα (λ = 0.71075 Å) radiation. The crystal structures were solved and refined using SHELXS and SHELXL Version 2013/1 packages. The structures were solved using the direct method and expanded using Fourier techniques, and refined by full-matrix least-squares methods with anisotropic parameters for all non-hydrogen atoms. Hydrogen atoms were refined using the riding models [15].

1.3 Results and Discussion

Preparation and characterization of the complexes

The complexes, [Ln(RR'dtc)$_3$(NN)] (Ln = Nd or Eu; RR' = Me$_2$, pyr or *S*-proOH; NN = phen or bpy), were prepared by a similar method reported previously [1,3,6] (Scheme 1.1) and characterized by elemental analysis and spectroscopic methods such as FT-IR and UV-vis absorption spectroscopy. Although, it was difficult to isolate analytically pure sample of the complex [Nd(*S*-proOHdtc)$_3$(bpy)], the reaction product from NdCl$_3$, K(*S*-proOHdtc) and bpy exhibited similar spectral patterns to those of the phen analogue. The isolated yields of these complexes were varied from 20% to 78% and exhibited the following tendency of the ligands: Me$_2$dtc < *S*-proOHdtc < pyrdtc. Because the cations of these dithiocarbamates used in the preparation were different as Na(Me$_2$dtc), K(*S*-proOHdtc) and NH$_4$(pyrdtc), the by-products (i.e., NaCl, KCl and NH$_4$Cl) were simultaneously formed with the desired Ln^{III} complexes. Thus, the solubility of the chloride salts, as well as the neutral complexes, in methanol gave a large effect in the isolated yields of the complexes.

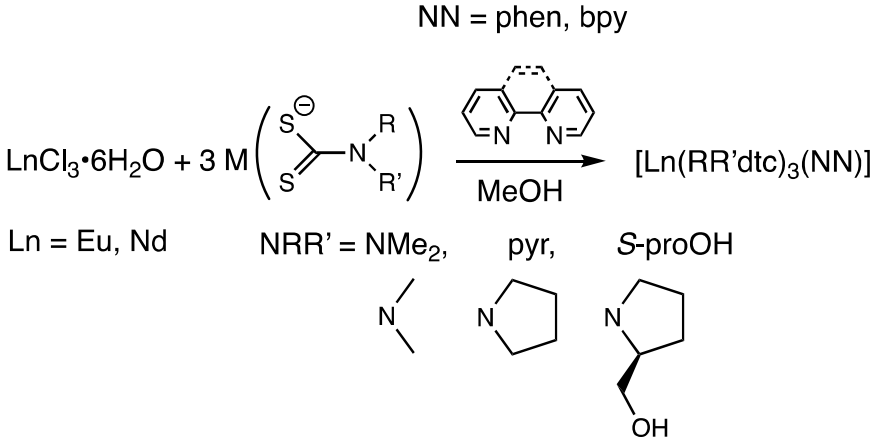

Scheme 1.1. Preparation of Ln^{III} complexes.

Crystal structures

The crystal structures of **1a**, **1b**, **1c**•0.5CH_2Cl_2, **2a**, **2b**, **2c** and **2e**•H_2O were determined by the single-crystal X-ray diffraction method, although the crystal structures of **1a** [5], **2c** [3a] and **2d**•3$CHCl_3$ [8] were reported previously. Crystallographic data and selected bond lengths and angles of the complexes are given in Table 1.1 and Table 1.2, respectively. The molecular structures of [Nd(pyrdtc)$_3$(phen)] (**1b**) and [Eu(Me_2dtc)$_3$(phen)] (**2a**), as examples, are shown in Figures 1.1 (and those of the other complexes are shown in figures 1.2), which are very similar to those of the related complexes reported previously with their comparable structural parameters (Table 1.2) [3,5,6,8]. The Ln^{III} (Nd^{III} or Eu^{III}) center is 8-coordinated by three dithiocarbamato ligands through two S donor atoms and a phenanthroline or bipyridine ligand through two N donor atoms. Interestingly, when the precise coordination geometry around Ln^{III} center is examined, there are two distinguishable structures observed in this series of complexes. Both bidentate ligands of dithiocarbamato (RR'dtc) and diimine (NN) are almost planar, and a set of mutually pseudo *trans*-positioned RR'dtc planes is co-planar in all complexes (Figure 1.1*c* and 1.1*d*). In complexes **1a** and **2a**, the other two ligand planes, i.e., phen and the pseudo *trans*-positioned Me_2dtc plane are nearly co-planar, as their dihedral angles are 13.67(5) and 12.77(9)°, respectively. In the other complexes, in contrast, the NN ligand plane and the pseudo *trans*-positioned RR'dtc ligand plane is not co-planar; the dihedral angles are in the range of 39.91(5)–45.21(7)° (Table 1.2). A similar coordination geometry has been recognized previously, and Regulacio et al. described it as a distorted square antiprism [6], while Pitchaimani et al. [9,14] and Raya et al. [3b] reported it as a distorted dodecahedron. It is also noted that there are no remarkable intermolecular interactions in these crystal structures.

The molecular structure of the [Eu(*S*-proOHdtc)$_3$(phen)]•H_2O (**2e**•H_2O) complex (Figure 1.3) was very interesting and worthy of further comments. It contained a set of unsymmetrical coordination (i.e., the direction of the hydroxymethyl substituent) of the three *S*-proOHdtc$^-$

ligands around the Eu^{III} center which gives rise to a variety of possible stereoisomers in the solid state (Scheme 1.2). This structural feature is observed because of the restricted rotation about the C–N bond in the RR'dtc$^-$ ligand due to the extended π-electron conjugation over the C–N bond, and the presence of the asymmetric carbon atom in the prolinol ring. The compound **2e**•H_2O was deposited as orange block crystals from a mixture of methanol and diethyl ether, one of the crystals used for X-ray analysis was revealed to be crystallized in a monoclinic space group *P*2 with $Z = 4$. There are two crystallographically independent molecules in the asymmetric unit, and they were found to be diastereoisomers due to the asymmetric coordination of the *S*-ProOHdtc$^-$ ligands: the *PMP* and *PPM* isomers (Figure 1.3). Interestingly, one of the molecules (*PMP* isomer with Eu1 center) showed a distorted square-antiprism or dodecahedron coordination geometry, likewise to the majority of the [Ln(RR'dtc)$_3$(NN)]-type complexes reported previously. In contrast, the coordination geometry of the other molecule (*PPM* isomer with Eu2 center) was apparently similar to those of **1a** and **2a**; the phen plane and the pseudo *trans*-positioned *S*-proOHdtc plane are nearly co-planar (Figure 1.3 and Table 1.2). In the crystal structure, these *PMP* and *PPM* isomers are connected by a hydrogen bond between their *S*-proOH moieties, together with the other hydrogen bond between the *PMP* isomers using the *S*-proOH group (Figure 1.4). Thus, the hydrogen-bonding interaction is one of the reasons why the crystals of **2e**•H_2O contains the *PMP* and *PPM* isomers in a 1:1 ratio. At this stage, however, we cannot deny a possibility that another crystal afforded might contain the other isomers. In the absorption, CD, MCD (*vide infra*) and ^{1}H NMR spectra (Figure 1.5), only the averaged structure of the possible diastereoisomers could be observed because of a rapid ligand exchange in solution. The IR spectrum of bulk sample of **2e**•H_2O (Figure 1.7) did not exhibit any complicated nature due to the mixture of the diastereoisomers.

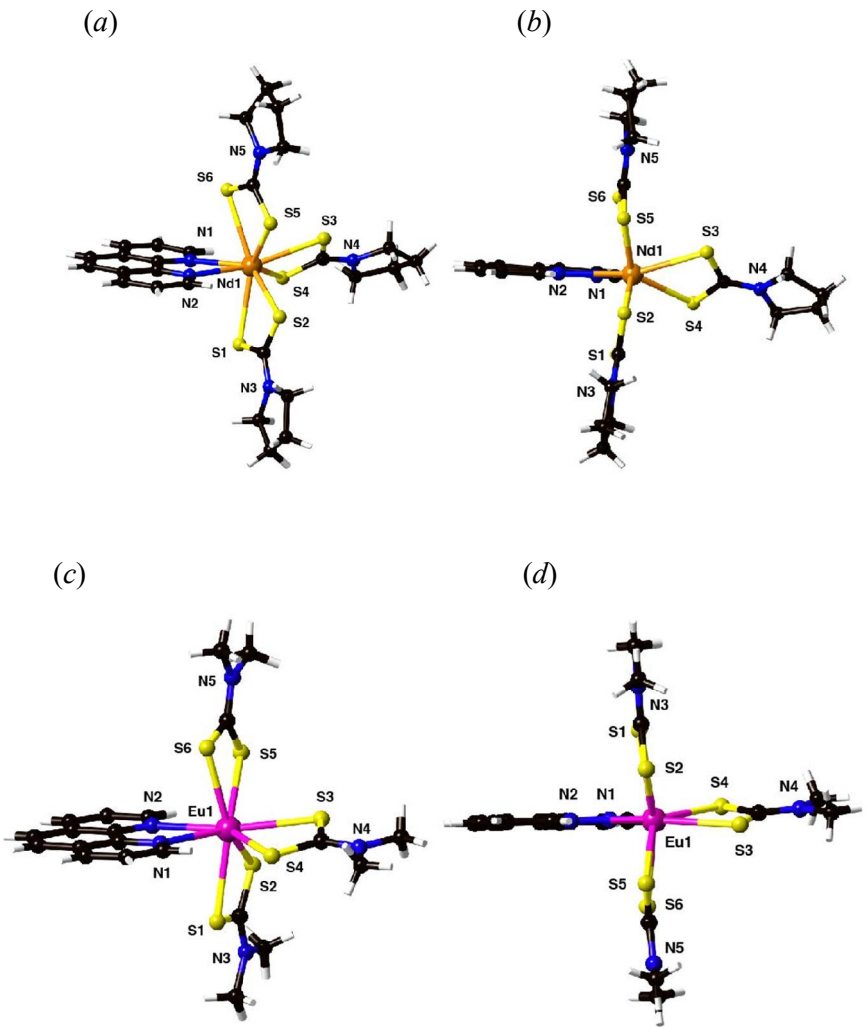

Figure 1.1. Perspective views of (*a* and *b*) [Nd(pyrdtc)$_3$(phen)] (**1b**) and (*c* and *d*) [Eu(Me$_2$dtc)$_3$(phen)] (**2a**). The views of (*b*) and (*d*) are from the direction that is perpendicular to the phen and two RR'dtc planes, showing the difference in the coordination geometry around Ln^{III} center.

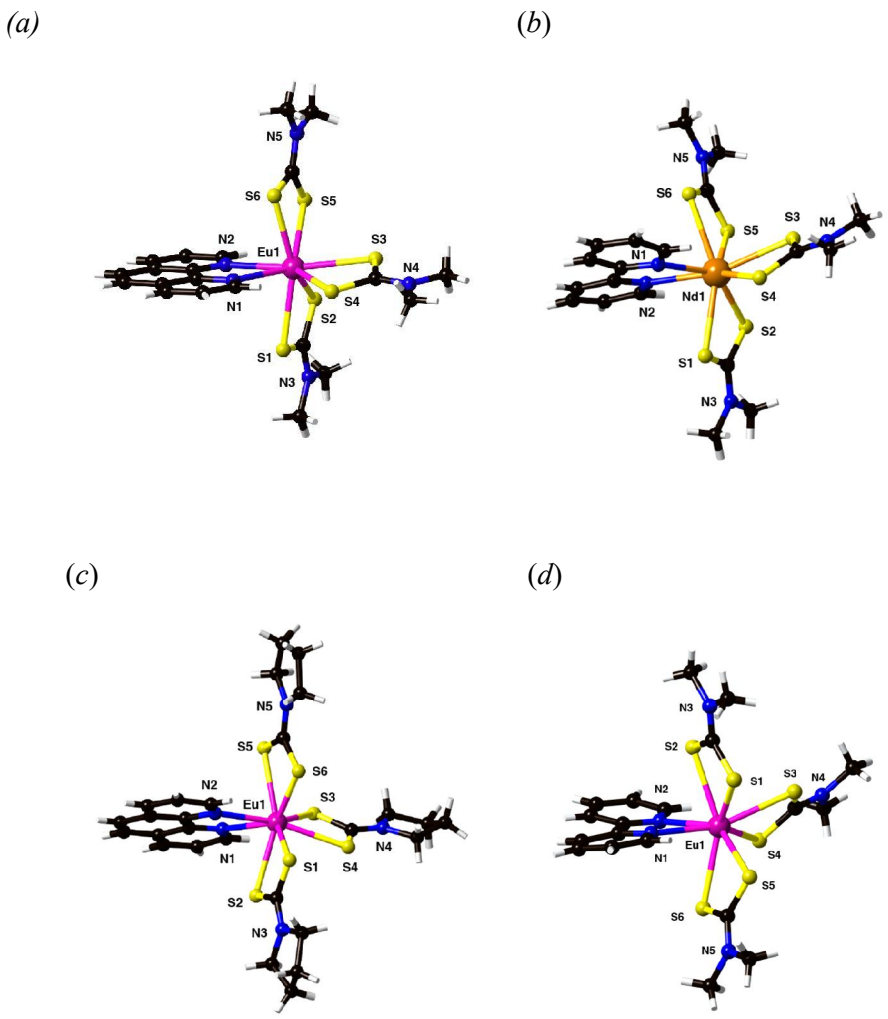

Figure 1.2. Perspective views of (*a*) [Nd(Me_2dtc)$_3$(phen)] (**1a**), (*b*) [Nd(Me_2dtc)$_3$(bpy)] (**1c**), (*c*) [Eu(pyrdtc)$_3$(phen)] (**2b**) and (*d*) [Eu(Me_2dtc)$_3$(bpy)] (**2c**).

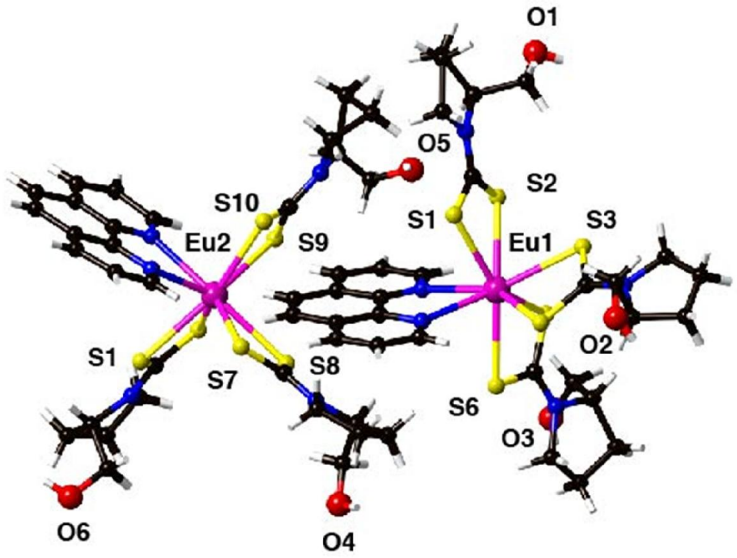

Figure 1.3. Perspective views of two crystallographically independent [Eu(*S*-proOHdtc)$_3$(phen)] molecules in **2e**•H_2O.

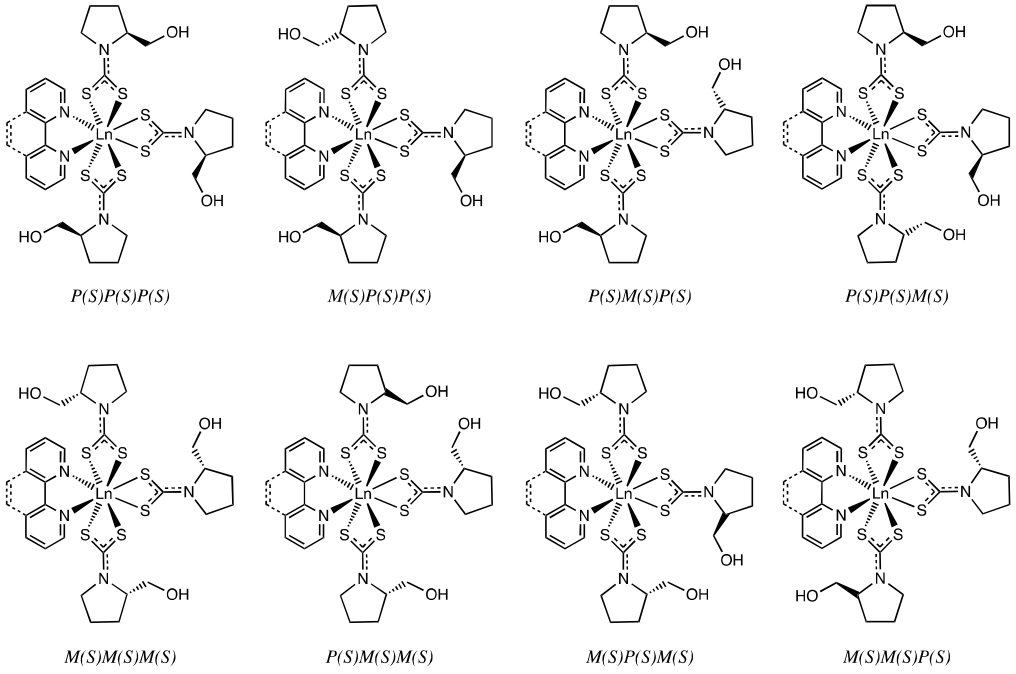

Scheme 1.2. Possible diastereoisomers for [Ln(*S*-proOHdtc)$_3$(NN)].

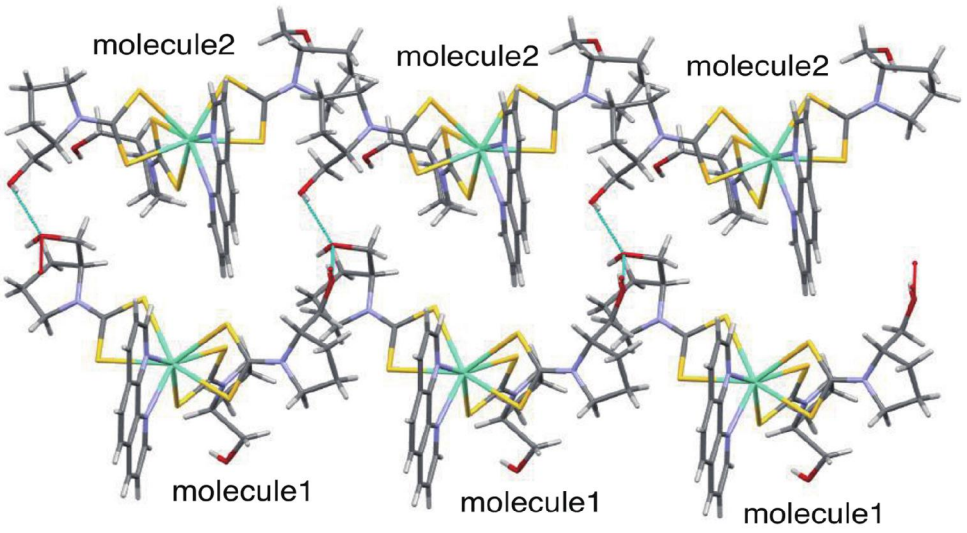

Figure 1.4. Hydrogen-bonding interactions between two crystallographically independent molecules in **2e**•H_2O.

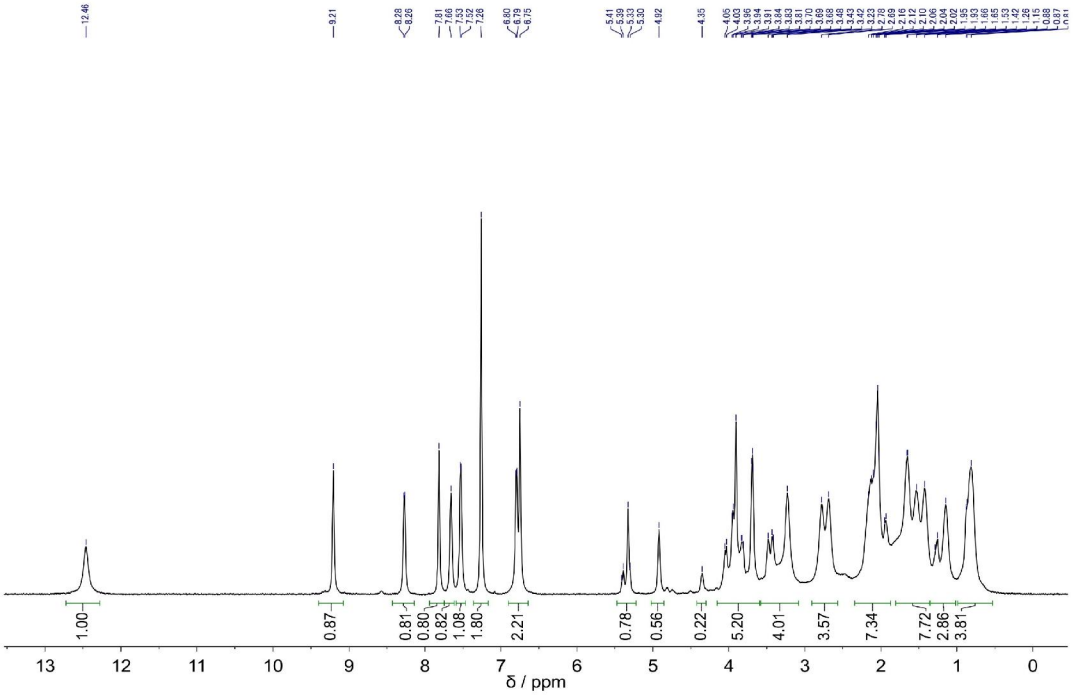

Figure 1.5. ^{1}H NMR spectrum of [Eu(*S*-proOHdtc)$_3$(phen)] (**2e**) in CD_3Cl at 22°C.

Spectroscopic Studies

FT-IR spectra

In the IR spectrum, the ν(C–N) stretching band of Na(Me_2dtc), NH_4(pyrdtc) and K(*S*-proOHdtc) appeared at 1359, 1413 and 1399 cm^{-1}, respectively, but those of the complexes **1a**–**2f** were observed in the range of 1374–1428 cm^{-1}. The ν(C–S) stretching band of Na(Me_2dtc), NH_4(pyrdtc) and K(*S*-proOHdtc) appeared at 963, 1001 and 966 cm^{-1}, respectively, but those of the complexes were exhibited in the range of 969–1011 cm^{-1}. These characteristic bands were similarly observed in the related complexes reported previously [3,16]. As representative spectra of the complexes, the IR spectra of **1d** and **2d** (Figure 1.6) and **1e** and **2e** (Figure 1.7) are compared with the respective free dithiocarbamate ligands.

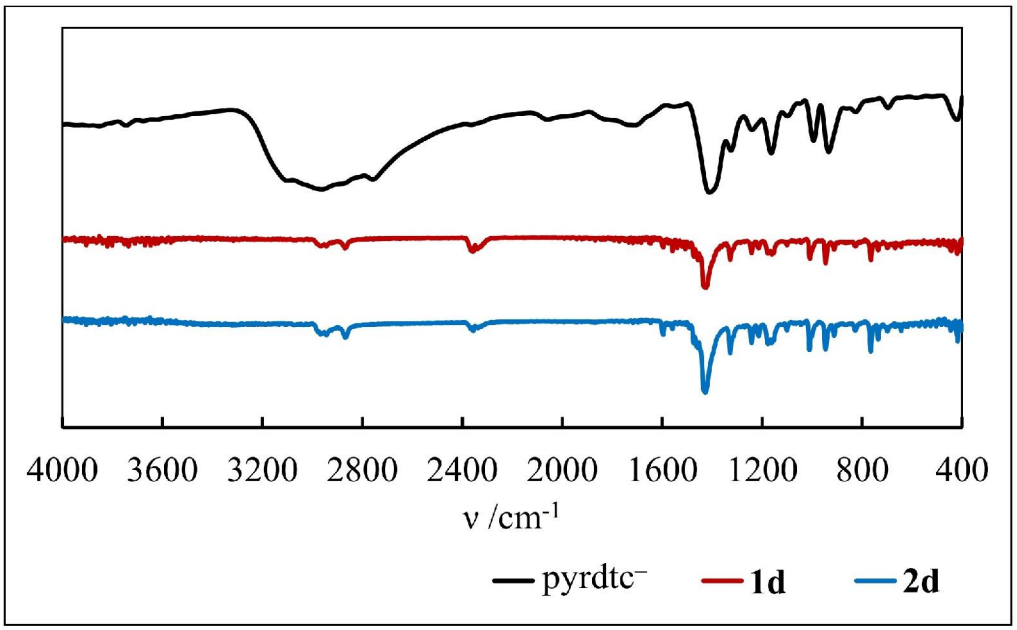

Figure 1.6. IR spectra of free pyrdtc⁻ ligand and [Nd(pyrdtc)$_3$(bpy)] **1d** and [Eu(pyrdtc)$_3$(bpy)] **2d** complexes.

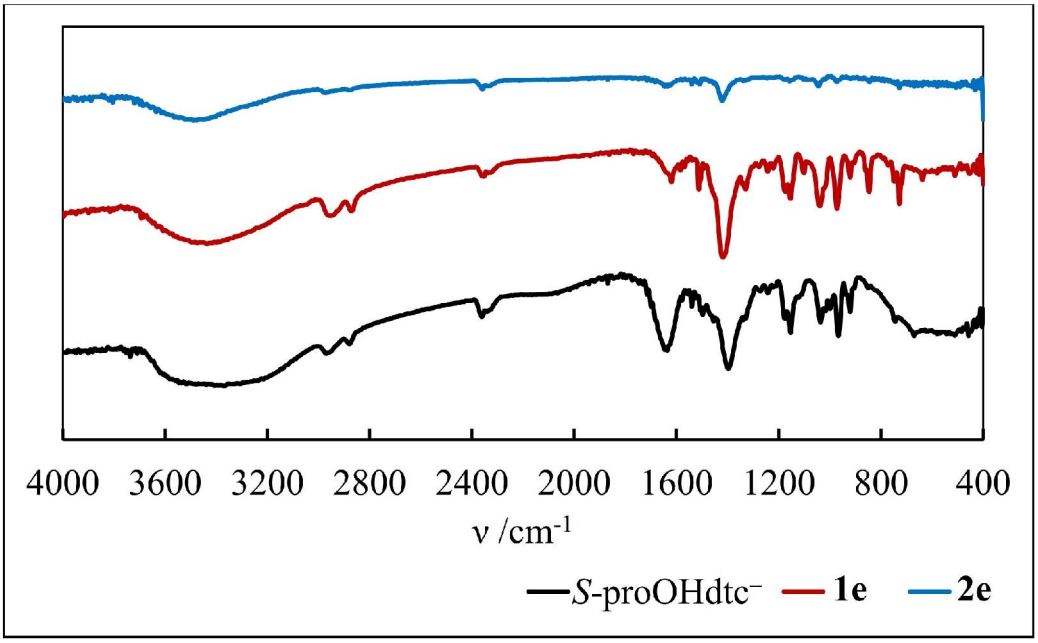

Figure 1.7. IR spectra of free *S*-proOHdtc⁻ ligand and [Nd(*S*-proOHdtc)$_3$(phen)] **1e** and [Eu(*S*-proOHdtc)$_3$(phen)] **2e** complexes.

UV-visible absorption, natural CD and MCD spectra

The Nd^{III} and Eu^{III} complexes with different dithiocarbamato ligands exhibited similar spectral patterns, respectively. The absorption, CD and MCD spectra of complexes [Nd(pyrdtc)$_3$(bpy)] (**1d**), [Eu(pyrdtc)$_3$(phen)] (**2b**), [Nd(*S*-proOHdtc)$_3$(phen)] (**1e**) and [Eu(*S*-proOHdtc)$_3$(phen)] (**2e**) are presented in Figures 1.8–1.19.

As shown in Figures 1.8 – 1.13, the Nd^{III} complexes exhibited sharp but weak f-f transitions at 19190, 18760, 16860, 13250 and 12350 cm^{-1}, which are assigned to the $^4G_{9/2}$, $^4G_{7/2}$, ($^2G_{7/2}$ and $^4G_{5/2}$), $^4S_{3/2}$ and $^4F_{5/2} \leftarrow {}^4I_{9/2}$ transitions, respectively. These assignments were consistent with the previous report [3a] and comparable with those of an octaaquaneodymium(III) ion [17] and a neodymium-doped fluorozirconate glass [18]. The observed bands for the complexes reported in this study were slightly shifted to lower energies relative to the corresponding absorption bands reported for neodymium(III) acetato complexes

[19], but they were in good agreement with the spectra of the related complexes [12, 20, 21]. In the MCD spectra (bottom), the MCD signals corresponding to the bands in the absorption spectra were observed for both Nd^{III} complexes with the achiral (i.e., Me_2dtc^- and $pyrdtc^-$) and the chiral (*S*-proOHdtc$^-$) dithiocarbamato ligands. These signals are characteristic of *C*-terms, except for the signal at 12350 cm^{-1} which appears as a positive pseudo *A*-term. In Figures 1.12 and 1.13 (top left), no CD signals characteristic of the f–f transitions were observed in the CD spectra of the Nd^{III} complexes of the Me_2dtc, pyrdtc and *S*-proOHdtc ligands. However, a CD band was observed around 368 nm in the *S*-proOHdtc complexes of Nd^{III}. These bands resulted from and are consistent with the bands (spectra not shown) observed in the free *S*-proOHdtc$^-$ ligand.

In Figures 1.14 – 1.19 (top), the Eu^{III} complexes exhibited a weak f–f transition band at 21460 cm^{-1} which is assigned to the $^5D_2 \leftarrow {}^7F_0$ induced electric dipole transition based on a comparison with the assignment for aqua Eu^{III} ion [17]. The position of this band is in good agreement with that observed in the Eu^{III} oxydiacetato and dipicolinato complexes [22] and is also consistent with the calculated energy levels for a free Eu^{III} ion [23]. In the MCD spectra (bottom), an MCD signal characteristic of a negative *B*-term was observed around 21460 cm^{-1} for the Eu^{III} complexes with the achiral (i.e. Me_2dtc^- and $pyrdtc^-$) and chiral (i.e. *S*-proOHdtc$^-$) dithiocarbamato ligands. As shown in Figure 1.18 and 1.19 (top left), no CD signals characteristic of f–f transitions were observed in the CD spectra of the Eu^{III} complexes with the *S*-proOHdtc ligands. In contrast, an MCD and a CD band were observed around 368 nm in the MCD and CD spectra, respectively, of [Eu(*S*-proOHdtc)$_3$(phen)] (**2e**). These bands resulted from the intraligand transition, because the spectra of K(*S*-proOHdtc) also exhibited a similar MCD and CD spectra in this region. The non-appearance of the f–f transition bands in CD spectra of the complexes containing the chiral *S*-proOHdtc$^-$ ligand suggests the lack of chirality around the Nd^{III} and Eu^{III} centers. It was expected that the chiral *S*-proOHdtc$^-$ ligand

coordinated to a Nd^{III} or Eu^{III} ion could not induce a chirality at the metal center, because the asymmetric center in the dithiocarbamato ligand is sterically far from the *S,S*-donor atoms to make the coordinated Ln^{III} site chiral, and because the Ln^{III} ions are substitutionally labile in solution.

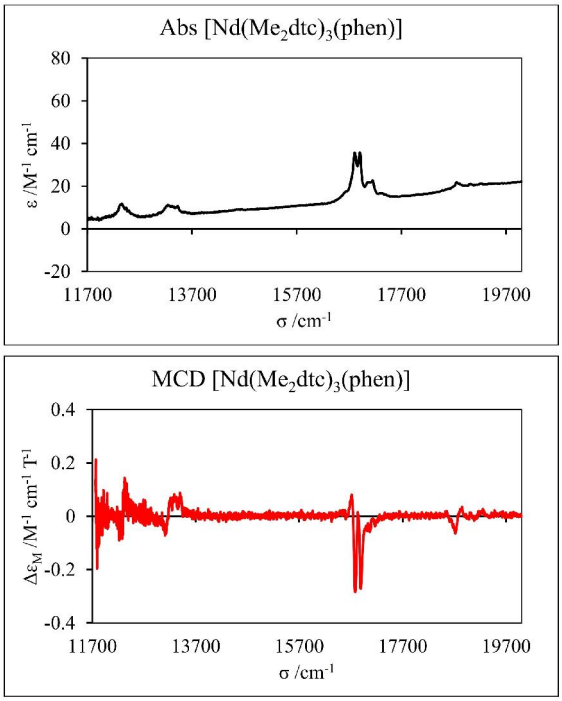

Figure 1.8. Absorption (top) and MCD (bottom) spectra of [Nd(Me$_2$dtc)$_3$(phen)] (**1a**).

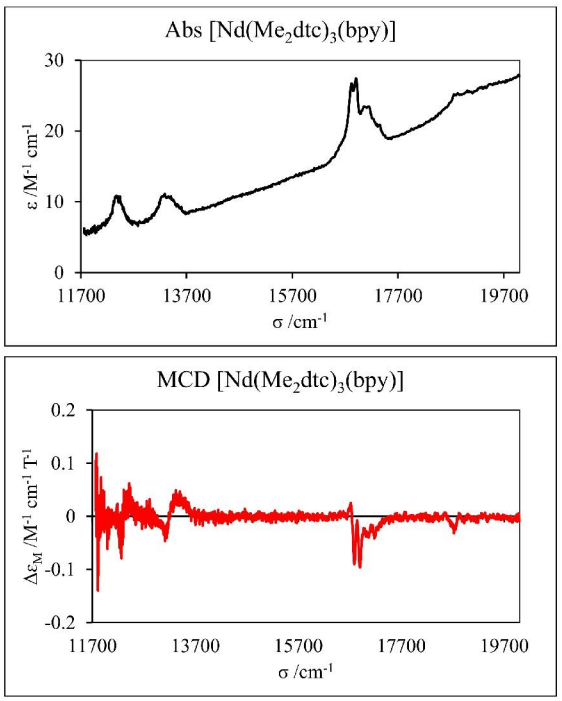

Figure 1.9. Absorption (top) and MCD (bottom) spectra of [Nd(Me$_2$dtc)$_3$(bpy)] (**1b**).

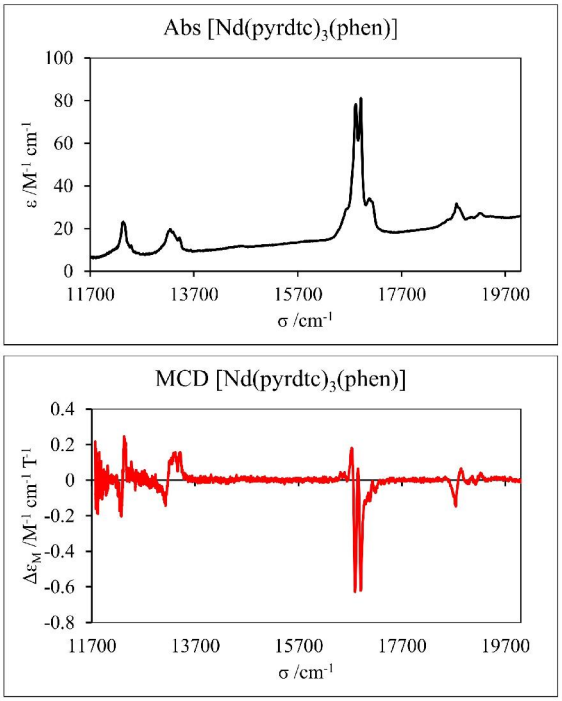

Figure 1.10. Absorption (top) and MCD (bottom) spectra of [Nd(pyrdtc)$_3$(phen)] (**1b**).

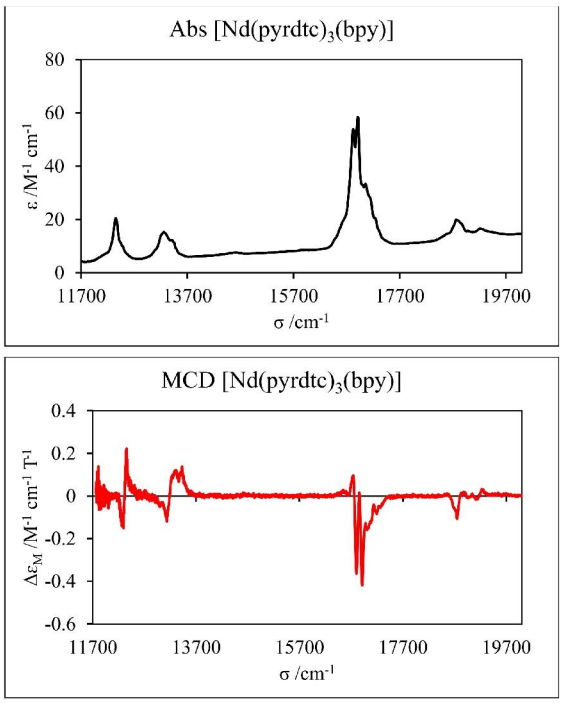

Figure 1.11. Absorption (top) and MCD (bottom) spectra of [Nd(pyrdtc)$_3$(bpy)] (**1d**).

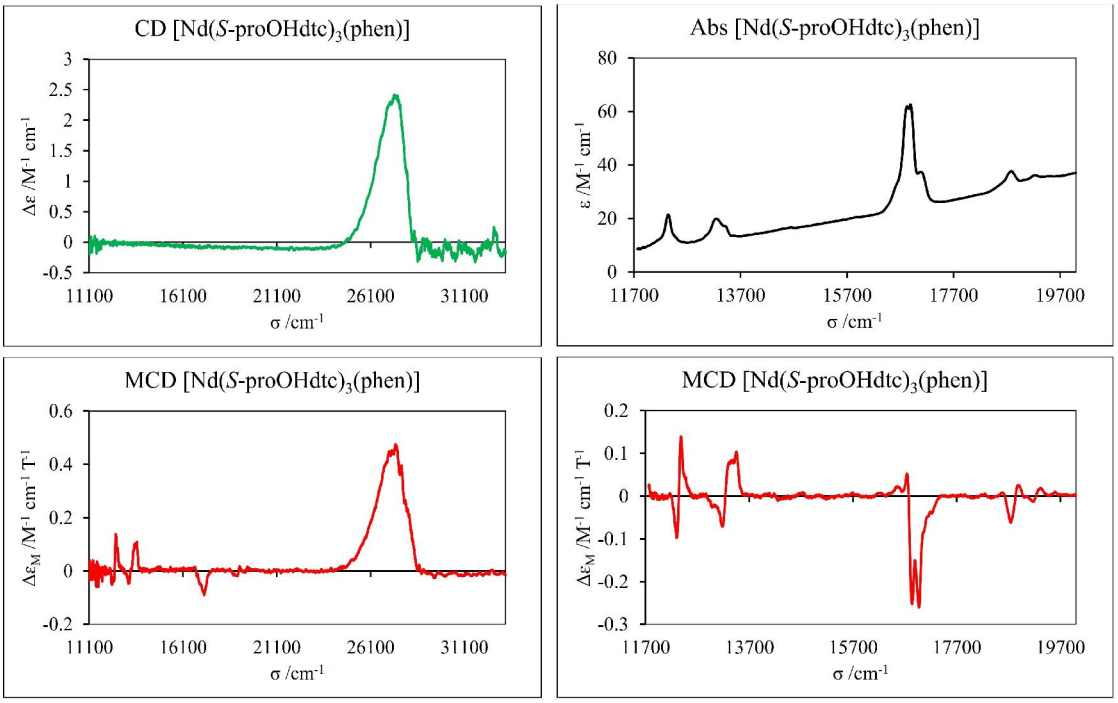

Figure 1.12. CD (top left), Absorption (top right) and MCD (bottom) spectra of [Nd(*S*-proOHdtc)$_3$(phen)] (**1e**).

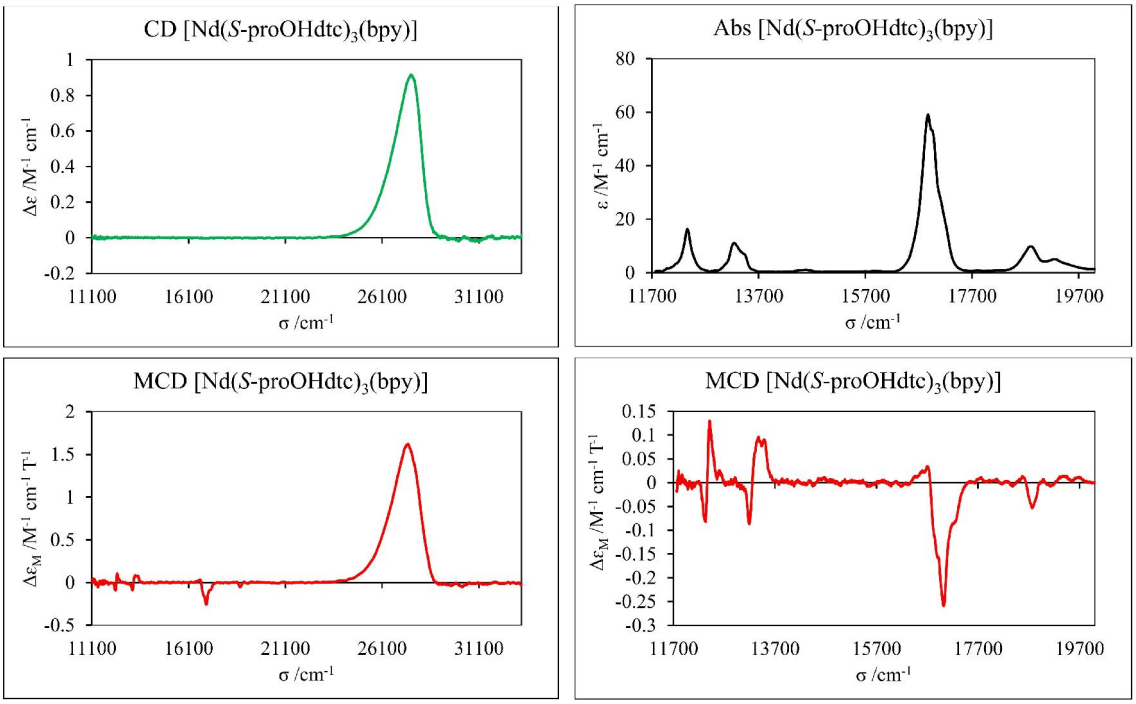

Figure 1.13. CD (top left), Absorption (top right) and MCD (bottom) spectra of [Nd(*S*-proOHdtc)$_3$(bpy)] (**1f**).

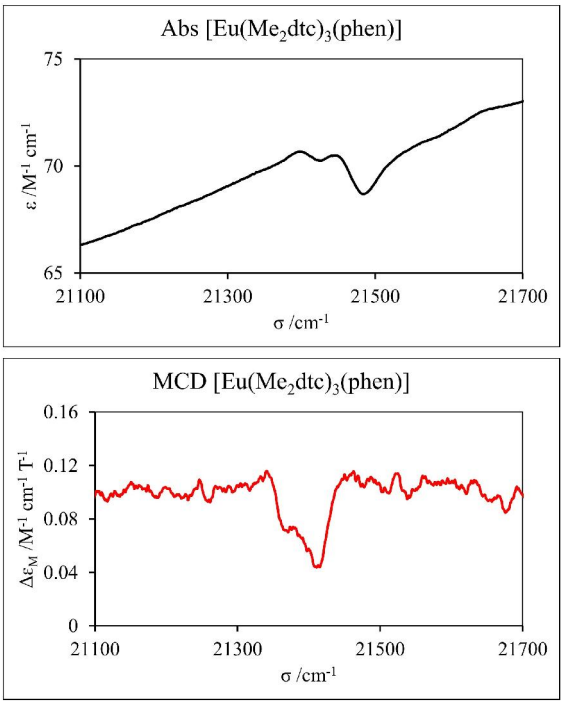

Figure 1.14. Absorption (top) and MCD (bottom) spectra of [Eu(Me$_2$dtc)$_3$(phen)] (**2a**).

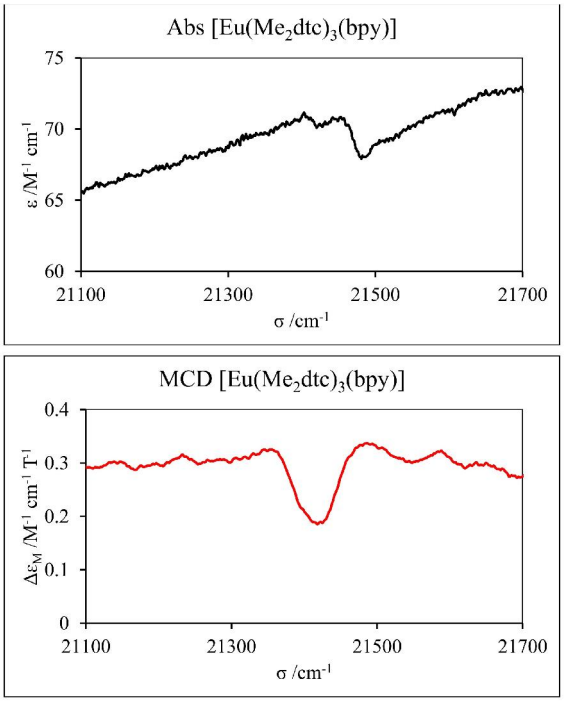

Figure 1.15. Absorption (top) and MCD (bottom) spectra of [Eu(Me$_2$dtc)$_3$(bpy)] (**2c**).

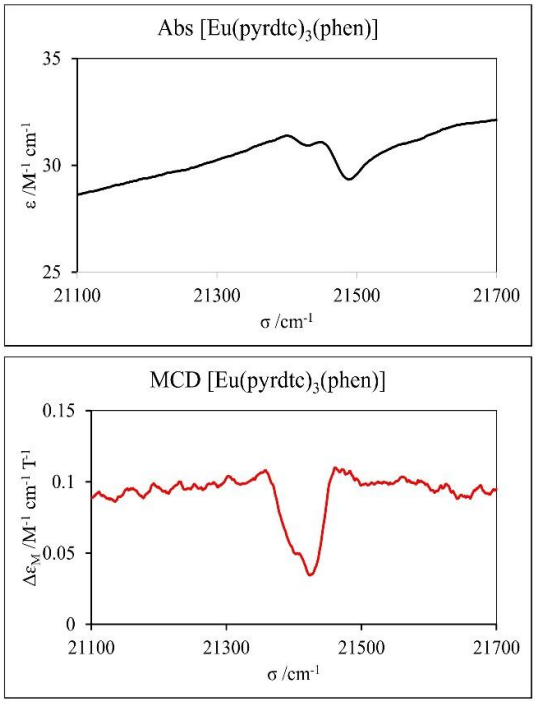

Figure 1.16. Absorption (top) and MCD (bottom) spectra of [Eu(pyrdtc)$_3$(phen)] (**2b**).

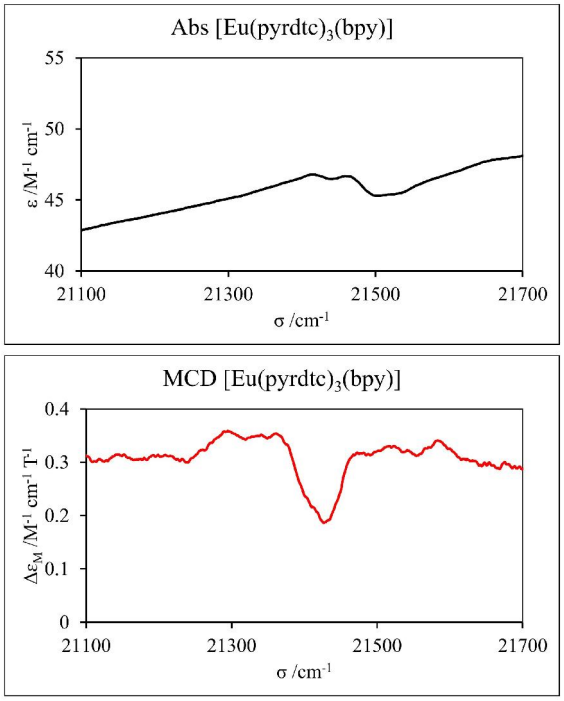

Figure 1.17. Absorption (top) and MCD (bottom) spectra of [Eu(pyrdtc)$_3$(bpy)] (**2d**).

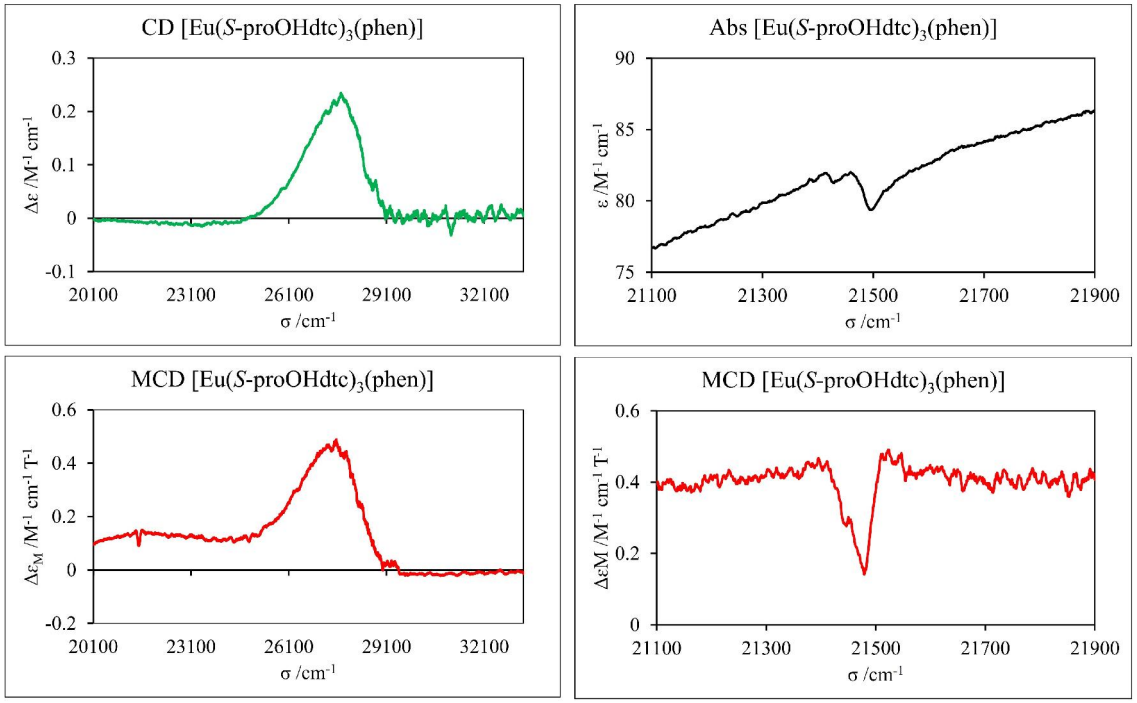

Figure 1.18. CD (top left), Absorption (top right) and MCD (bottom) spectra of [Eu(*S*-proOHdtc)$_3$(phen)] (**2e**).

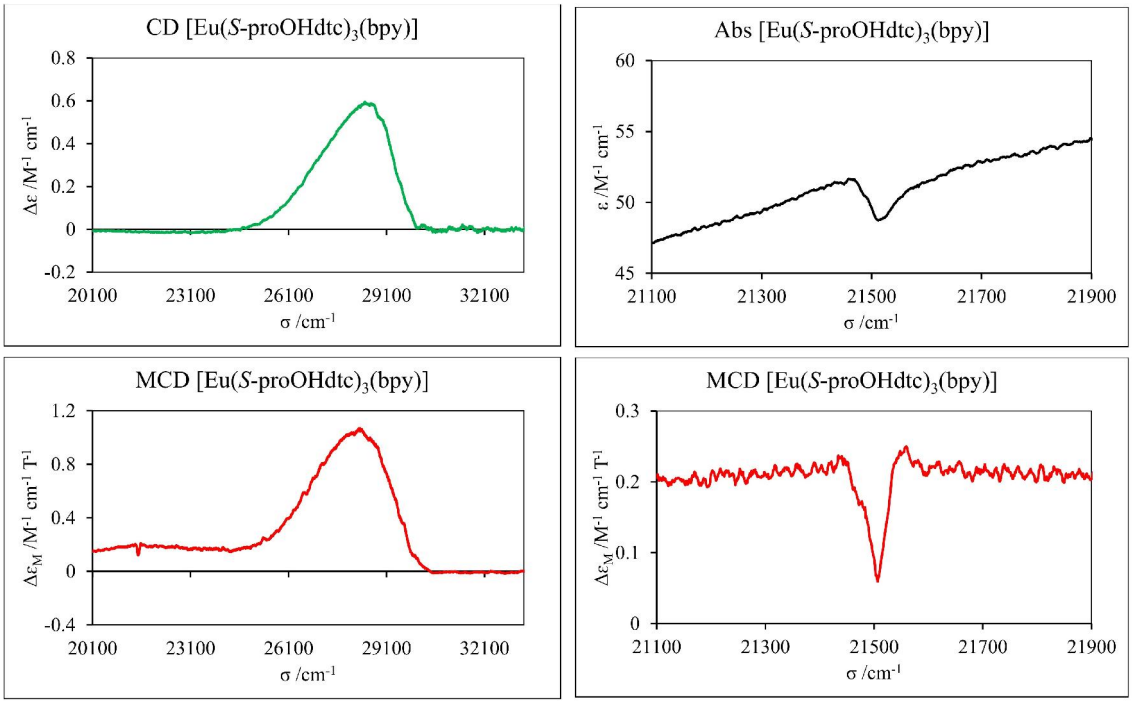

Figure 1.19. CD (top left), Absorption (top right) and MCD (bottom) spectra of [Eu(*S*-proOHdtc)$_3$(bpy)] (**1f**).

Coordination Symmetry of Ln^{III} Dithiocarbamato Complexes

The MCD signal for the induced electric dipole $^5D_2 \leftarrow {}^7F_0$ transition of the Eu^{III} complexes exhibited a characteristic pattern (Figure 6), as compared to the signals observed in the MCD spectra of $[Eu(H_2O)_8]^{3+}$ and [Eu(dpp)$_3$(phen)] (dpp = 1,3-diphenyl-1,3-propanedione) (Figure 1.20). The present dithiocarbamato complexes showed a negative *B*-term MCD signal, while the latter complexes gave a negative *A*-term MCD signal. Based on the suggestion by Görller-Walrand [24], the MCD spectral pattern of the $^5D_2 \leftarrow {}^7F_0$ induced electric dipole transition can be a probe of the coordination symmetry of the Eu^{III} complexes. Thus, it is deduced that the present dithiocarbamato complexes have a local C_{2v} symmetry at the Eu^{III} site in solution. In contrast, the β-diketonato complex showing a negative *A*-term MCD signal suggests a local D_{2d} symmetry at the Eu^{III} site. The difference in coordination

symmetry indicates that a mixed donor atoms set of O (of β-diketonato) and N (of diimine) in [Ln(dpp)$_3$(phen)] did not give a significant difference in the electronic structure of Ln^{III}, but the S donor atoms of dithiocarbamate showed a significant difference in the electronic structure of the Ln^{III} complexes from that of the N donor atoms of the diimine ligands.

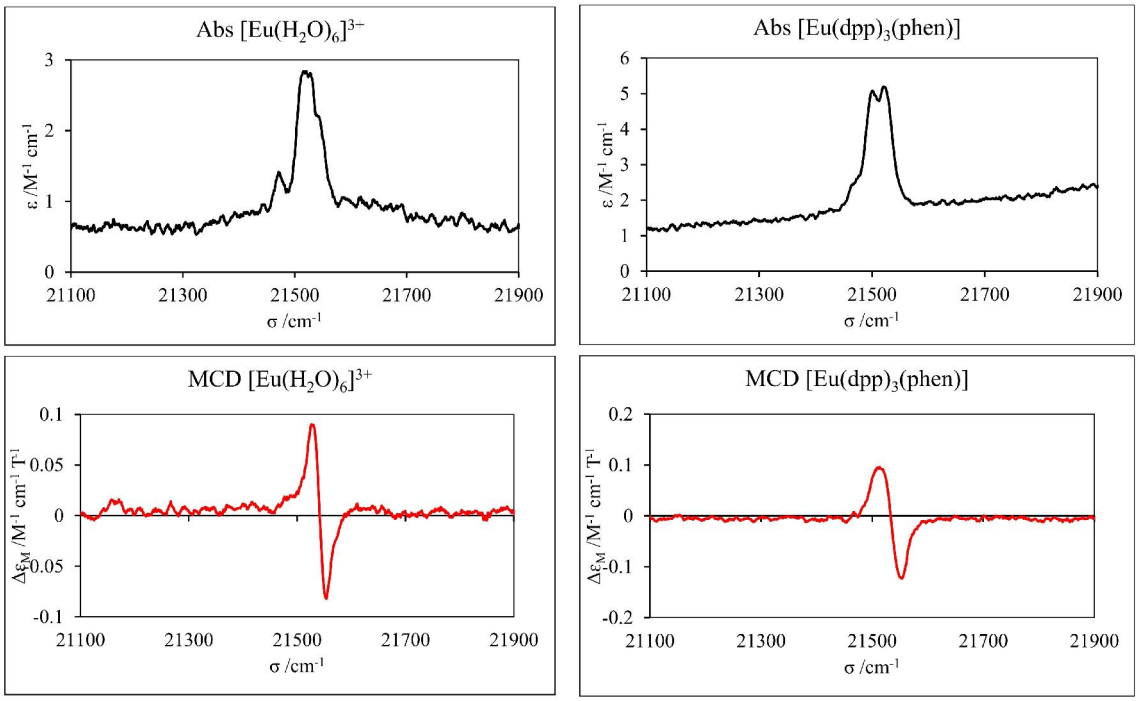

Figure 1.20. Absorption (top) and MCD (bottom) spectra of aqua (left) and β-diketonato (right) Eu^{III} complexes.

1.3 Conclusion

A series of lanthanoid(III) dithiocarbamato complexes have been synthesized and characterized through various spectroscopic methods. The molecular structures are all 8-coordinate geometry with insignificant differences in the structural parameters. The complexes showed no CD signals associated with the f–f transitions; however, MCD signals of these transitions were observed in all complexes. The MCD spectral pattern suggests that the dithiocarbamato complexes of lanthanide(III) have a site (coordination) symmetry different from those of the related β-diketonato complexes.

Table 1.1. Crystal data and structure refinement details

Parameters	**1a**	**1b**	**1c**•0.5CH_2Cl_2	**2a**
Molecular formula	$C_{21}H_{26}N_5NdS_6$	$C_{27}H_{32}N_5NdS_6$	$C_{19.5}H_{27}ClN_5NdS_6$	$C_{21}H_{26}N_5EuS_6$
Molecular weight	685.07	763.18	703.52	692.79
Crystal system	Triclinic	Triclinic	Tetragonal	Triclinic
Space group, Z	$P\bar{1}$	$P\bar{1}$	$I4_1/a$	$P\bar{1}$
a / Å	9.570(2)	10.0851(17)	16.6985(7)	9.5498(6)
b / Å	10.089(2)	10.4426(16)	–	10.0688(4)
c / Å	16.343(4)	17.221(3)	39.7858(17)	16.3618(8)
α / °	93.271(4)	96.922(5)	–	93.292(3)
β / °	103.863(4)	102.713(5)	–	104.420(3)
γ / °	113.752(4)	113.109(4)	–	113.678(4)
V / Å^3	1381.2(5)	1583.4(5)	11093.8(8)	1373.28(13)
Z	2	2	8	2
D_{calc} / g cm^{-3}	1.647	1.601	1.685	1.675
μ(Mo K$_\alpha$) / mm^{-1}	23.516	20.605	24.374	27.544
F(000)	686.00	770.00	5632.00	692.00
R_{int}	0.0433	0.0754	0.0478	0.0347
$R1$ [$I > 2\sigma(I)$]	0.0293	0.0448	0.0415	0.0289
$wR2$ [all data]	0.0813	0.1351	0.1142	0.1102
GOF on F^2	1.093	1.186	1.143	1.127
Flack parameter	–	–	–	–

Table 1.1. Continued.

Parameters	**2b**	**2c**	**2e•H_2O**
Molecular formula	$C_{27}H_{32}N_5EuS_6$	$C_{19}H_{26}N_5EuS_6$	$C_{30}H_{40}EuN_5O_4S_6$
Molecular weight	770.90	668.77	878.98
Temperature (K)	188	188	188
Crystal system	Triclinic	Tetragonal	Monoclinic
Space group, Z	$P\bar{1}$,	$I4_1/a$,	$P2$
a / Å	9.9956(12)	16.6431(10)	19.7161(8)
b / Å	10.3900(14)	16.6431	10.7864(5)
c / Å	17.198(3)	39.431(2)	20.2944(10)
α / °	96.603(4)	90	90
β / °	102.653(4)	90	115.367(2)
γ / °	112.806(4)	90	90
V / Å^3	1566.3(4)	10922.1(15)	3899.8(3)
Z	2	16	4
D_{calc} / g cm^{-3}	1.634	1.627	1.494
μ(Mo K$_\alpha$) / mm^{-1}	2.4243	2.772	1.968
F(000)	776	5344	1780
R_{int}	0.0286	0.0573	0.0396
$R1$ [$I > 2\sigma(I)$]	0.0248	0.0316	0.0433
$wR2$ [all data]	0.0861	0.0737	0.1181
GOF on F^2	1.000	1.087	1.072
Flack parameter	–	–	0.005(5)

Table 1.2. Selected bond parameters of complexes

Complexes	**1a**	**1b**	**1c**	**2a**	**2b**	**2c**	**2e•H_2O** molecule1	molecule2[a]
Bond lengths (Å)								
Ln1─S1	2.8664(12)	2.9324(16)	2.9191(14)	2.8540(18)	2.8243(12)	2.8533(10)	2.823(3)	2.855(3)
Ln1─S2	2.8576(12)	2.8811(17)	2.8723(14)	2.8658(12)	2.8657(11)	2.8344(10)	2.912(3)	2.839(3)
Ln1─S3	2.9062(12)	2.8737(15)	2.8924(14)	2.8306(15)	2.8798(12)	2.9012(13)	2.855(3)	2.844(4)
Ln1─S4	2.8692(11)	2.923(2)	2.9426(16)	2.8860(17)	2.8399(10)	2.8553(11)	2.863(3)	2.831(3)
Ln1─S5	2.8900(12)	2.864(2)	2.8874(13)	2.8477(18)	2.8943(10)	2.8768(11)	2.841(3)	2.845(2)
Ln1─S6	2.8997(9)	2.9122(19)	2.8709(13)	2.8219(14)	2.8413(11)	2.8256(11)	2.843(3)	2.911(3)
Ln1─N1	2.635(3)	2.613(5)	2.647(4)	2.605(4)	2.585(3)	2.566(3)	2.580(9)	2.591(8)
Ln1─N2	2.662(2)	2.639(5)	2.617(4)	2.597(5)	2.581(3)	2.582(3)	2.573(7)	2.594(7)
Bond angles (°)								
S1─Ln1─S2	62.33(3)	61.69(5)	61.54(4)	62.50(4)	62.90(3)	62.49(2)	62.46(8)	61.79(10)
S3─Ln1─S4	61.55(3)	61.64(5)	60.48(4)	61.96(4)	62.33(3)	61.18(3)	62.09(10)	62.50(11)
S5─Ln1─S6	61.73(3)	62.14(5)	61.74(3)	62.85(4)	62.49(3)	62.58(3)	63.31(9)	62.09(8)
N1─Ln1─N2	62.71(9)	62.88(17)	62.27(12)	64.00(15)	63.91(11)	63.74(9)	64.1(3)	63.3(3)
Dihedral angles (°)								
pl(NN)[b] vs. pl(dtc1)[c]	13.67(5)	41.35(8)	40.78(9)	12.77(9)	39.91(5)	45.21(7)	32.9(2)	13.1(2)
pl(dtc2)[d] vs. pl(dtc3)[d]	0.53(6)	5.89(7)	23.00(1)	1.60(2)	5.18(2)	27.15(2)	15.7(2)	5.0(4)
Average Bond length (Å)								
Ln─S	2.882(3)	2.893(4)	2.898(3)	2.851(4)	2.858(3)	2.858(3)	2.856(7)	2.854(7)
Ln─N	2.649(4)	2.626(7)	2.632(6)	2.601(6)	2.583(4)	2.574(4)	2.576(11)	2.593(11)
Average Bond angles (°)								
S─Ln─S	61.87(5)	61.82(9)	62.25(6)	62.44(7)	62.57(5)	62.08(5)	62.62(16)	62.13(17)

[a] The atomic numbers should be modified adequately. [b] pl(NN) was defined by all non-H atoms of phen or bpy. [c] pl(dtc1) was defined by the S_2CN atoms of the pseudo *trans*-positioned dtc ligand to the NN ligand. [d] pl(dtc2) and pl(dtc3) were defined by the S_2CN atoms, respectively, of the pseudo *cis*-positioned dtc ligands to the NN ligand.

References

[1] W.M. Faustino, O.L. Malta, E.E.S. Teotonio, H.F. Brito, A.M. Simas, G.F. de Sá, J. Phys. Chem. A110 (2006) 2510.

[2] M. Mahato, P.P. Jana, K. Harms, H.P. Nayek, RSC Adv. 5 (2015) 62167.

[3] (a) C. Su, M. Tan, N. Tang, X. Gan, W. Liu, X. Wang, J. Coord. Chem. 38 (1996) 207; (b) I. Raya, I. Baba, B.M. Yamin, Malaysia J. Anal. Sci. 10 (2006) 93.

[4] H. P. S. Chauhan, J. Carpenter, J. Saudi Chem. Soc. 19 (2015) 417.

[5] V. Kubat, G. Demo, L. Jeremias, J. Novosad, Z. Kristallogr. 228 (2013) 369.

[6] M.D. Regulacio, N. Tomson, S.L. Stoll, Chem. Mater. 17 (2005) 3114.

[7] W. L. Boncher, M. D. Regulacio, S. L. Stoll, J. Solid State Chem. 183 (2010) 52.

[8] R.S. Selinsky, J.H. Han, E.A.M. Pérez, I.A. Guzei, S. Jin, J. Am. Chem. Soc. 132 (2010) 15997.

[9] (a) P. Pitchaimani, K.M. Lo, K.P. Elango, Polyhedron. 93 (2015) 8; (b) P. Pitchaimani, K.M. Lo, K.P. Elango, J. Coord. Chem. 68 (2015) 2167.

[10] M. T. Berry, C. Schwieters, F. S. Richardson, Chem. Phy. 122 (1988) 125.

[11] D. Shirotani, T. Suzuki, K. Yamanari, S. Kaizaki, J. Alloys and Comp. 451 (2008) 325.

[12] P. Biscarini, Inorg. Chim. Acta. 74 (1983) 65.

[13] A. Yakubu, T. Suzuki, M. Kita, J. Chem. Educ. 94 (2017) 1357.

[14] P. Pitchaimani, K.M. Lo, K.P. Elango, Polyhedron. 54 (2013) 60.

[15] G.M. Sheldrick, SHELXS Version 2013/1. Acta Cryst, A64 (2008) 112.

[16] D. A. Brown, W. K. Glass, M. A. Burke, Spectrochimica Acta. 32A (1976) 137.

[17] C. Görller-Walrand, L. Fluyt, Magnetic Circular Dicroism of Lanthanides. Handbook on the Physics and Chemistry of Rare Earths, 40 (2010) 1-107.

[18] K. Binnemans, D. Verboven, C. Görller-Warlrand, J. Lucas, N. Duhamel-Henry, J.L. Adam, J. Non-Crystalline Solids. 204 (1996) 178.

[19] S. V. J. Laksham, S. Buddhudu, Proc. Indian natn. Sci. Acad., 47, A. 6 (1981) 721.

[20] M. Iwamuro, T. Adachi, Y. Wada, T. Kitamura, N. Nakashima, S. Yanagida, Bull. Chem. Soc. Jpn. 73 (2000) 1359.

[21] R. Ilmi, K. Iftikhar, Inorg. Chem. Commun. 13 (2010) 1552.

[22] J. G. Kim, S. K. Yoon, J. G. Kang, Bull. Korean Chem. Soc. 17 (1996) 854.

[23] K. Binnemans, Coord. Chem. Rev. 295 (2015) 1.

[24] C. Görller-Walrand, Chem. Phys. Lett. 115 (1985) 333.

Chapter 2

Syntheses, structures and spectroscopic properties of homodinuclear lanthanoid(III) dithiocarbamato complexes bridged by 2,2'-bipyrimidine

Abstract

Four new homodinuclear lanthanoid(III) dithiocarbamato (*RR′*dtc^{-}) complexes bridged by 2,2'-bipyrimidine (bpm) of the form [{Ln(*RR′*dtc)$_3$}$_2$(μ-bpm)] {Ln = Nd or Eu; *RR′* = dimethyl- (Me_2) or pyrrolidine- (pyr)} were prepared and their crystal structures and spectroscopic properties were characterized. Crystallographic studies revealed that all of the complexes possess a similar structural motif with an 8:8-coordination geometry, in which bpm bridges two Ln^{III} centers in the $\kappa^2N^{1,1'}$:$\kappa^2N^{3,3'}$ mode and three *RR′*dtc^{-} ligands coordinate to each Ln^{III} center. The complexes exhibited weak but relatively sharp f–f transition bands in the absorption and magnetic circular dichroism (MCD) spectra recorded in the visible region. The MCD spectral studies demonstrated the magneto-optical behavior of the complexes. The spectral features of the dithiocarbamato complexes were distinctly different from those of the β-diketonato analogues, suggesting the coordination environment around the Ln^{III} center influences the electronic structure and spectroscopic symmetry of the complexes in solution.

2.1 Introduction

The role of homo- and hetero-dinuclear lanthanoid complexes as building blocks for coordination polymers and supramolecular assemblies is a significant field of study in recent years. Dinuclear lanthanoid complexes with intriguing structural diversity, spectroscopic, magnetic and physicochemical properties have been studied for many reasons including catalysis, optical probes, magnetic materials, biological assays, display devices, and microelectronics [1,2]. Many dinuclear complexes and coordination polymers with a variety of bridging ligands have been reported [3], and 2,2'-bipyrimidine (bpm) is one of the heterocyclic bridging ligands, which have been shown to afford diverse structural architectures with different dimensionalities [3,4]. The coordination chemistry of polyazine bridging ligands and transition metals is a well-established field of study [2], but it is only recently that the coordination ability of bpm to form complexes with lanthanoids has been explored [4]. In addition to studies on the structures and photophysical properties of heterometallic d-f systems [5,6], several examples of homodinuclear lanthanoid complexes bearing β-diketonato co-ligands appeared in the literature. D'Cunha et al. reported the synthesis of homodinuclear lanthanoid complexes bridged by bpm and capped with terminal β-diketonato ligands [7]. Yu et al. have reported the molecular structures and magnetic properties of bpm bridged homodinuclear lanthanoid complexes of 2,2',6,6'-tetramethyl-3,5-heptanedionate [8]. Sun et al. have reported the single-molecule magnetic behavior of bpm bridged Dy^{III}_2 β-diketonato dimers [9]. Absorption and photoluminescence properties of bpm-bridged homodinuclear lanthanoid(III) 2,4-pentanedionato complexes have also been reported [10]. On the other hand, the analogous lanthanoid chemistry with dithiocarbamato co-ligands and polyazine bridging ligands has not yet been studied.

Lanthanoid dithiocarbamato complexes have been studied sporadically since the 1960s. However, interests in these complexes have recently resurfaced for practical applications in catalysis, nanotechnology, and microelectronics [11,12]. The syntheses, crystallographic and spectroscopic characterizations of some mononuclear lanthanoid complexes of various dialkyl-substituted dithiocarbamates with 1,10-phenanthroline (phen) and 2,2'-bipyridine (bpy) have been reported [13-17]. In a previous study [17], we investigated the crystal structures and spectroscopic properties of the Nd^{III} and Eu^{III} complexes containing chiral or achiral dithiocarbamates. In particular, their natural circular dichroism (CD) and magnetic circular dichroism (MCD) spectra were discussed in relation to the coordination environment and electronic structure around the lanthanoid center, because Nd^{III} and Eu^{III} often give representative examples showing CD- and MCD-active f–f transition bands. In this study, we will describe four new homodinuclear lanthanoid dithiocarbamato complexes using 2,2'-bipyrimidine (bpm) as a bridging unit and compare their structures and spectroscopic properties with those of the mononuclear phen or bpy complexes and with those of the corresponding dinuclear β-diketonato complexes.

2.1 Experimental section

Synthesis of Dithiocarbamato Complexes

The complexes were prepared by a similar procedure (Scheme 2.1) to that for mononuclear 2,2'-bipyridine (bpy) and 1,10-phenanthroline (phen) complexes [17]. To a

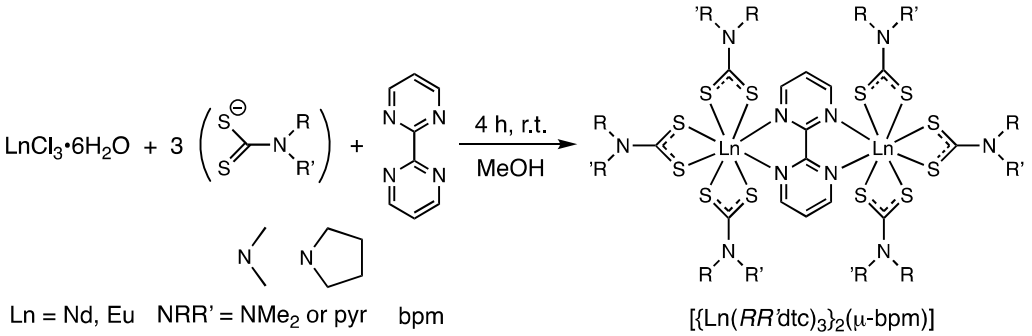

Scheme 2.1. Synthesis of [{Ln(*RR'*dtc)$_3$}$_2$(μ-bpm)] complexes.

mixture of 2,2'-bipyrimidine, bpm (1.00 mmol) and sodium dimethyldithiocarbamate, Na(Me$_2$dtc) or ammonium pyrrolidine dithiocarbamate, NH$_4$(pyrdtc) (3.00 mmol) in MeOH (20 mL) was added a methanol solution (10 mL) of $LnCl_3 \cdot 6H_2O$ (Ln = Nd or Eu) (1.00 mmol). The mixture was stirred for 4 h at room temperature and the resulting precipitate was collected by filtration, washed with MeOH and dried in air. The crude product was purified by recrystallization. The method of recrystallization, the results of elemental analysis and the FT-IR spectral data of respective complexes are given below.

[{Nd(Me$_2$dtc)$_3$}$_2$(μ-bpm)] (**1a**)

Green crystals were grown from a CH_2Cl_2 solution layered with Et_2O in 37% yield, while single-crystals suitable for X-ray diffraction analysis were obtained from $CHCl_3/Et_2O$. Anal. Found: C, 25.04; H, 3.67; N, 10.57; S, 29.06%. Calcd. for $C_{26}H_{42}N_{10}Nd_2S_{12} \cdot 2CH_2Cl_2$: C, 25.14; H, 3.47; N, 10.47; S, 28.76%. IR (KBr disc) cm^{-1}: *ν*(C–N) 1374; *ν*(C–S) 983.

[{Nd(pyrdtc)$_3$}$_2$(μ-bpm)] (1b)

Greenish-yellow crystals were obtained from a mixture of $CHCl_3$ and EtOH in 46% yield. Anal. Found: C, 33.34; H, 3.99; N, 9.97; S, 27.18%. Calcd. for $C_{38}H_{54}N_{10}Nd_2S_{12}\cdot 0.5CHCl_3$: C, 33.41; H, 3.97; N, 10.12; S, 27.81%. IR (KBr disc) cm^{-1}: *ν*(C–N) 1436; *ν*(C–S) 948.

[{Eu(Me$_2$dtc)$_3$}$_2$(μ-bpm)] (2a)

Orange crystals were obtained from a mixture of CH_2Cl_2 and Et_2O in 38% yield, while single-crystals suitable for X-ray diffraction analysis were obtained from a mixture of $CHCl_3$ and Et_2O. Anal. Found: C, 24.39; H, 3.29; N, 10.56; S, 28.10%. Calcd. for $C_{26}H_{42}N_{10}Eu_2S_{12}\cdot 2CH_2Cl_2$: C, 24.85; H, 3.43; N, 10.35; S, 28.43%. IR (KBr disc) cm^{-1}: *ν*(C–N) 1399; *ν*(C–S) 984.

[Eu$_2$(pyrdtc)$_6$(μ-bpm)] (2b)

Orange crystals were obtained from a mixture of CH_2Cl_2 and Et_2O mixture in 48% yield, while single-crystals suitable for X-ray diffraction analysis were obtained from a CH_2Cl_2 solution by adding a 1:1 mixture of EtOH/Et_2O. Anal. Found: C, 34.28; H, 4.17; N, 10.35; S, 27.95%. Calcd. for $C_{38}H_{54}N_{10}Eu_2S_{12}$: C, 34.07; H, 4.06; N, 10.46; S, 28.72%. IR (KBr disc) cm^{-1}: *ν*(C–N) 1436; *ν*(C–S) 949.

Synthesis of Acetylacetonato Complexes

The complexes, [{Ln(acac)$_3$}$_2$(μ-bpm)] (Ln = Nd (**1c**) and Eu (**2c**)) were prepared, following the procedure described by Ilmi *et al*. with some modification [10]. To a mixture of 2,2'-bipyrimidine, bpm (0.50 mmol) and lithium acetylacetonate, Li(acac) (3.00 mmol) in absolute EtOH (20 mL) was added an absolute EtOH solution (10 mL) of $LnCl_3 \cdot 6H_2O$ (1.00 mmol) (Ln = Nd or Eu). The mixture was stirred on a hot plate at an elevated temperature below the boiling point of the solvent for 4 h and the resulting solution (concentrated to ca. 15 mL) was filtered. The filtrate was kept at room temperature for slow evaporation of the solvent. Single-crystals suitable for X-ray diffraction study were obtained within 24 h. The crystals were collected by filtration and dried in air.

Structural Characterization

X-ray diffraction data of all complexes were collected on a Rigaku R-AXIS Rapid diffractometer using a graphite-monochromatized Mo-Kα (λ = 0.71075Å) radiation. Data were collected and processed using a program package, process-auto [18]. The structures were solved by the direct methods [19,20] and expanded using Fourier techniques. The non-hydrogen atoms were refined anisotropically. Hydrogen atoms were introduced at theoretical positions and treated with the riding models. All calculations were performed using a program package, CrystalStructure [21], except for the refinement, which was performed using SHELXL Version 2014/7 [22].

Physical Measurements

C, H, N and S analysis of the complexes were carried out on a Perkin Elmer Series II CHNS/O Analyzer 2400 at Advanced Science Research Center, Okayama University. The FT-IR spectra were recorded on a JASCO FT-001 FT-IR spectrophotometer in KBr disc in the 4000–400 cm^{-1} range. The UV-visible absorption spectra of the complexes in a CH_2Cl_2 solution were obtained on a JASCO V-550 UV/VIS spectrophotometer at room temperature. Room temperature magnetic circular dichroism (MCD) spectra were measured on a JASCO J-1500 CD spectropolarimeter equipped with a home-made 0.5 T neodymium magnet [23].

2.3 Results and Discussion

Synthesis of 2,2'-bipyrimidine-bridged Ln^{III}_2 complexes

The 2,2'-bipyrimidine-bridged dinuclear lanthanoid(III) complexes with dithiocarbamato co-ligands were prepared by a one-pot reaction from $LnCl_3 \cdot 6H_2O$ (Ln = Nd^{III} (**1**) and Eu^{III} (**2**)), 2,2'-bipyrimidine (bpm) and sodium *N,N*-dimethyldithiocarbamate (Me_2dtc^-) or ammonium pyrrolidine dithiocarbamate ($pyrdtc^-$) in a 1:1:3 molar ratio in methanol at room temperature. These dithiocarbamato complexes were isolated in 37–48% yields. The acetylacetonato analogues were prepared similarly by a reaction of $LnCl_3 \cdot 6H_2O$, bpm and lithium acetylacetonate ($acac^-$) in a 2:1:6 molar ratio in absolute ethanol at an elevated temperature, and isolated in 23–24% yields. All of the complexes prepared were characterized by elemental analyses, single-crystal X-ray diffraction analysis, FT-IR, absorption and magnetic circular dichroism (MCD) spectroscopy.

Crystal Structures

Single-crystal X-ray diffraction analysis revealed that all complexes investigated in this study, **1a**–**1c** and **2a**–**2c**, have a centrosymmetric homodinuclear structure. Complexes of $[\{Nd(Me_2dtc)_3\}_2(\mu\text{-bpm})]\cdot 2CHCl_3$ (**1a**$\cdot 2CHCl_3$) and $[\{Eu(Me_2dtc)_3\}_2(\mu\text{-bpm})]\cdot 2CHCl_3$ (**2a**$\cdot 2CHCl_3$) are isomorphous and crystallized in the monoclinic space group $P2_1/n$ with Z = 2, while $[\{Nd(pyrdtc)_3\}_2(\mu\text{-bpm})]\cdot 2CHCl_3$ (**1b**$\cdot 2CHCl_3$) crystallized in the monoclinic space group $C2/c$ with Z = 4. The corresponding Eu^{III}–pyrdtc complex, **2b**, afforded two kinds of pseudo-polymorphic crystals: one is of the formula $[\{Eu(pyrdtc)_3\}_2(\mu\text{-bpm})]\cdot 4CH_2Cl_2$ (**2b**$\cdot 4CH_2Cl_2$) and crystallized in the monoclinic space group $C2/c$ with Z = 4, and the other, $[\{Eu(pyrdtc)_3\}_2(\mu\text{-bpm})]\cdot CH_2Cl_2$ (**2b**$\cdot CH_2Cl_2$) crystallized in the triclinic space group $P\bar{1}$ with Z = 2. The acetylacetonato analogues, $[\{Nd(acac)_3\}_2(\mu\text{-bpm})]$ (**1c**) and $[\{Eu(acac)_3\}_2(\mu\text{-bpm})]$ (**2c**), are also isomorphous and crystallized in the triclinic space group $P\bar{1}$ with Z = 1, although the crystallographic data of **2c** has been reported previously [24]. The crystallographic data of the complexes **1a**–**1c** and **2a**-**2c** are summarized in Table 2.1, while their selected bond parameters are listed in Table 2.2.

The molecular structures of **1a** and **2a** (Figure 2.1 and Figure 2.2, respectively) have a similar core structure, in which each Ln^{III} center is 8-coordinated by three bidentate *S*,*S*-donating Me_2dtc^- ligands with a chelating and bridging bpm ligand in a $\kappa^2N^{1,1'}$:$\kappa^2N^{3,3'}$ bonding mode. The coordination geometry around each Ln^{III} center is similar to those of previously reported 1,10-phenanthroline and 2,2'-bipyridine coordinated mononuclear analogues [17]. The two pyrimidine rings of the bridging bpm ligand are almost planar (mean deviation of each atom from the plane is 0.010(5) Å in **1a**$\cdot 2CHCl_3$ and 0.008(7) Å in **2a**$\cdot 2CHCl_3$) [25]. The Ln^{III} atom is located slightly above the bpm ligand plane by 0.262(9) and 0.272(9) Å in **1a**$\cdot 2CHCl_3$ and **2a**$\cdot 2CHCl_3$, respectively. The pseudo *trans*-positioned Me_2dtc ligand plane is slightly tilted from the bridging bpm plane with the dihedral angles of 14.09(5) and 15.22(5)° in **1a**$\cdot 2CHCl_3$

and **2a**·2CHCl$_3$, respectively. The other set of mutually pseudo *trans*-positioned Me$_2$dtc ligands perpendicular to the bridging bpm plane (Figure 2.1*b*), are co-planar to each other with the dihedral angles of 5.16(5) and 5.90(1)° in **1a**·2CHCl$_3$ and **2a**·2CHCl$_3$, respectively. The intramolecular Ln···Ln distances across the bridging bpm ligand are 6.9744(5) Å in **1a**·2CHCl$_3$ and 6.8602(6) Å in **2a**·2CHCl$_3$.

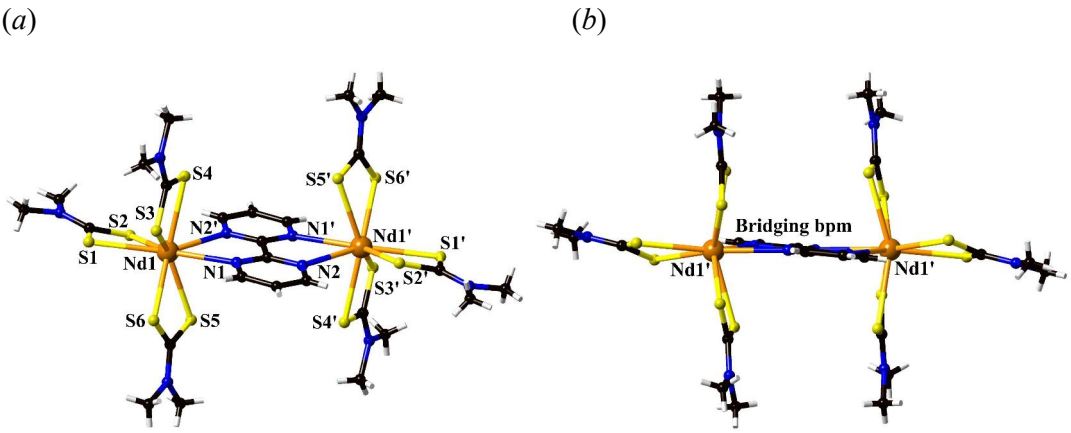

Figure 2.1. (*a*) A perspective view of [{Nd(Me$_2$dtc)$_3$}$_2$(μ-bpm)] (**1a**) with atom-numbering scheme. (*b*) A view of the same complex from a direction parallel to the bridging bpm and the mutually *trans*-positioned Me$_2$dtc ligand planes.

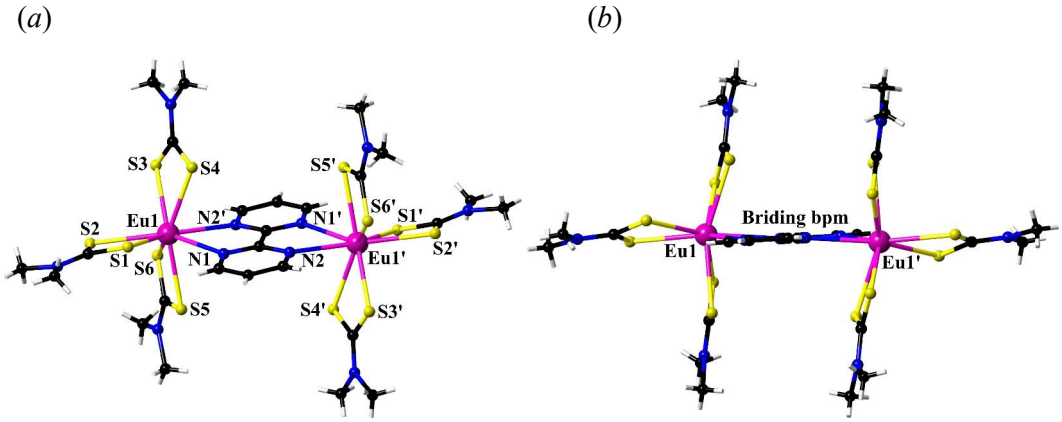

Figure 2.2. (*a*) A perspective view of [{Eu(Me$_2$dtc)$_3$}$_2$(μ-bpm)] (**2a**·2CHCl$_3$) with atom-numbering scheme. (*b*) a view of the same complex from a direction parallel to the bridging bpm and the mutually *trans*-positioned Me$_2$dtc ligand planes.

In the case of pyrdtc complexes, three pseudo-polymorphs with different kinds and/or number of solvent molecules of crystallization were analyzed by the X-ray diffraction method: the Nd^{III} complex with two $CHCl_3$ molecules, **1b**·$2CHCl_3$, and the Eu^{III} complex with four or one CH_2Cl_2 molecule(s), **2b**·$4CH_2Cl_2$ and **2b**·CH_2Cl_2. The molecular structure of bpm-bridged dinuclear Nd^{III} complex in **1b**·$2CHCl_3$ is illustrated in Figure 2.3, and those of the corresponding Eu^{III} complexes in **2b**·$4CH_2Cl_2$ and **2b**·CH_2Cl_2 are in Figure 2.4. The overall structural characteristics of dinuclear [{Eu(pyrdtc)$_3$}$_2$(μ-bpm)] complex in **2b**·$4CH_2Cl_2$ (Figure 2.4*a*) is similar to those of the above-mentioned Me_2dtc complexes in **1a**·$2CHCl_3$ and **2a**·$2CHCl_3$ and the corresponding mononuclear pyrdtc complexes with bpy or phen co-ligand [17]. In **2b**·$4CH_2Cl_2$ the Eu^{III} atom is located on the bridging-bpm ligand plane, the deviation being only 0.059(5) Å. The dihedral angle between the bridging-bpm and its pseudo *trans*-positioned pyrdtc ligand planes is 35.27(8)° in **2b**·$4CH_2Cl_2$, while the mutually *trans*-positioned pyrdtc ligand planes are almost co-planar, the dihedral angle between them being 12.91(1)° (Figure 2.4*b*). In contrast, the Nd^{III} complex, **1b**·$2CHCl_3$ gave a severe structural distortion for one of the coordinated pyrdtc ligands, as shown in Figure 2.3*a*. The dihedral angle between the mutually *trans*-positioned pyrdtc ligand planes is as large as 53.71(7)° (Figure 2.3*b*). In addition, the Nd^{III} atom is deviated by 0.327(9) Å from the bridging-bpm plane. Other structural parameters as well as the coordination geometry around Nd^{III} center is similar to those of the non-distorted Eu^{III} complex in **2b**·$4CH_2Cl_2$; the equatorial-positioned pyrdtc plane is twisted out of the bridging-bpm plane by 34.02(4)° in **1b**·$2CHCl_3$. The characteristic distortion is possibly due either to the intramolecular π–π stacking interaction between the bpm and pyrdtc ligands or to the packing effects from the solvent $CHCl_3$ molecule (Figure 2.3*c*).

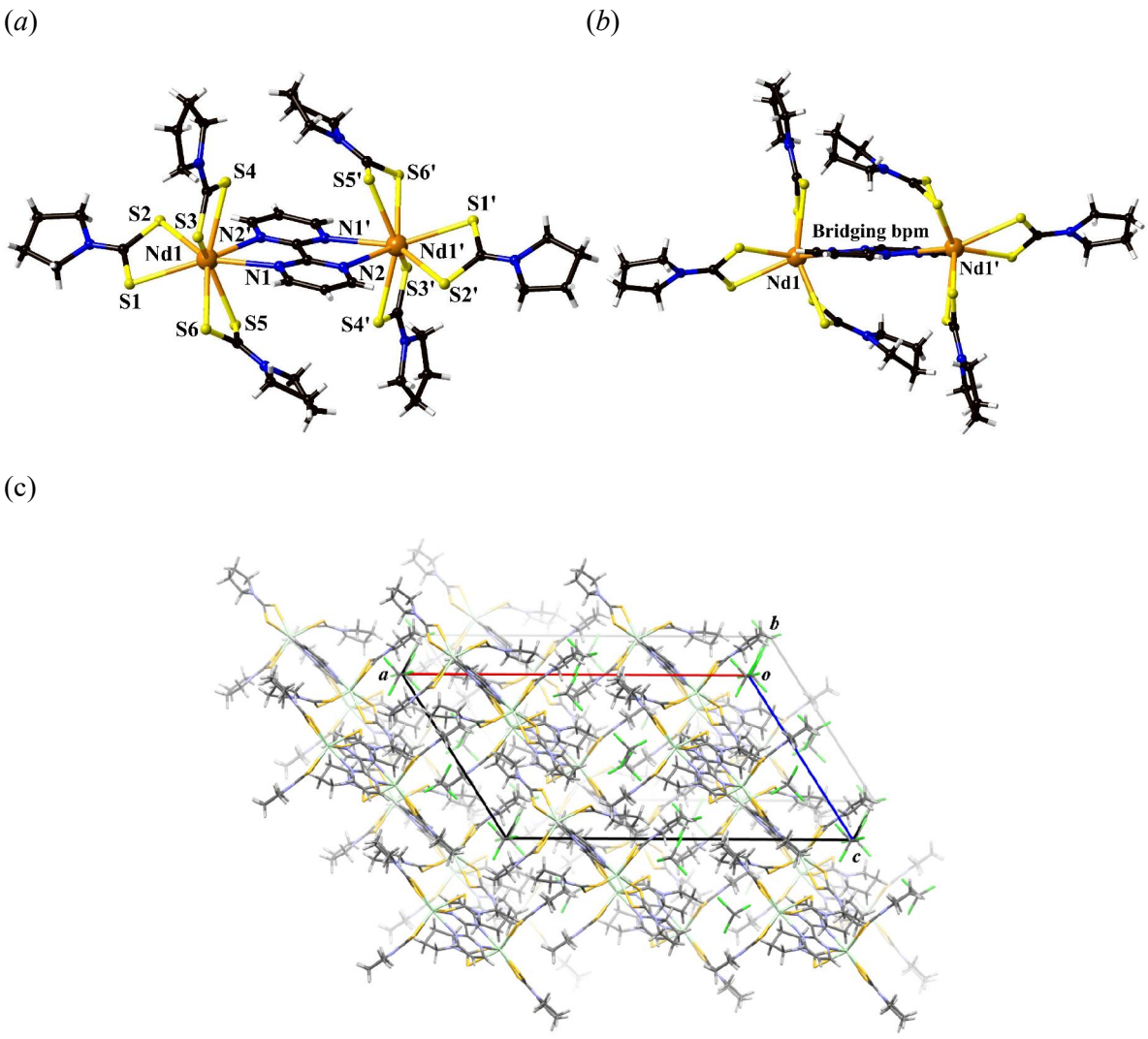

Figure 2.3. (*a*) Molecular structures of [{Nd(pyrdtc)$_3$}$_2$(μ-bpm)] in **1b**·2CHCl$_3$ with atom-numbering scheme. (*b*) A view of the same complex from a direction parallel to the bridging bpm and the mutually *trans*-positioned pyrdtc ligand planes. (*c*) A packing diagram of **1b**·2CHCl$_3$.

Interestingly, the crystal of **2b**·CH_2Cl_2 contains both structural types of dinuclear Eu^{III} complexes (Figure 2.4*c*), although the accuracy of the analysis was not perfect due to its poor crystallinity. In this triclinic crystal (space group $P\bar{1}$ with $Z = 2$) the asymmetric unit consists of two half-molecules of the bpm-bridged dinuclear Eu^{III} complexes and a CH_2Cl_2 molecule of crystallization, and one of the dinuclear complex having Eu1 showed a distorted structural feature similar to that of the above-mentioned Nd^{III} complex in **1b**·2CHCl$_3$, while the other having Eu2 gave a non-distorted structure as in **2b**·4CH_2Cl_2. The intramolecular $Ln^{III}\cdots Ln^{III}$

distances across the bridging bpm ligand is 6.9908(5) Å in **1b**·2$CHCl_3$, 6.8673(4) Å in **2b**·4CH_2Cl_2, and 6.832(1) and 6.848(1) Å in **2b**·CH_2Cl_2. The average Ln^{III}–S bond lengths in **1a**–**2b**, 2.831(4)–2.869(4) Å, are in good agreement with the corresponding values reported for the mononuclear analogues with phen or bpy co-ligand. On the other hand, the average Ln^{III}–N bond lengths in **1a**–**2b**, 2.620(6)–2.672(6) are longer than those in the mononuclear phen complexes [17]. This difference in the Ln^{III}–N(bpm) and Ln^{III}–N(phen) bond lengths may be related to the less pronounced basic character of bpm [1,4].

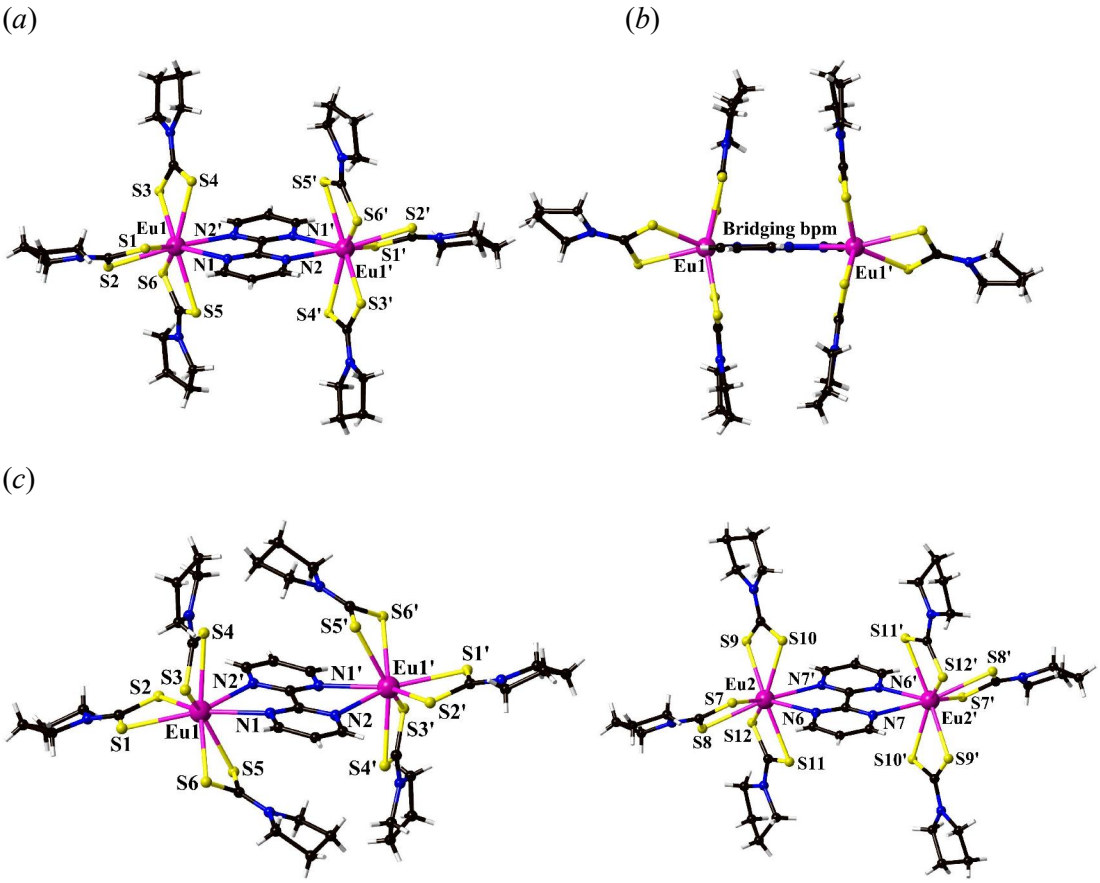

Figure 2.4. (*a*) A perspective view of [{Eu(pyrdtc)$_3$}$_2$(μ-bpm)] in **2b**·4CH_2Cl_2. (*b*) a view of the same complex from a direction parallel to the bridging bpm and the mutually *trans*-positioned pyrdtc ligand planes. (*c*) A perspective view of two crystallographically independent complex molecules in **2b**·CH_2Cl_2.

As a structural comparison, the crystal structure of the analogous acac complex **1c** is illustrated in Figure 2.5, while that of **2c** was previously reported [24] and presented in Figure 2.6. Each Nd^{III} center has a similar coordination geometry to that of the Me_2dtc complex, **1a**, described above. A characteristic difference between **1a** and **1c** was found in the coordination geometry around the Nd^{III} center; in contrast to the structure shown in Figure 2.1*b*, the bridging bpm and the pseudo *trans*-positioned acac ligand planes of complex **1c** are almost co-planar as depicted in Figure 2.5*b*. The dihedral angle between these ligand planes is only 5.24(4)°. The intramolecular Nd···Nd distance across the bridging bpm ligand of 7.0702(5) Å in **1c** is slightly longer than the corresponding values in **1a** and **1b**. The Ln–N length of 2.704(3) Å in **1c** is in good agreement with those of **1a** and **1b**. The structural characteristics of **1c** are very similar to those of **2c**.

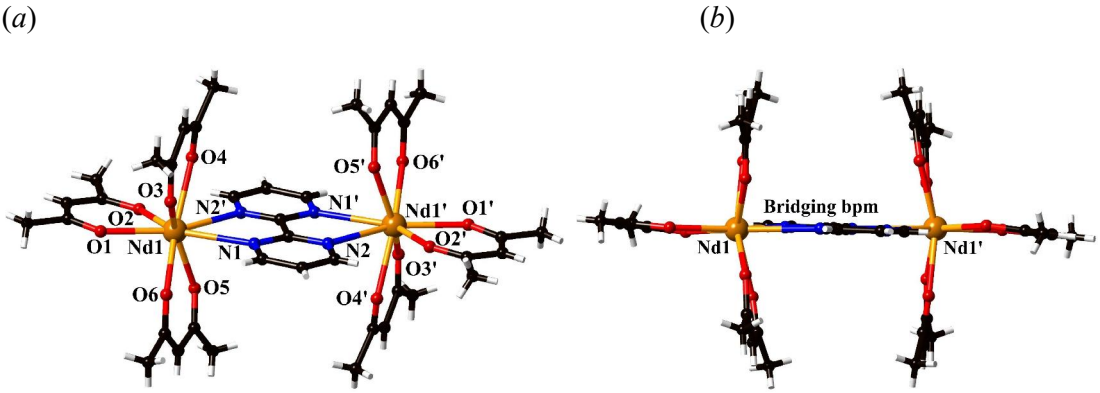

Figure 2.5. (*a*) A perspective view of [{Nd(acac)$_3$}$_2$(μ-bpm)] (**1c**) and (*b*) a view of the same complex from a direction parallel to the bridging bpm and the mutually *trans*-positioned acac ligand planes.

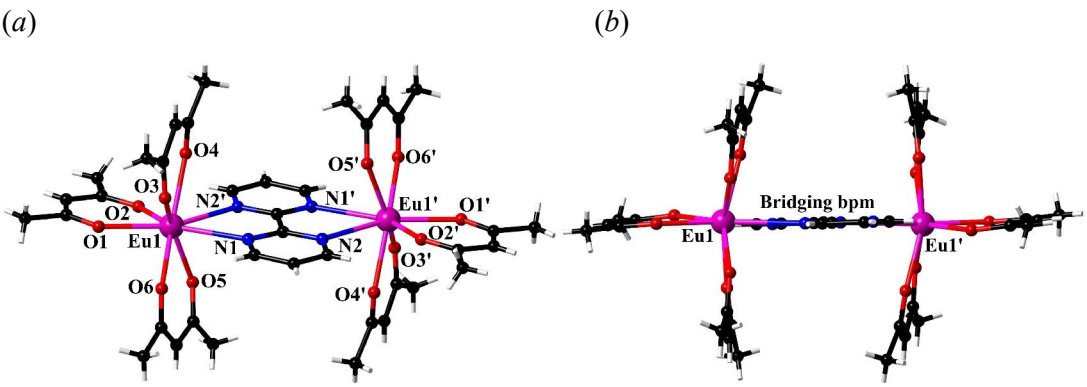

Figure 2.6. (*a*) A perspective view of [{Eu(acac)$_3$}$_2$(μ-bpm)] (**2c**) and (*b*) a view of the same complex from a direction parallel to the bridging bpm and the mutually *trans*-positioned acac ligand planes.

Spectroscopic studies

FT-IR Spectral Study

The infrared spectra of the complexes in the regions of 1450–1550 and 950–1050 cm^{-1} are of interest, because the *ν*(C–N) and *ν*(C–S) stretching bands are appeared in these regions [26,27]. The [{Nd(Me$_2$dtc)$_3$}$_2$(μ-bpm)] (**1a**) and [{Eu(Me$_2$dtc)$_3$}$_2$(μ-bpm)] (**2a**) complexes (Figure 2.7) exhibited the *ν*(C–N) band between 1374–1418 cm^{-1}, while [{Nd(pyrdtc)$_3$}$_2$(μ-bpm)] (**1b**) and [[{Eu(pyrdtc)$_3$}$_2$(μ-bpm)] (**2b**) complexes (Figure 2.8) showed the band around 1436 cm^{-1}. The *ν*(C–S) bands of the complexes above were observed in the range of 948–984 cm^{-1}. These band positions of the dinuclear complexes are consistent with those reported for the related mononuclear analogues [17].

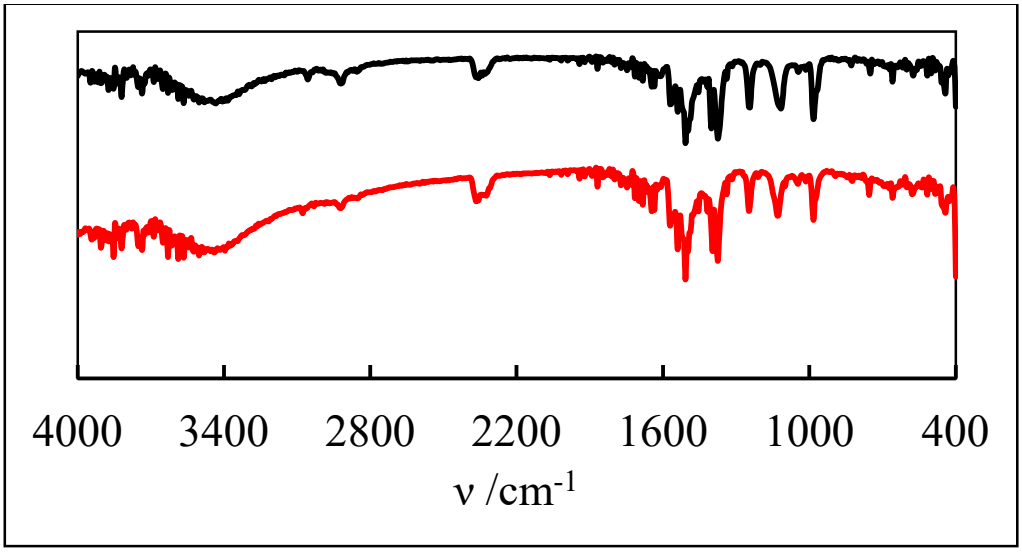

Figure 2.7. IR spectra of [{Nd(Me_2dtc)$_3$}$_2$(μ-bpm)] (black) and [{Eu(Me_2dtc)$_3$}$_2$(μ-bpm)] (red).

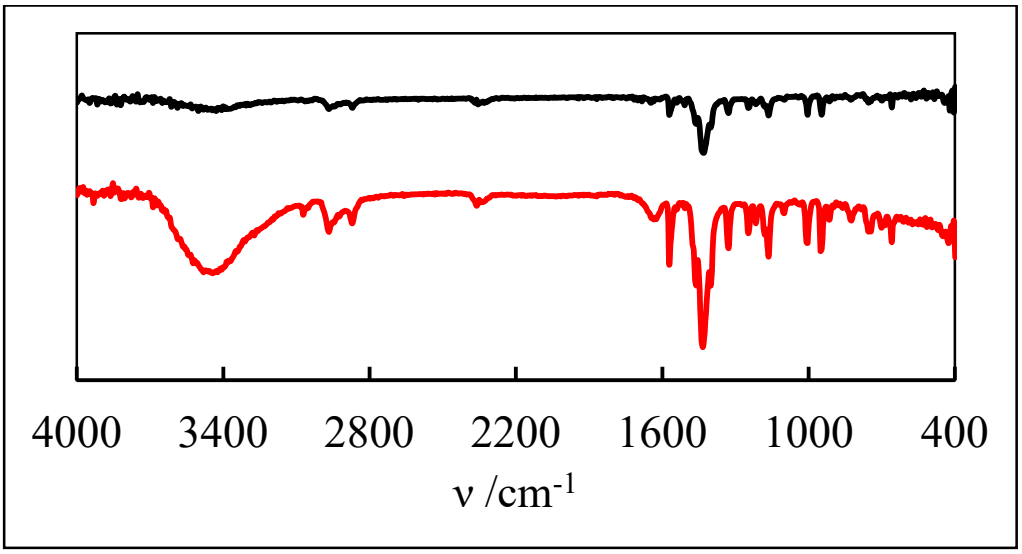

Figure 2.8. IR spectra of [{Nd(pyrdtc)$_3$}$_2$(μ-bpm) (black) and [{Eu(pyrdtc)$_3$}$_2$(μ-bpm) (red).

Absorption and magnetic circular dichroism (MCD) studies

Absorption and MCD spectra associated with f–f transitions were measured in dichloromethane at room temperature. As seen in the previous study on the mononuclear phen and bpy complexes [17], the structural deformation found in the crystal structure would be defused in solution due to the flexible coordination bonds around Ln^{III} center. For instance, two dichloromethane solutions dissolving crystals of **2b**•$4CH_2Cl_2$ and **2b**•CH_2Cl_2 showed the identical spectra. Thus, this discussion is on the spectroscopic properties of the bpm-bridged dithiocarbamato complexes with the ideal C_{2v} local symmetry at each Ln^{III} center. In Figures 2.9 and 2.10, the absorption and MCD spectra of Nd^{III}_2 and Eu^{III}_2 dithiocarbamato series of complexes are presented, respectively.

As shown in Figure 2.9*a* (top), the absorption spectrum of [{Nd(Me_2dtc)$_3$}$_2$(μ-bpm)] (**1a**) gives four sharp but weak f–f bands with their maxima at 12340, 13240, (16790, 16890) and 18762 cm^{-1}, assignable to the transition from the ground state $^4I_{9/2}$ to the excited states

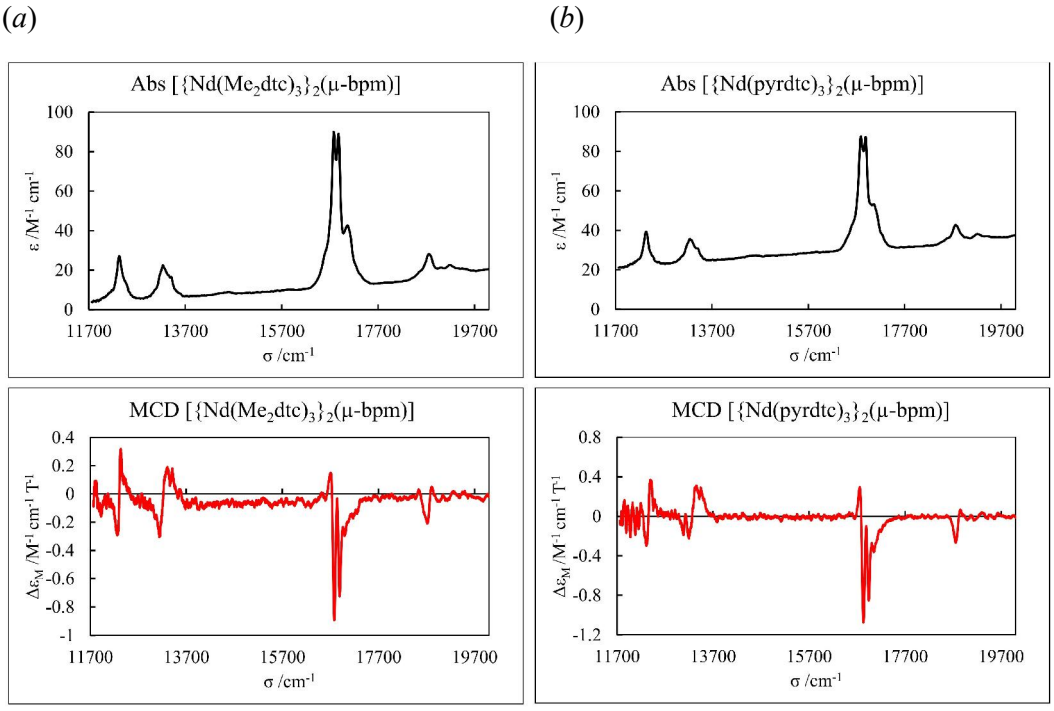

Figure 2.9. Absorption (top) and MCD (bottom) spectra of (*a*) [{Nd(Me_2dtc)$_3$}$_2$(μ-bpm)] and (*b*) [{Nd(pyrdtc)$_3$}$_2$(μ-bpm)] complexes.

$^4F_{5/2}$, $^4S_{3/2}$, ($^4G_{5/2}$, $^2G_{7/2}$) and $^4G_{7/2}$, respectively. The intense band arising from the $^4I_{9/2} \rightarrow$ ($^4G_{5/2}$, $^2G_{7/2}$) hypersensitive transition showed a weak splitting to 16790 and 16890 cm^{-1} with a pronged peak at 17090 cm^{-1}. In Figure 2.9*a* (bottom), the MCD signals at 12300, 13210, (16770, 16890) and 18710 cm^{-1} correspond to the above-mentioned absorption bands. The MCD signals are dominated by room temperature *C*-terms except for that at 12340 cm^{-1} which appeared as a positive *A*-term. The characteristic $^4I_{9/2} \rightarrow$ ($^4G_{5/2}$, $^2G_{7/2}$) hypersensitive transition splits into a closely spaced *C*-terms at 16780 and 16890 cm^{-1}. Similar spectral features were observed for the [{Nd(pyrdtc)$_3$}$_2$(μ-bpm)] (**1b**) complex (Figure 2.9*b*).

In Figure 2.10*a* (top) the absorption spectrum of [{Eu(Me$_2$dtc)$_3$}$_2$(μ-bpm)] (**2a**) was shown to exhibit a characteristic weak f–f bands at 21450 cm^{-1} assignable to the transition from the ground state $^7F_0$ to the excited state $^5D_2$. In the corresponding MCD spectrum (bottom), a characteristic negative *B*-term MCD signal is observed at 21450 cm^{-1}. Similar spectral features were observed for [{Eu(pyrdtc)$_3$}$_2$(μ-bpm)] (**2b**) (Figure 2.10*b*).

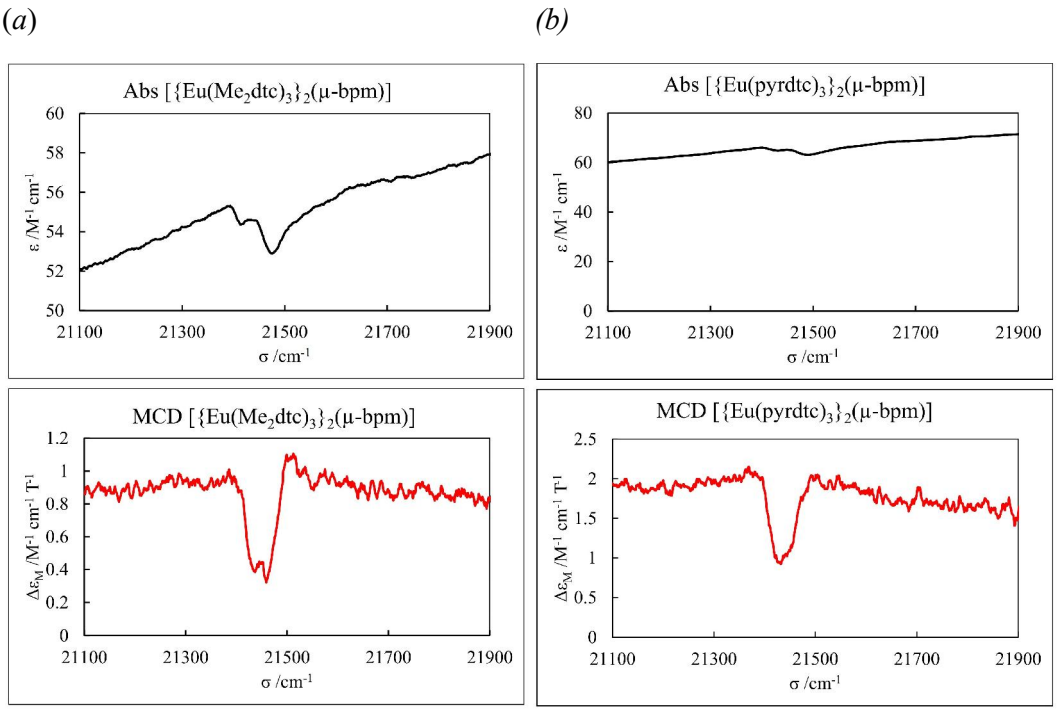

Figure 2.10. Absorption (top) and MCD (bottom) spectra of (*a*) [{Eu(Me$_2$dtc)$_3$}$_2$(μ-bpm)] and (*b*) [{Eu(pyrdtc)$_3$}$_2$(μ-bpm)] complexes.

Spectral comparisons

Comparison of the absorption and MCD spectra of the bpm-bridged dinuclear complexes (Figures 2.9 and 2.10) to those of the mononuclear phen or bpy analogues [17] revealed very similar spectral features. This suggests that there is no significant $Ln^{III}\cdots Ln^{III}$ electronic interaction in the dinuclear complexes, which may induce a different electronic structure or spectroscopic symmetry around the central Ln^{III} ion. For another spectral comparison, the *β*-diketonato analogues of [{Ln(acac)$_3$}$_2$(μ-bpm)] (Ln = Nd^{III} **1c** or Eu^{III} **2c**, $acac^-$ = 2,4-pentanedionate) were prepared and their absorption and MCD spectra were measured. The absorption and MCD spectra of **1c** are presented in Figure 2.11, where a shape absorption band associated with the hypersensitive transition $^4I_{9/2} \rightarrow (^4G_{5/2}, {}^2G_{7/2})$ at 17210 cm^{-1} is distinctively different from that of the dithiocarbamato complexes **1a** and **1b** (Figure 2.9). The room temperature *C*-terms in the MCD spectrum associated with the $^4I_{9/2} \rightarrow (^4G_{5/2}, {}^2G_{7/2})$ transition at (17150, 17450 cm^{-1}) are more clearly resolved in **1c** than in complexes **1a** and **1b** (Figure 2.9).

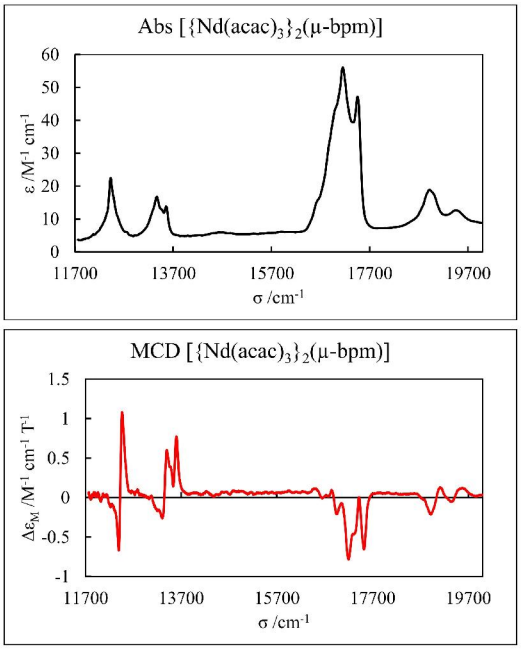

Figure 2.11. Absorption (top) and MCD (bottom) spectra of [Nd_2(acac)$_6$(μ-bpm)] (**1c**).

The Eu^{III} complex, [{Eu(acac)$_3$}$_2$(μ-bpm)] (**2c**), on the other hand, exhibited a relatively intense absorption band and a negative *A*-term MCD signal at 21490 cm^{-1} assigned to the $^7F_0 \rightarrow {}^5D_2$ transition (Figure 2.12). This feature is a remarkable contrast to the dithiocarbamato complexes of **2a** and **2b**, which exhibited a very weak absorption band and a negative *B*-term MCD signals at 21450 cm^{-1} (Figure 2.10). A similar difference in the spectral features were observed in the previously reported mononuclear complexes [17], where it was concluded that the electronic structure of Ln^{III} complexes in solution may be largely related to the coordination environment of the central Ln^{III} ion. That is, also in the bpm-bridged dinuclear complexes, it is deduced that the dithiocarbamato and acetylacetonato complexes possess a C_{2v} and D_{2d} local symmetry, respectively [17].

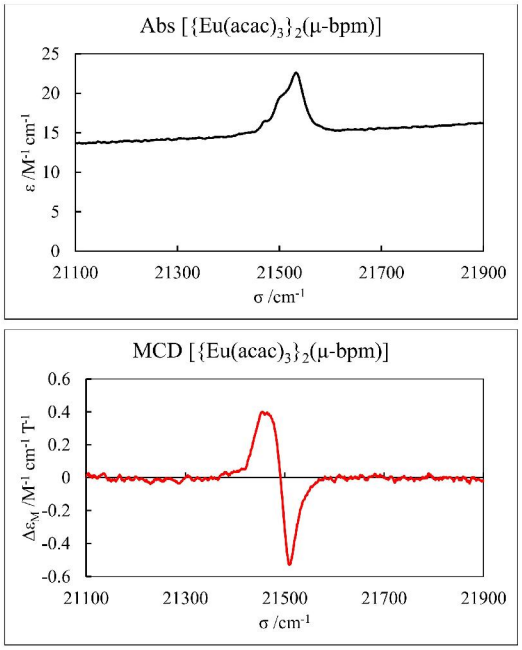

Figure 2.12. Absorption (top) and MCD (bottom) spectra of [{Eu(acac)$_3$}$_2$(μ-bpm)] (**2c**).

2.4 Conclusion

In this study, four new novel 2,2'-bipyrimidine (bpm)-bridged homodinuclear Ln^{III}_2 complexes bearing dithiocarbamato co-ligands have been prepared and their crystal structures have been analyzed. In the dinuclear complexes each Ln^{III} ion is 8-coordinated and situated in a distorted square antiprismatic geometry. In contrast to the corresponding mononuclear complexes with phen or bpy co-ligand, a severe distortion of one of the pyrdtc coordination structures was observed in some pseudo-polymorphs. The MCD spectral properties of the complexes were also investigated which revealed a distinctly different spectral features of the dithiocarbamato complexes from their corresponding β-diketonato analogues, owing to the effect of the coordination environment on the electronic structure and spectroscopic symmetry around the central Ln^{III} ions in solution.

Table 2.1. Crystallographic data of dinuclear Ln^{III}_2 complexes.

Parameter	**1a**·2$CHCl_3$	**1b**·2$CHCl_3$	**1c**	**2a**·2$CHCl_3$	**2b**·4CH_2Cl_2
Molecular formula	$C_{28}H_{44}Cl_6N_{10}Nd_2S_{12}$	$C_{40}H_{56}N_{10}Cl_6Nd_2S_{12}$	$C_{38}H_{48}N_4Nd_2O_{12}$	$C_{28}H_{44}Cl_6N_{10}Eu_2S_{12}$	$C_{42}H_{60}N_{10}Cl_8Eu_2S_{12}$
Molecular weight	1406.64	1562.87	1041.30	1422.08	1677.27
Temperature (K)	188	188	188	188	188
Crystal system	Monoclinic	Monoclinic	Triclinic	Monoclinic	Monoclinic
Space group, Z	$P2_1/n$, 2	$C2/c$, 4	$P\bar{1}$, 1	$P2_1/n$, 2	$C2/c$, 4
a (Å)	16.0903(8)	27.2998(11)	9.3304(3)	16.0722(14)	24.4037(14)
b (Å)	11.1735(6)	18.0517(7)	10.1142(9)	11.0919(10)	17.9989(10)
c (Å)	16.6342(6)	15.3180(8)	12.4276(4)	16.6771(14)	15.0300(9)
α (°)	90	90	108.662(5)	90	90
β (°)	116.4757(15)	121.8007(14)	95.9487(17)	116.559(3)	94.5797(19)
γ (°)	90	90	95.150(5)	90	90
V (Å^3)	2677.0(2)	6415.7(5)	1095.69(11)	2659.3(4)	6580.7(7)
D_{calcd} (g cm^{-3})	1.745	1.618	1.578	1.776	1.693
μ(Mo Kα) (cm^{-1})	27.177	22.770	24.022	31.378	26.287
F(000)	1392	3120	520	1404	3344
R_{int}	0.0715	0.0487	0.0440	0.1034	0.0463
$R1$ [$I > 2\sigma(I)$]	0.0458	0.0434	0.0256	0.0516	0.0291
$wR2$ [all data]	0.1275	0.1415	0.0894	0.1023	0.0714
GOF on F^2	1.066	1.058	1.237	1.055	1.048

Table 2.1. (Continued)

Parameter	**2b**·CH_2Cl_2	**2c**
Molecular formula	$C_{39}H_{56}N_{10}Cl_2Eu_2S_{12}$	$C_{38}H_{48}N_4Eu_2O_{12}$
Molecular weight	1424.47	1056.74
Temperature (K)	188	188
Crystal system	Triclinic	Triclinic
Space group, Z	$P\bar{1}$, 2	*P*-1, 1
a (Å)	10.7040(19)	9.2886(13)
b (Å)	15.200(3)	10.0402(15)
c (Å)	17.936(3)	12.4853(15)
α (°)	80.020(5)	108.251(4)
β (°)	73.696(5)	96.325(4)
γ (°)	75.939(5)	95.943(4)
V (Å^3)	2699.5(9)	1087.2(3)
D_{calcd} (g cm^{-3})	1.752	1.614
μ(Mo Kα) (cm^{-1})	29.06	29.125
F(000)	1424	526
R_{int}	0.1136	0.0581
*R*1 [$I > 2\sigma(I)$]	0.0754	0.0244
*wR*2 [all data]	0.2370	0.0662
GOF on F^2	1.161	0.872

Table 2.2. Selected Bond lengths and angles of Ln^{III}_2 complexes.

Parameter	**1a**	**1b**	**2a**	**2b**	**1c**	**2c**
Bond Lengths (Å)					Bond Lengths (Å)	
Ln1─S1 (O1)	2.8790(17)	2.9091(12)	2.8161(17)	2.8642(11)	Ln1─O1	2.389(3)	2.350(3)
Ln1─S2	2.8574(14)	2.8873(16)	2.8496(17)	2.8311(9)	Ln1─O2	2.416(3)	2.349(2)
Ln1─S3	2.8830(19)	2.9131(11)	2.812(2)	2.8706(8)	Ln1─O3	2.383(3)	2.3576(18)
Ln1─S4	2.8593(18)	2.8626(13)	2.8447(14)	2.8458(9)	Ln1─O4	2.395(3)	2.342(2)
Ln1─S5	2.8860(14)	2.883(3)	2.8269(15)	2.8701(8)	Ln1─O5	2.371(3)	2.376(2)
Ln1─S6	2.849(2)	2.915(2)	2.8380(19)	2.8474(8)	Ln1─O6	2.402(2)	2.359(3)
Ln1─N1	2.658(4)	2.682(4)	2.604(4)	2.613(2)	Ln1─N	2.697(2)	2.6456(19)
Ln1─N2[1]	2.686(5)	2.687(5)	2.635(5)	2.627(2)	Ln1─N2[1]	2.710(2)	2.663(2)
Ln···Ln	6.9744(5)	6.9908(5)	6.8602(6)	2.8671(5)	Ln···Ln	7.072(5)	6.9474(8)
Bond angles (°)					Bond angles (°)		
S1─Ln1─S2	62.13(5)	62.33(4)	63.16(5)	63.13(3)	O1─Ln1─O2	70.65(10)	72.49(8)
S3─Ln1─S4	62.52(5)	62.53(4)	62.17(6)	62.60(2)	O3─Ln1─O4	71.90(9)	72.36(7)
S5─Ln1─S6	61.35(6)	61.11(5)	62.82(5)	62.14(2)	O5─Ln1─O6	71.57(9)	71.52(8)
N1─Eu1─N2[1]	61.00(11)	61.02(13)	62.55(13)	62.29(7)	N1─Ln1─N2[1]	59.87(8)	61.18(6)
Average					Average		
Bond length (Å)	2.8690(37)				*Bond length (Å)*		
Ln─S	2.672(6)	2.8950(27)	2.8312(37)	2.8549(22)	Ln─O	2.393(7)	2.356(19)
Ln─N		2.685(6)	2.620(6)	2.62(3)	Ln─N	2.704(3)	2.654(19)
Bond angles (°)	62.00(9)				*Bond angles (°)*		
S─Ln─S		61.99(8)	62.72(9)	62.62(4)	O─Ln─O	71.37(16)	72.12(13)
Dihedral angle (°)	14.09(5)				Dihedral angle (°)		
pl(bpm)[a] vs pl(dtc 1)[b]	5.16(5)	34.02(4)	15.22(5)	35.27(8)	pl(bpm)[a] vs pl(acac 1)[d]	5.24(4)	5.64(1)
pl(dtc 2)[c] vs pl(dtc 3)[c]		53.71(7)	5.90(1)	12.91(1)	pl(acac 2)[e] vs pl(acac 3)[e]	9.93(6)	9.81(1)

[a] pl(bpm) was defined by all non-H atoms of bpm. [b] pl(dtc 1) was defined by S_2CN atoms of the pseudo *trans*-positioned dtc ligand to the bpm ligand. [c] pl(dtc 2) and pl(dtc 3) were defined by the S_2CN atoms, respectively, of the pseudo *cis*-positioned dtc ligands to the bpm ligand. [d] pl(acac 1) was defined by O_2C_3 atoms of the pseudo *trans*-positioned acac ligand to the bpm ligand. [e] pl(acac 2) and pl(acac 3) were defined by the O_2C_3 atoms, respectively, of the pseudo *cis*-positioned acac ligands to the bpm ligand.

Reference

1. G. Zucchi, O. Maury, P. Thuery, M. Ephritikhine, *Inorg. Chem.,* 47 (2008) 10398.
2. S. Swavey, R. Swavey, *Coord. Chem. Rev.,* 253 (2009) 2627.
3. A. Fratini, G. Richards, E. Larder, S. Swavey, *Inorg. Chem.,* 47 (2008) 1030.
4. G. Zucchi, *Internat. J. Inorg. Chem.*, (2011) 1.
5. N. M. Shavaleev, G. Accorsi, D. Virgili, Z. R. Bell, T. Lazarides, G. Calogero, N. Armaroli, M. D. Ward, *Inorg. Chem.,* 44 (2005) 61.
6. M. D. Ward, T. Lazarides, H. Adams, D. Sykes, S. Faulkner, G. Calogero, *Dalton Trans.,* (2008) 691.
7. D. D'Cunha, D. Collins, G. Richards, S. Gilford G. S. Vincent, S. Swavey, *Inorg. Chem. Comm.,* 9 (2006) 979.
8. W. Yu, F. Schramm, E. M. Pineda, Y. Lan, O. Fuhr, J. Chen, H. Isshiki, W. Wernsdorfer, W. Wulfhekel, M. Ruben,. *Beilstein J. Nanotechnol.,* 7 (2016) 126.
9. W. -B. Sun, B. Yan, L. -H. Jia, B. -W. Wang, Q. Yang, X. Cheng, H. -F. Li, P. Chen, Z. -M. Wang, S. Gao, *Dalton Trans.,* 45 (2016) 8790.
10. R. Ilmi, K. Iftikhar, *Inorg. Chem. Comm., 13* (2010) 1552.
11. W.M. Faustino, O.L. Malta, E.E.S. Teotonio, H.F. Brito, A.M. Simas, G.F. de Sá, *J. Phys*. *Chem*., A110 (2006) 2510.
12. P. Pitchaimani, K.M. Lo, K.P. Elango, *Polyhedron*, 93 (2015) 8.
13. M.D. Regulacio, N. Tomson, S.L. Stoll, *Chem*. *Mater*., 17 (2005) 3114.
14. J. A. Vale, W. M. Faustino, P. H. Menezes, G. F. de Sá, *J. Braz. Chem. Soc.,* 17 (2006) 829.
15. P. Pitchaimani, K.M. Lo, K.P. Elango, *Polyhedron*, 54 (2013) 60.
16. V. Kubat, G. Demo, L. Jeremias, J. Novosad, *Z. Kristallogr.,* 228 (2013) 369.
17. A. Yakubu, T. Suzuki, M. Kita, *Inorg. Chim. Acta*, 484 (2019) 394.

18. Rigaku Co. Ltd., Process−Auto, Automatic Data Acquisition and Processing Package for Imaging Plate Diffractometer, Akishima, Tokyo, 1998.
19. C.M. Burla, R. Caliandro, M. Camalli, B. Carrozzini, L.G. Cascarano, L. De Caro, C. Giacovazzo, G. Polidori, D. Siliqi, R. Spagna, SIR2008. *J. Appl. Cryst.*, 40 (2007) 609.
20. M.G. Sheldrick, SHELXT Version 2014/5, *Acta Cryst.,* A70 (2014) C1437.
21. Rigaku Co. Ltd., CrystalStructure, Akishima, Tokyo, 2000−2014.
22. M.G. Sheldrick, SHELXL Version 2014/7, *Acta Cryst.,* A64 (2008) 112.
23. A. Yakubu, T. Suzuki, M. Kita. *J. Chem*. *Educ*., 94 (2017) 1357.
24. G. Zucchi, T. Jeon, D. Tondelier, D. Aldakov, P. Thuery, M. Ephritikhine, B. Geffroy, *J. Mater. Chem.,* 20 (2010) 2114.
25. A. Fratini, G. Richards, E. Larder, S. Swavey, *Inorg. Chem. Comm., 12* (2009) 509.
26. D. A. Brown, W. K. Glass, M. A. Burke. *Spectrochim. Acta,* 32A, (1976) 137.
27. I. Raya, I. Baba, B. M. Yamin. *Malaysia Journal of Analytical Sciences,* 10 (2006) 93.

Chapter 3

Syntheses, structures and spectroscopic properties of homodinuclear lanthanoid(III) dithiocarbamato complexes bridged by (*E*)-*N*-benzylidenepicolinohydrazonate

Abstract

(*E*)-*N*-Benzylidenepicolinohydrazide (Hbphz) was used to synthesize a series of hydrazonato-bridged homodinuclear Ln^{III}_2 dithiocarbamato (*RR′*dtc$^-$) complexes of the form [{Ln(*RR′* dtc)$_2$}$_2$(μ-bphz)$_2$] {Ln = La, Pr, Nd, Sm or Eu; *RR′* = dimethyl- (Me_2) or pyrrolidine-(pyr)}. X-ray crystallographic studies revealed that these complexes possessed a common head-to-tail type dinuclear structural motif in which two hydrazonato ligands bridged two Ln^{III} centers in the μ-1κ^2*N*(py),*O*:2κ^2*O*,*N*(imine) mode and two *RR′*dtc ligands are coordinated to each Ln^{III} center. Interestingly, while the Sm^{III} and Eu^{III} complexes crystallized as simple 8:8-coordinate dinuclear molecules, the lighter Ln^{III} (i.e. La^{III}, Pr^{III} and Nd^{III}) complexes afforded in some cases 9:9-coordinate molecules, where the ninth coordination site was occupied by a solvent ethanol or methanol molecule. Even for the lighter Ln^{III} complexes, the complexes were solved in dichloromethane or chloroform as the 8:8-coordinate dimer, as revealed by ^{1}H NMR spectroscopy. In the UV-visible absorption and magnetic circular dichroism (MCD) spectra of the complexes, similar spectral patterns for ligand-centered and Laporte forbidden f–f transitions were observed. The MCD spectral studies demonstrated the characteristic magneto-optical behavior of the complexes.

3.1 Introduction

The coordination chemistry of hydrazones is an active research area in view of their general interests and application of hydrazone complexes [1,2]. Hydrazones can coordinate to a metal center either as neutral molecules or deprotonated anionic forms; therefore, the hydrazone complexes often exhibit interesting reversible properties dependent on the solvent acidity [3,4]. In addition, the exploitation of possible ligating substitutional groups affords a variety of coordination modes of the hydrazones which would give the complexes with interesting structural diversity, magnetic and spectroscopic properties [5].

Lanthanoid complexes of hydrazones are being investigated for potential applications in various fields including supramolecular assemblies and magnetic materials. Chandrasekhar et al. have prepared a series of hydrazone-based homodinuclear lanthanoid complexes and revealed the presence of weak antiferromagnetic coupling between the Ln^{III} centers at low temperature [6]. Thompson and co-authors have investigated the coordination chemistry of tritopic pyridinebis(hydrazone) with some Ln^{III} ions [**7**]. Klouras, Perlepes and their collaborators characterized dinuclear 2-acetylpyridine-substituted hydrazone complexes with four bridging acetate groups [8]. The structural characterizations and magnetic properties of other hydrazone-based dinuclear Dy^{III}_2 [9] and tetranuclear Ln^{III}_4 [10] complexes have also been reported. In addition, several mixed-ligand lanthanoid complexes bearing hydrazones (or the deprotonated hydrazonates) and β-diketonates (or other oxygen-donor ligands) have been reported; however, those of the analogous mixed-ligand complexes with dithiocarbamates have not yet been investigated. Lanthanoid dithiocarbamato compounds have important practical applications in catalysis, nanotechnology and microelectronics, and, therefore, their structural, thermodynamical and spectroscopic properties have been studied in detail [11, 12]. So far, most of the mixed-ligand dithiocarbamato lanthanoid complexes studied involve 1,10-phenanthroline or 2,2'-bipyridine as an ancillary ligand.

In this study, a hydrazone derived from picolinohydrazide and benzaldehyde, (*E*)-*N*-benzylidenepicolinohydrazide (Hbphz) was synthesized and used to prepare a series of lanthanoid dithiocarbamato complexes (Scheme 3.1). The structural features and spectroscopic properties of these hydrazonato-bridged homodinuclear lanthanoid dithiocarbamato complexes were investigated.

3.2 Experimental section

Synthesis of (*E*)-*N*-benzylidenepicolinohydrazide (Hbphz)

The Hbphz was prepared by a condensation reaction (Scheme 3.1) between a hydrazide and an aldehyde. 2-Pyridinecarboxylic acid hydrazide (= picolinohydrazide) (343 mg, 2.5 mmol) was dissolved in ethanol (20 mL) and benzaldehyde (265 mg, 2.5 mmol) was added. The mixture was stirred for 3 h at room temperature and, then, allowed to stand overnight. A slight shaking of the mixture triggered precipitation of the product. Analytically pure white fluffy product was isolated in 73% yield. Slow evaporation of a methanolic solution of the product yielded colorless needle-shaped crystals suitable for X-ray diffraction analysis. Anal. Found: C, 69.23; H, 4.67; N, 18.55%. Calcd. for $C_{13}H_{11}N_3O$: C, 69.32; H, 4.92; N, 18.66%. IR (KBr disc)/cm^{-1}: ν(N–H), 3212; ν(C=O), 1664; ν(C=N), 1522; ν(N–N), 1141. ^{1}H NMR (300 MHz, Chloroform-*d*, 22 °C): δ 10.99 (s, 1H), 8.58 (ddd, *J* = 4.8, 1.8, 0.9 Hz, 1H), 8.42–8.16 (m, 2H), 8.02–7.64 (m, 3H), 7.60–7.31 (m, 4H).

Synthesis of complexes

All complexes described in this study were similarly prepared by a method described below (Scheme 3.2). To a mixture of Hbphz (1.00 mmol) and Et_3N (1.00 mmol) in MeOH (10 mL) was added a methanolic solution (10 mL) of $LnX_3•6H_2O$ (Ln = La, Pr, Nd, Sm or Eu; X^- = Cl^- or NO_3^-) (1.00 mmol) with stirring. Na(Me_2dtc) or NH_4(pyrdtc) (2.00 mmol) in MeOH (10 mL) was added. The mixture was stirred for 5 h at room temperature and the resulting precipitate was collected by filtration, washed with MeOH and dried in air. The crude product was purified by recrystallization from a dichloromethane or chloroform solution by layering of ethanol, methanol or diethyl ether. The analytical and FT-IR spectral data are given below.

[{La(Me$_2$dtc)$_2$}$_2$(μ-bphz)$_2$] (1a)

Pale green crystals were obtained from a mixture of CH_2Cl_2 and EtOH in 18% yield. Anal. Found: C, 36.29; H, 3.77; N, 11.21; S, 19.30%. Calcd. for $C_{38}H_{44}N_{10}O_2La_2S_8$•$2CH_3OH$•$2H_2O$: C, 36.75; H, 4.32; N, 10.71; S, 19.62%. IR (KBr disc)/cm^{-1}: ν(C=N),1540; ν(N–N), 1161; ν(C–N), 1349; ν(C–S) 982.

[{La(pyrdtc)$_2$}$_2$(μ-bphz)$_2$] (1b)

Pale green crystals were obtained from a mixture of $CHCl_3$ and EtOH in 21% yield. Anal. Found: C, 40.55; H, 3.99; N, 10.37; S, 18.65%. Calcd for $C_{46}H_{52}N_{10}O_2La_2S_8$•$CH_3OH$•$2H_2O$: C, 40.92; H, 4.38; N, 10.15; S, 18.60%. IR (KBr disc)/cm^{-1}: ν(C=N), 1539; ν(N–N), 1163; ν(C–N), 1430; ν(C–S) 1005.

[{Pr(Me$_2$dtc)$_2$}$_2$(μ-bphz)$_2$] (2a)

Green crystals were obtained from a mixture of CH_2Cl_2 and EtOH in 19% yield. Anal. Found: C, 37.23; H, 3.50; N, 11.41; S, 19.85%. Calcd. for $C_{38}H_{44}N_{10}O_2Pr_2S_8$•$0.5CH_2Cl_2$: C, 36.89; H, 3.62; N, 11.17; S, 20.46%. IR (KBr disc)/cm^{-1}: ν(C=N), 1540; ν(N–N), 1158; ν(C–N), 1347; ν(C–S) 979.

[{Pr(pyrdtc)$_2$}$_2$(μ-bphz)$_2$] (2b)

Green crystals were obtained from CH_2Cl_2 and EtOH in 21% yield. Anal. Found: C, 41.49; H, 4.25; N, 9.86; S, 18.90%. Calcd. for $C_{46}H_{52}N_{10}O_2Pr_2S_8$•$2H_2O$: C, 40.88; H, 4.18; N, 10.37; S, 18.98%. IR (KBr disc)/cm^{-1}: ν(C=N), 1540; ν(N–N), 1163; ν(C–N), 1430; ν(C–S) 1006.

[{Nd(Me$_2$dtc)$_2$}$_2$(μ-bphz)$_2$] (3a)

Pale green crystals were obtained from $CHCl_3$ and MeOH mixture in 42% yield. Anal. Found: C, 36.82; H, 3.70; N, 11.16; S, 18.87%. Calcd. for $C_{38}H_{44}N_{10}O_2Nd_2S_8$•2$CH_3OH$•0.5$CHCl_3$: C, 36.26; H, 3.95; N, 10.44; S, 19.12%. IR (KBr disc)/cm^{-1}: ν(C=N), 1543; ν(N–N), 1159; ν(C–N), 1349; ν(C–S) 980.

[{Nd(pyrdtc)$_2$}$_2$(μ-bphz)$_2$] (3b)

Pale green crystals were obtained from CH_2Cl_2 and EtOH mixture in 43% yield. Anal. Found: C, 41.56; H, 4.56; N, 9.78; S, 17.57%. Calcd. for $C_{46}H_{52}N_{10}O_2Nd_2S_8$•2$CH_3CH_2OH$•$CH_2Cl_2$•$H_2O$: C, 41.25; H, 4.62; N, 9.43; S, 17.27%. IR (KBr disc)/cm^{-1}: ν(C=N), 1541; ν(N–N), 1163; ν(C–N), 1431; ν(C–S) 1007. ^{1}H NMR (300 MHz, Chloroform-*d*, 22°C) δ 9.56 (dd, *J* = 14.6, 7.2 Hz, 1H), 8.94–8.23 (m, 2H), 7.99–7.70 (m, 1H), 7.69–7.37 (m, 1H), 7.26 (s, 1H), 4.39–3.40 (m, 8H), 1.67–1.04 (m, 8H).

[{Nd(pyrdtc)$_2$}$_2$(μ-bphz)$_2$] (3b')

Pale green crystals were obtained from CH_2Cl_2 and Et_2O. Anal. Found: C, 41.58; H, 4.00; N, 10.56; S, 19.20%. Calcd. for $C_{46}H_{52}N_{10}O_2Nd_2S_8$: C, 41.79; H, 3.96; N, 10.60; S, 19.40%. IR (KBr disc)/cm^{-1}: ν(C=N), 1544; ν(N–N), 1163; ν(C–N), 1436; ν(C–S) 1004. ^{1}H NMR (300 MHz, Chloroform-*d*, 22°C) δ 9.56 (t, *J* = 10.2 Hz, 1H), 8.89–8.21 (m, 2H), 7.77 (t, *J* = 8.7 Hz, 1H), 7.69–7.37 (m, 1H), 7.26 (s, 2H), 4.27–3.47 (m, 6H), 1.61–1.03 (m, 6H).

[{Sm(Me$_2$dtc)$_2$}$_2$(μ-bphz)$_2$] (4a)

Pale yellow crystals were obtained from $CHCl_3$ and EtOH in 18% yield. Anal. Found: C, 35.97; H, 3.33; N, 10.93; S, 20.37%. Calcd. for $C_{38}H_{44}N_{10}O_2Sm_2S_8$•0.5$CHCl_3$: C, 35.85; H, 3.48; N, 10.86; S 19.89%. IR (KBr disc)/cm^{-1}: ν(C=N), 1545; ν(N–N), 1129; ν(C–N), 1351; ν(C–S) 982.

[{Sm(pyrdtc)$_2$}$_2$(μ-bphz)$_2$] (4b)

Pale yellow crystals were obtained from CH_2Cl_2 and EtOH in 22% yield. Anal. Found: C, 40.69; H, 3.71; N, 10.36; S, 19.06%. Calcd. for $C_{46}H_{52}N_{10}O_2Sm_2S_8$•0.5$CH_2Cl_2$: C, 40.57; H, 3.88; N, 10.17; S, 18.63. IR (KBr disc)/cm^{-1}: ν(C=N), 1545; ν(N–N), 1164; ν(C–N), 1437; ν(C–S) 1005.

[{Eu(Me$_2$dtc)$_2$}$_2$(μ-bphz)$_2$] (5a)

Orange crystals were obtained from $CHCl_3$ and MeOH in 37% yield. Anal. Found: C, 35.12; H, 3.41; N, 10.55; S, 19.20%. Calcd. for $C_{38}H_{44}N_{10}O_2Eu_2S_8$•$CHCl_3$: C, 35.04; H, 3.39; N, 10.48; S, 19.19%. IR (KBr disc)/cm^{-1}: ν(C=N), 1545; ν(N–N), 1131; ν(C–N), 1351; ν(C–S) 982.

[{Eu(pyrdtc)$_2$}$_2$(μ-bphz)$_2$] (5b)

Orange crystals were obtained from $CHCl_3$ and EtOH in 40% yield. Anal. Found: C, 38.03; H, 3.70; N, 9.41; S, 17.23%. Calcd. for $C_{46}H_{52}N_{10}O_2Eu_2S_8$•$CHCl_3$: C, 38.76; H, 3.67; N, 9.62; S, 17.61%. IR (KBr disc)/cm^{-1}: ν(C=N), 1545; ν(N–N), 1165; ν(C–N), 1436; ν(C–S) 1005.

Physical Measurements

C, H, N and S analysis were carried out on a Perkin Elmer Series II CHNS/O Analyzer 2400 at Department of Instrumental Analyses, Advanced Science Research Center, Okayama University. The FT-IR spectra were recorded on a JASCO FT-001 FT-IR spectrophotometer by a KBr disc method in the 400–4000 cm^{-1} range. The UV-visible absorption spectra of the complexes in dichloromethane were obtained on a JASCO V-550 UV/VIS spectrophotometer at room temperature. Room temperature magnetic circular dichroism (MCD) spectra were measured on a JASCO J-1500 CD spectropolarimeter equipped with a home-made neodymium magnet apparatus (ca. 0.5 T magnetic field) [13].

X-ray crystallographic study

X-ray diffraction intensity data were collected on a Rigaku R-AXIS Rapid diffractometer, except for those of compound **5b** which were obtained on a Rigaku VariMax diffractometer with a Saturn-70 CCD detector, using graphite or multi-layered mirror monochromated Mo Kα (λ = 0.71075 Å) radiation. The diffraction data were processed using the PROCESS-AUTO or CrystalClear software package [14] and the numerical absorption corrections were applied [15]. The structures were solved by the direct method employing the SIR2008 [16] or SHELXT [17] software package and expanded using Fourier techniques, and refined on F^2 (with all independent reflections) using SHELXL Version 2014/7 software package [18]. All non-hydrogen atoms were refined anisotropically. Hydrogen atoms were introduced at the theoretical positions and refined using riding models. All calculations were performed using the CrystalStructure software package [19].

3.3 Results and discussion

Synthesis and characterization of (*E*)-*N*-benzylidenepicolinohydrazide (Hbphz)

The hydrazone, Hbphz, was synthesized by a one-pot condensation reaction of equimolar amounts of 2-pyridinecarboxylic acid hydrazide and benzaldehyde in ethanol in 73% yield (Scheme 3.1) [20,21]. The product was characterized by elemental analysis, X-ray diffraction analysis, and IR and ^{1}H NMR spectroscopy.

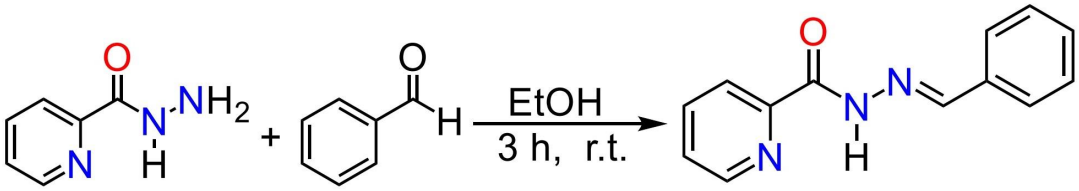

Scheme 3.1. Synthetic route of Hbphz.

The X-ray crystallographic analysis (Table 3.1) revealed the molecular structure of Hbphz as an *E*-isomer, which is depicted in Figure 3.1*a*. The molecule has an almost planar structure; the planes of the pyridyl (N1, C1–C5) and phenyl (C8–C13) rings form a dihedral angle of 10.4(1)°. The plane defined by the central hydrazone linkage, –C=N–N–C(=O)–, is tilted by 8.0(1) and 16.4(1)°, respectively, to the planes of the pyridyl and phenyl rings. The hydrazone C6=O1 bond length, 1.226(3) Å, indicates a ketonic character [7], and the imine N3=C7 bond length, 1.279(3) Å, shows its double bond character, while the N2–N3 and N2–C6 bond lengths are 1.381(2) and 1.356(3) Å, respectively. Therefore, the N2 atom should have an amide-H atom. Intermolecular N–H···O hydrogen bonds form a one-dimensional chain structure (Figure 3.1*b*), running along the *b* axis.

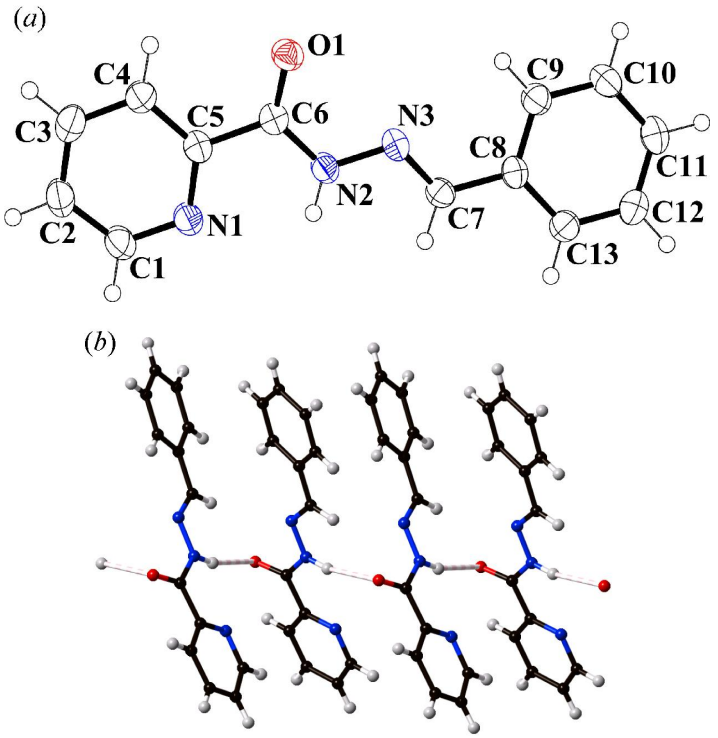

Figure 3.1. (*a*) An ORTEP drawing of Hbphz (at 50% probability level), and (*b*) hydrogen-bonding interaction in the crystal of Hbphz.

Synthesis and characterization of Ln^{III}_2 complexes with the hydrazonate, $bphz^-$

A reaction of Hbphz, $LnX_3•6H_2O$ (Ln = La, Pr, Nd, Sm or Eu; X = Cl^- or NO_3^-), and sodium dimethyldithiocarbamate {$Na(Me_2dtc)$} or ammonium pyrrolidinedithiocarbamate {$NH_4(pyrdtc)$} in a 1:1:2 molar ratio in the presence of Et_3N in methanol at room temperature gave a pale-yellow or green precipitate of the respective $Ln^{III}(bphz)(RR'dtc)_2$ complexes {Ln = La (**1x**), Pr (**2x**), Nd (**3x**), Sm (**4x**) or Eu (**5x**); *RR′* = Me_2 (**x** = **a**) or pyr (**x** = **b**)} (Scheme 3.2). Recrystallization of each product from dichloromethane (or chloroform) and ethanol (or methanol) afforded single-crystals suitable for the X-ray diffraction study. The elemental analysis of these products suggested the composition of $Ln(bphz)(RR'dtc)_2•n$(solvent).

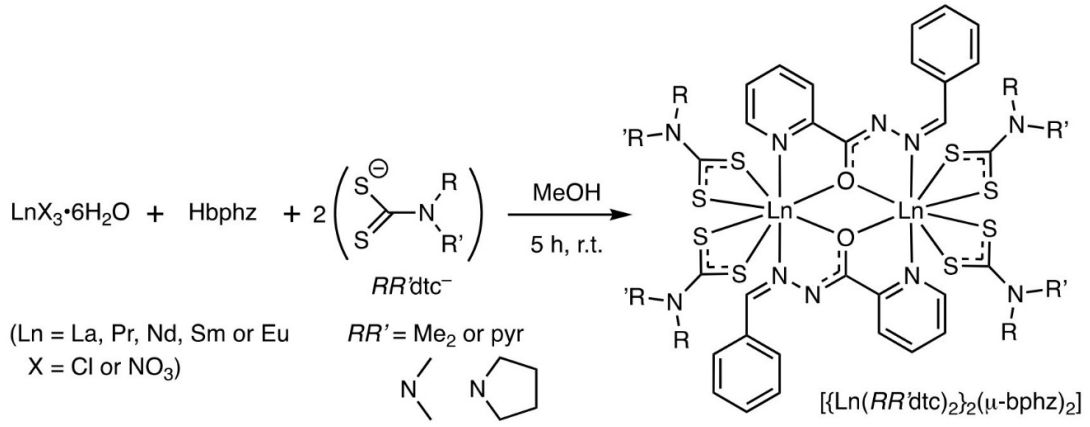

Scheme 3.2. Synthetic route of Ln^{III}_2 complexes.

Crystal structure of the complexes

Further characterization of the bphz complexes, **1a**–**5b**, were performed by the single-crystal X-ray analysis. The crystallographic data are summarized in Table 3.1. The selected structural parameters are listed in Table 3.2 in the Supporting Information.

The Eu^{III}–pyrdtc complex, **5b**, was crystallized in a monoclinic space group *Cc* (with *Z* = 4), and the asymmetric unit contains two Eu^{III} ions, each of which attaches two bidentate *S,S'*-donating pyrdtc$^-$ ligands, two bridging bphz$^-$ (deprotonated hydrazonate) anions and three chloroform molecules of crystallization: $[\{Eu(pyrdtc)_2\}_2(\mu\text{-bphz})_2]\bullet 3CHCl_3$ (Figure 3.2). The bphz$^-$ anions are bridged to two Eu^{III} ions in a $\mu\text{-}1\kappa^2N(py),O:2\kappa^2O,N(imine)$ mode and form a head-to-tail type $Eu_2(\mu\text{-bphz})_2$ core. Each Eu^{III} center accomplishes a distorted dodecahedral 8-coordination geometry with $N_2O_2S_4$ donor atoms, and two pyrdtc ligands in the mutually pseudo-*trans* positions are almost co-planar and perpendicular to the $Eu_2(bphz)_2$ plane (Figure 3.2*b*). Analogous Eu^{III}–Me_2dtc complex, **5a**, was crystallized in a triclinic space group $P\bar{1}$ with *Z* = 1 (based on the dinuclear unit). The asymmetric unit consists of an Eu^{III} ion, two bidentate *S,S'*-donating Me_2dtc$^-$ anions, and a bidentate *N*(py),*O*-bonding bphz$^-$ anion, but the symmetry expansion by the crystallographic inversion center forms further coordination of the

neighboring $bphz^-$ anion via a bidentate *O*,*N*(imine) mode. Thus, the molecule has a C_i symmetric (head-to-tail type) bphz-bridged dinuclear structure, as similar to the above pyrdtc complex: $[\{Eu(Me_2dtc)_2\}(\mu\text{-}bphz)_2]$ (Figure 3.3).

The Sm^{III}–Me_2dtc complex, **4a**, is isomorphorous to that of **5a**, and a similar molecular structure is resulted: $[\{Sm(Me_2dtc)_2\}(\mu\text{-}bphz)_2]$ (Figure 3.4). In the case of Sm^{III}–pyrdtc complex of **4b**, a similar dinuclear molecular structure with two solvent CH_2Cl_2 molecules of crystallization, $[\{Sm(pyrdtc)_2\}_2(\mu\text{-}bphz)_2]\bullet 2CH_2Cl_2$ (Figure 3.5) was obtained in a triclinic space group $P\bar{1}$ with $Z = 1$ (based on the dinuclear unit).

All four complexes of Eu^{III} and Sm^{III}, **4a**, **4b**, **5a** and **5b**, have similar structural features with two Ln^{III} ions having a $N_2O_2S_4$ dodecahedral 8-coordination and two bridging monodeprotonated hydrazonate anions ($bphz^-$). Compared to the metric parameters of the complexes with those of free Hbphz, the C=O and C–N bonds become longer (by ca. 0.07 Å) and shorter (by ca. 0.05 Å), respectively, while the N–N and N=C(imine) bond lengths are not different so much. This fact indicates that delocalization of the anionic character of the hydrazonate is limited in the [O=C–N] moiety, although the whole hydrazonato moiety [–C(=O)–N–N=C–] has a planar structure. Two Ln^{III} ions are placed on the hydrazonato planes, and the pyridine ring is also coplanar, while the phenyl ring of $bphz^-$ is slightly tilted from the planes (Table 3.3). Two *RR'*dtc ligands at each Ln^{III} ion are located above and below the $Ln_2(\mu\text{-}bphz)_2$ plane, i.e., at mutually pseudo *trans*-positions, and their coordination planes are almost parallel to each other but perpendicular to the $Ln_2(\mu\text{-}bphz)_2$ plane. The coordination bond lengths around Eu^{III} or Sm^{III} centers are: Ln–S, 2.85–2.93 Å; Ln–N, 2.50–2.62 Å; Ln–O, 2.75–2.41 Å, the bite angles of *RR'*dtc are 61.8–62.5°, and the bridging angles of Ln–O–Ln are 112.2–113.6°.

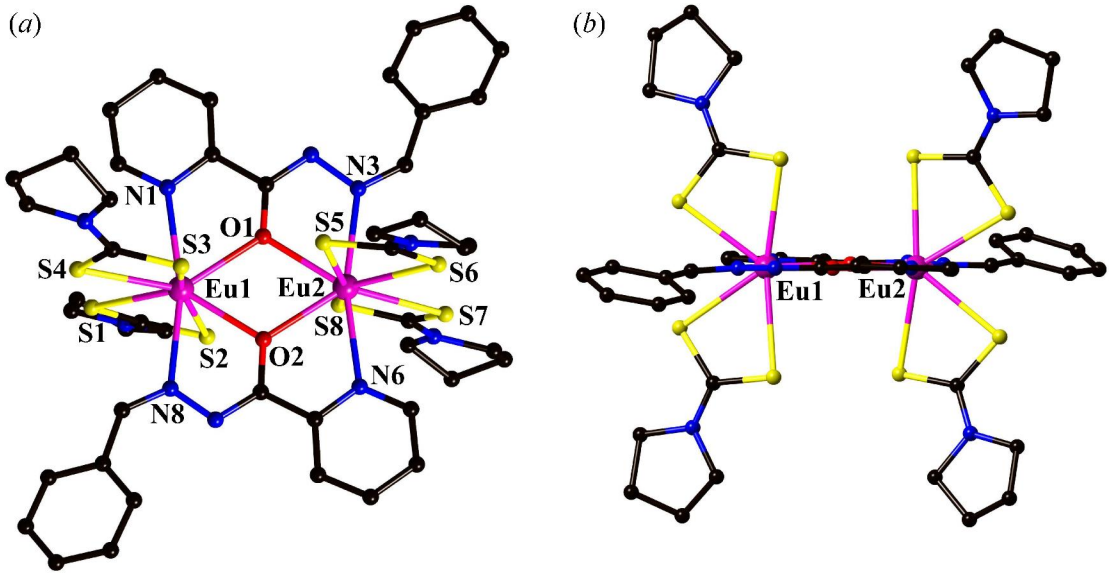

Figure 3.2. (*a*) A perspective view of dinuclear complex of [{Eu(pyrdtc)$_2$}$_2$(μ-bphz)$_2$] in **5b**•3CHCl$_3$ and (*b*) its side view from the Eu$_2$(bphz)$_2$ plane. Hydrogen atoms and lattice solvent molecules are omitted for clarity.

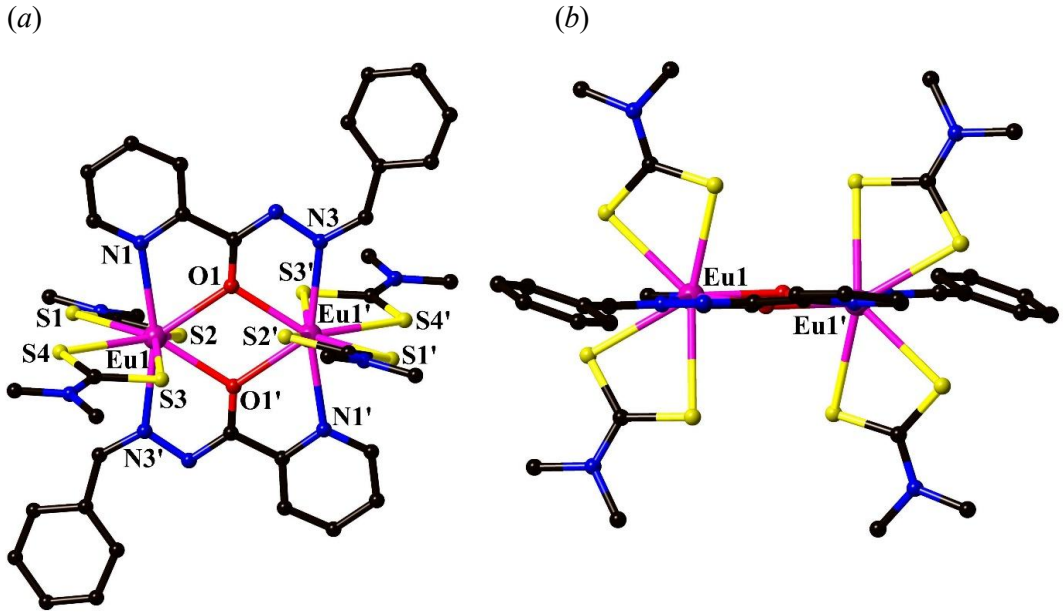

Figure 3.3. (*a*) A perspective view of molecular structures of [{Eu(Me$_2$dtc)$_2$}$_2$(μ-bphz)$_2$] in **5a** and (*b*) its perpendicular view of the Me$_2$dtc planes to the Eu$_2$(bphz)$_2$ plane. Hydrogen atoms and lattice solvent molecules are omitted for clarity.

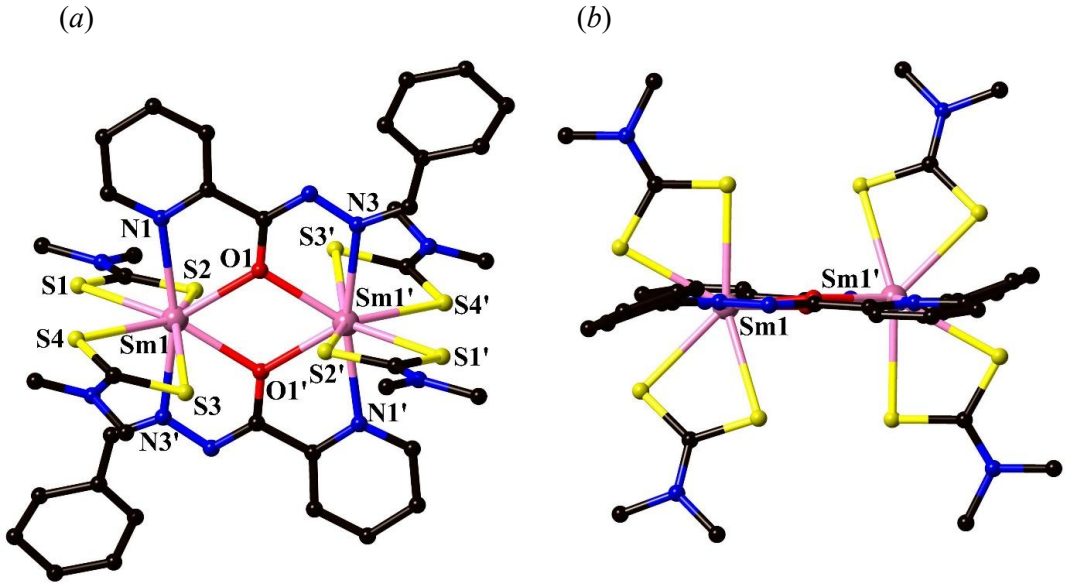

Figure 3.4. (*a*) A perspective view of molecular structures of [{Sm(Me$_2$dtc)$_2$}$_2$(μ-bphz)$_2$] in **4a** and (*b*) its perpendicular view of the Me$_2$dtc planes to the Sm$_2$(bphz)$_2$ plane. Hydrogen atoms and lattice solvent molecules are omitted for clarity.

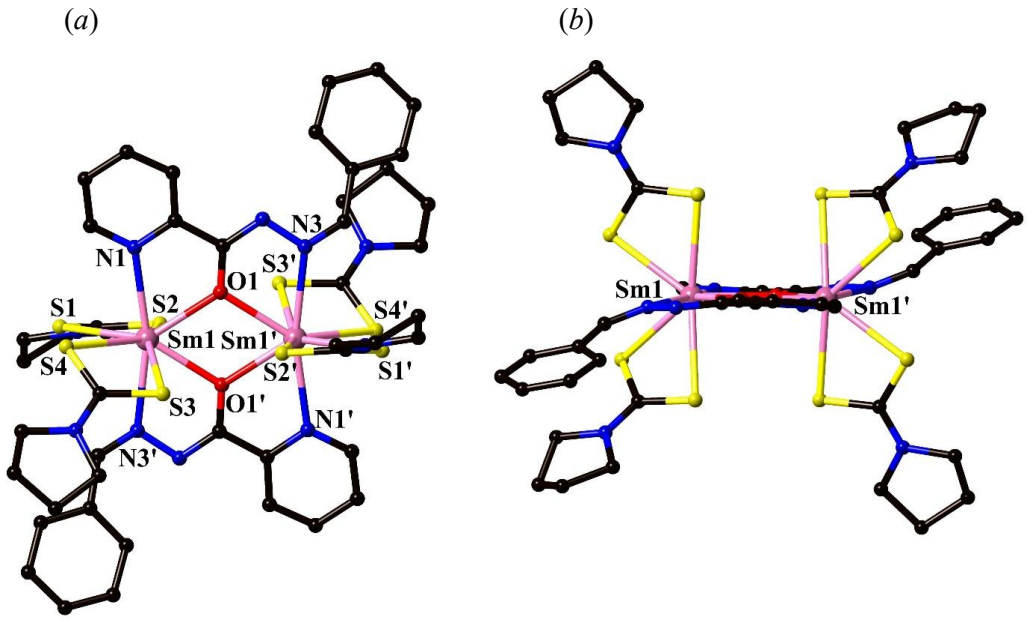

Figure 3.5. (*a*) A perspective view of molecular structures of [{Sm(pyrdtc)$_2$}$_2$(μ-bphz)$_2$] in **4b** and (*b*) its perpendicular view of the Me$_2$dtc planes to the Sm$_2$(bphz)$_2$ plane. Hydrogen atoms and lattice solvent molecules are omitted for clarity.

In contrast to the above complexes, the La^{III} complexes of **1a** and **1b** were found to have a different molecular structure (Figure 3.6 and Figure 3.7, respectively) in the crystals. The Me_2dtc complex of **1a** was crystallized in a monoclinic space group $P2_1/n$ with $Z = 2$ (based on the dinuclear unit), and the pyrdtc complex of **1b** was crystallized in a triclinic space group $P\bar{1}$ with $Z = 1$ (based on the dinuclear unit). Both complexes showed a dinuclear bphz-bridged $La^{III}_2(\mu\text{-bphz})_2$ structure having a crystallographic inversion center in the molecule. The bridging mode of the hydrazonato is the same as those in the Eu^{III} and Sm^{III} complexes, but the coordination bond lengths around the La^{III} are longer by 0.15–0.20 Å, which is consistent with the longer ionic radius of La^{III} than Eu^{III} and Sm^{III}. Because of the larger ionic size, the La^{III} center is deviated from the plane defined by two bridging ligands (Figure 3.6*b*). In addition, the La^{III} center is coordinated by an ethanol molecule as well as two dithiocarbamato ($RR'dtc^-$) ligands. The coordinated ethanol molecule is hydrogen-bonded to one of the S atoms of $RR'dtc^-$ ligand coordinated to the other La^{III} center (O2–H···S4: Figure 3.6*a*). Two dithiocarbamato ligand planes are almost perpendicular to each other and to the bridging bphz ligand plane, and, therefore, the coordination geometry around each La^{III} center is characterized as a 9-coordinate tricapped trigonal prism.

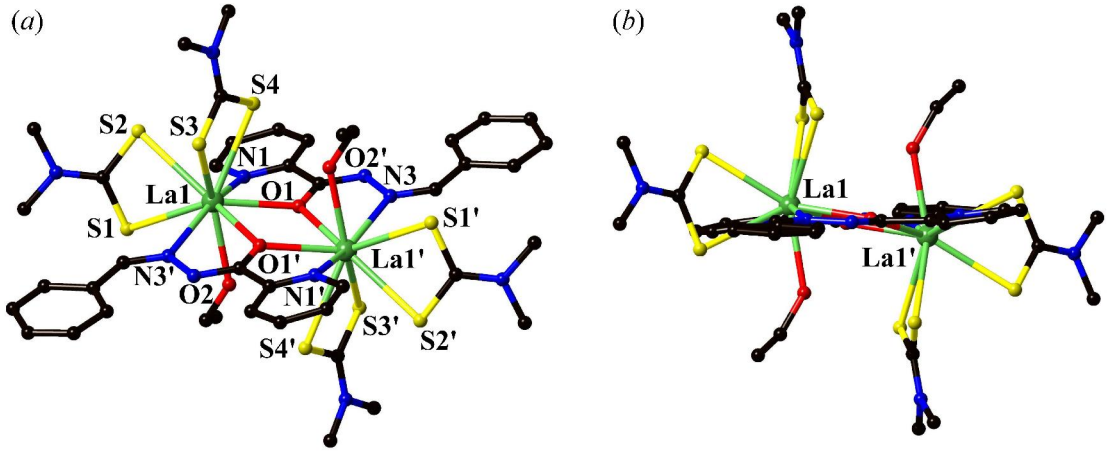

Figure 3.6. (*a*) A perspective view of dinuclear complex of [{La(Me$_2$dtc)$_2$(EtOH)}$_2$(μ-bphz)$_2$] in **1a** and (*b*) its side view from the (μ-bphz)$_2$ plane. Hydrogen atoms and lattice solvent molecules are omitted for clarity.

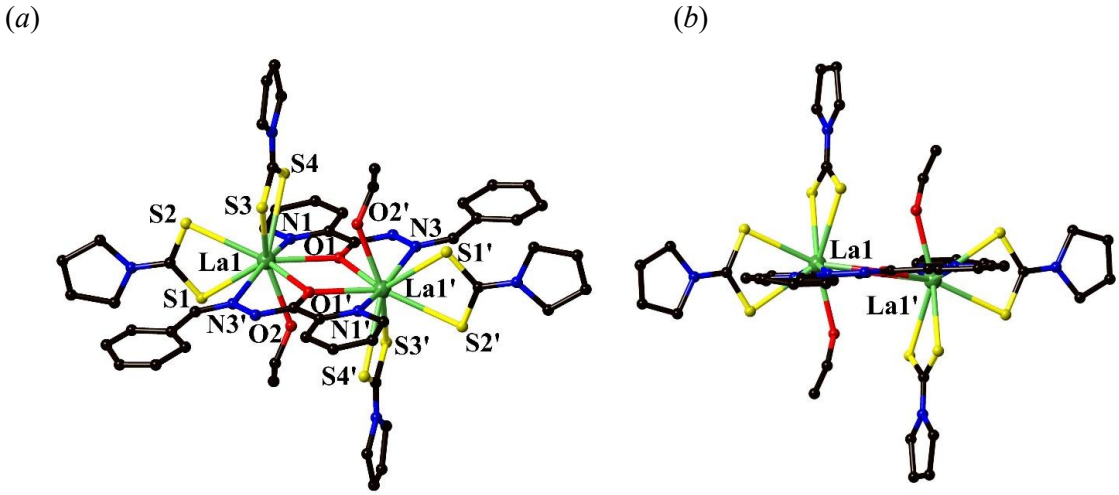

Figure 3.7. (*a*) A perspective view of molecular structures of [{La(pyrdtc)$_2$(EtOH)}$_2$(μ-bphz)$_2$] in **1b** and (*b*) its perpendicular view of the pyrdtc planes to the La$_2$(bphz)$_2$ plane. Hydrogen atoms and lattice solvent molecules are omitted for clarity.

Since the $La^{III}(RR'dtc)_2$ fragments form a 9-coordinate dinuclear bphz-bridged complex with a coordinated EtOH ligand, while the corresponding Sm^{III} and Eu^{III} ones gave an 8-coordinate dinuclear complexes where two dithiocarbamato ligand planes at each Ln^{III} center are co-planar, it is interesting to investigate the molecular structures of the Pr^{III} and Nd^{III} analogues. The Pr^{III}–pyrdtc complex of **2b** and the Nd^{III}–pyrdtc complex of **3b** were found to be isomorphous to the La^{III}–pyrdtc complex of **1b**, and a similar molecular structure with 9-coordinate Pr^{III} ions (Figure 3.8) or Nd^{III} ions (Figure 3.9) resulted in. The structural characteristics of **2b** and **3b** are also the same as those of **1b**. The coordination bond lengths around Pr^{III} center in **2b** are slightly shorter than the corresponding ones around La^{III} in **1b** by 0.02–0.06 Å and those around Nd^{III} in **3b** are further shorter by ca. 0.01 Å, although the Pr^{III} and Nd^{III} centers in **2b** and **3b** are still not on the plane of the bridging bphz ligands (Figures 3.8*b* and 3.9*b*).

The crystal structure of Pr^{III}–Me_2dtc complex, **2a**, was found to be rather different from the above examples. It was crystallized in a triclinic space group $P\bar{1}$ with $Z = 4$ (based on the dinuclear unit), and its asymmetric unit contains a whole molecule of bphz-bridged dinuclear Pr^{III} complex, two fragments of '$Pr^{III}(Me_2dtc)_2(bphz)$' which gives a dinuclear bphz-bridged complex by symmetry operation, and four molecules of solvent CH_2Cl_2 molecules; thus, the crystals of **2a** can be assigned as $[\{Pr(Me_2dtc)_2\}_2(\mu\text{-bphz})_2]\bullet 2CH_2Cl_2$. There are three kinds of crystallographically different dinuclear complexes, but all of them are found to be 8-coordinate around the Pr^{III} centers (Figure 3.10). The characteristics of the molecular structures are also similar to those of the Sm^{III}_2 and Eu^{III}_2 complexes of **4a** and **5a**.

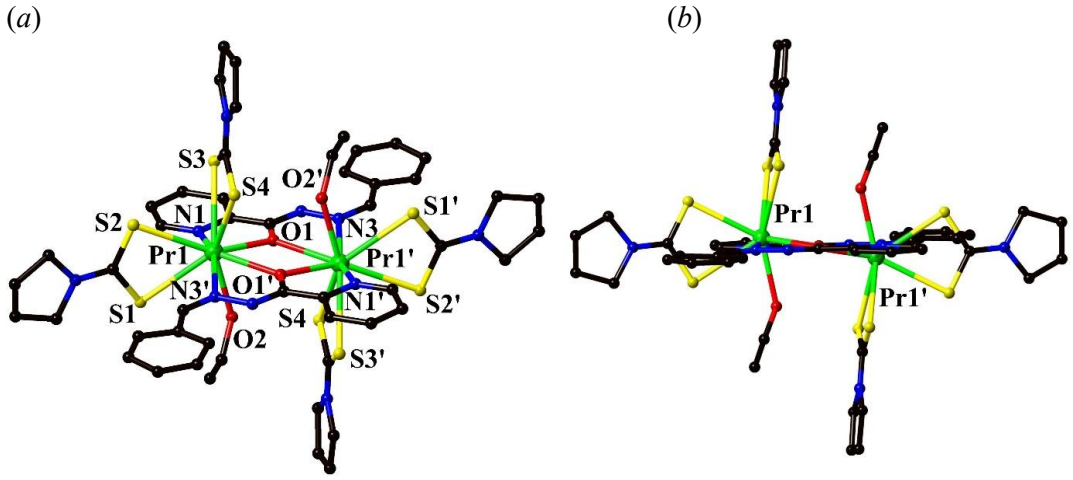

Figure 3.8. (*a*) A perspective view of molecular structures of [{Pr(pyrdtc)$_2$(EtOH)}$_2$(μ-bphz)$_2$] in **2b** and (*b*) its perpendicular view of the pyrdtc planes to the Pr$_2$(bphz)$_2$ plane. Hydrogen atoms and lattice solvent molecules are omitted for clarity.

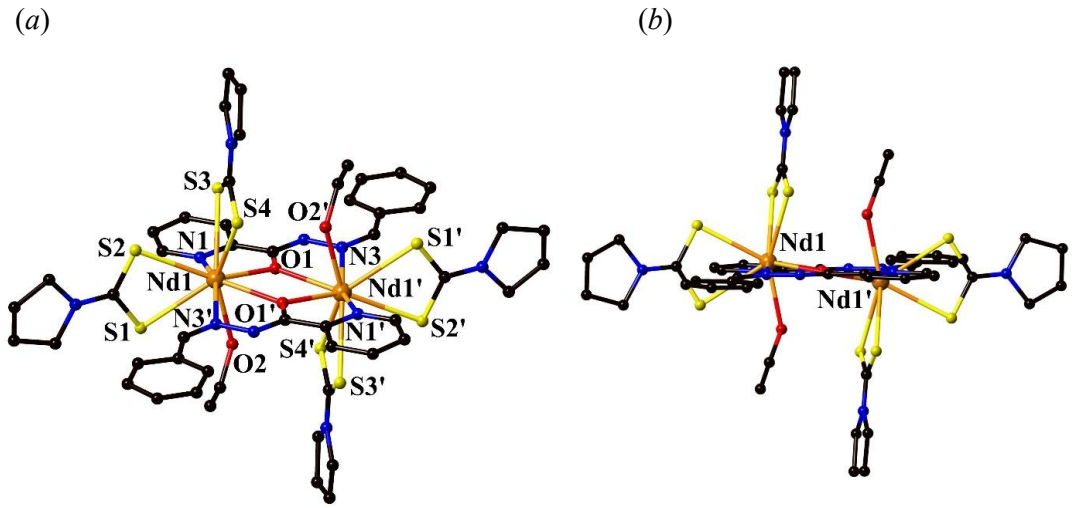

Figure 3.9. (*a*) A perspective view of molecular structures of [{Nd(pyrdtc)$_2$(EtOH)}$_2$(μ-bphz)$_2$] in **3b** and (*b*) its perpendicular view of the pyrdtc planes to the Nd$_2$(bphz)$_2$ plane. Hydrogen atoms and lattice solvent molecules are omitted for clarity.

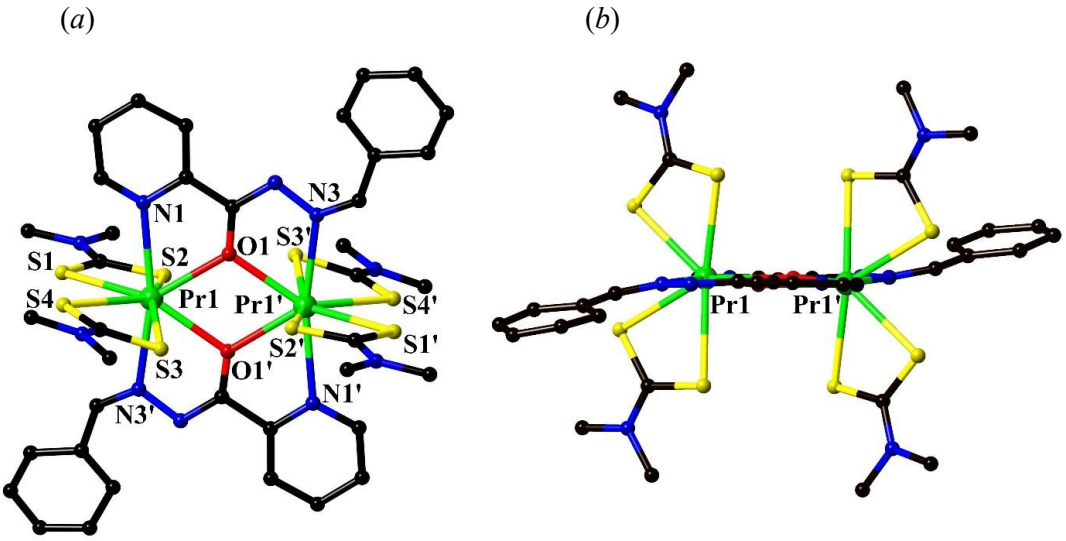

Figure 10. (*a*) A perspective view of molecular structures of [{Pr(Me$_2$dtc)$_2$}$_2$(μ-bphz)$_2$] in **2a** and (*b*) its perpendicular view of the Me$_2$dtc planes to the Pr$_2$(bphz)$_2$ plane. Hydrogen atoms and lattice solvent molecules are omitted for clarity.

The Nd^{III}–Me$_2$dtc complex, **3a**, showed a further characteristic crystal structure (Figure 3.11). It was crystalized in a triclinic space group $P\bar{1}$ with $Z = 2$ (based on the dinuclear unit), and the asymmetric unit contains two halves of the dinuclear bphz-bridged Nd^{III} molecules and two solvent $CHCl_3$ molecules. Interestingly, these two fragments have different molecular structures; one of the molecules (with Nd1) has a similar 8-coordinate structure (Figure 3.11*a* and *b*) to those of the Sm^{III} (**4a**) and Eu^{III} (**5a**) analogues (where two mutually *trans*-positioned Me$_2$dtc ligand planes are co-planar to each other), while the other molecule (with Nd2) is coordinated by an additional MeOH molecule to complete a 9-coordinate coordination geometry (Figure 3.11*c* and *d*). Therefore, the crystals are assigned as [{Nd(Me$_2$dtc)$_2$}$_2$(μ-bphz)$_2$]•[{Nd(Me$_2$dtc)$_2$(MeOH)}$_2$(μ-bphz)$_2$]•4$CHCl_3$.

The above-mentioned crystallographic analyses suggested that the bphz-bridged dinuclear lanthanoid dithiocarbamato complexes tend to form a 9-coordinate complex by a coordination of solvent EtOH (or MeOH) molecule used for recrystallization, when a larger Ln^{III} ion (e.g., La^{III}, Pr^{III} or Nd^{III}) was applied. Then, an interesting question arose; would an

8:8- or 9:9-coordinate molecule be obtained by recrystallizing these complexes from non-coordinating solvents? We attempted several recrystallizations and finally isolated pale green and block single-crystals of the Nd^{III}–pyrdtc complex, **3b'**, from a mixture of dichloromethane and diethyl ether. Although the crystallinity was not good enough to obtain a satisfactory *R* value, we have been able to confirm the successful crystallization of the 8:8-coordinate [{Nd(pyrdtc)$_2$}$_2$(μ-bphz)$_2$] (**3b'**) complex (Table 3.1 and Figure 12).

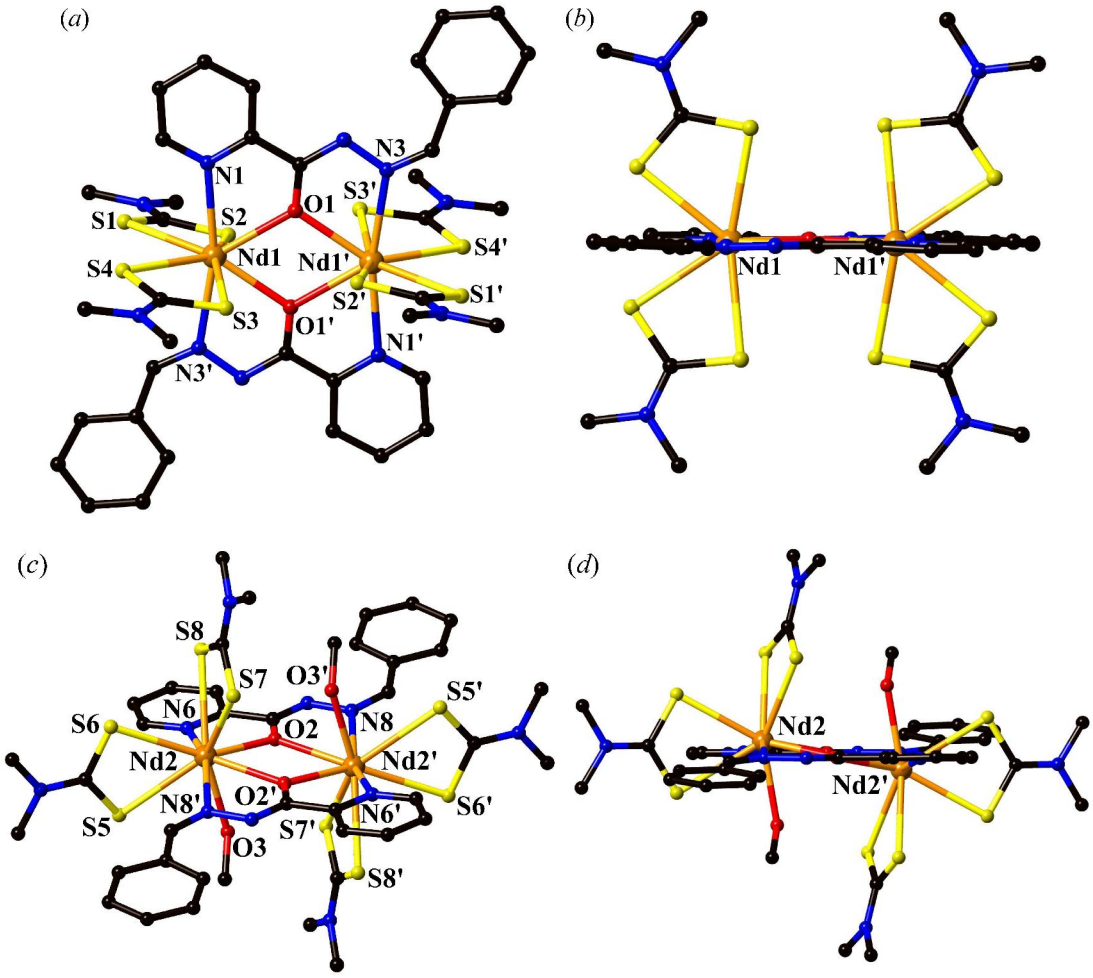

Figure 3.11. Perspective views of (*a* and *b*) a 8:8-coordinate dinuclear complex of [{Nd(Me$_2$dtc)$_2$}$_2$(μ-bphz)$_2$] and (*c* and *d*) a 9:9-coordinate dinuclear complex of [{Nd(Me$_2$dtc)$_2$(MeOH)}$_2$(μ-bphz)$_2$] in **3a** (*b* and *d* are their side views from the (μ-bphz)$_2$ plane. Hydrogen atoms and lattice solvent molecules are omitted for clarity.

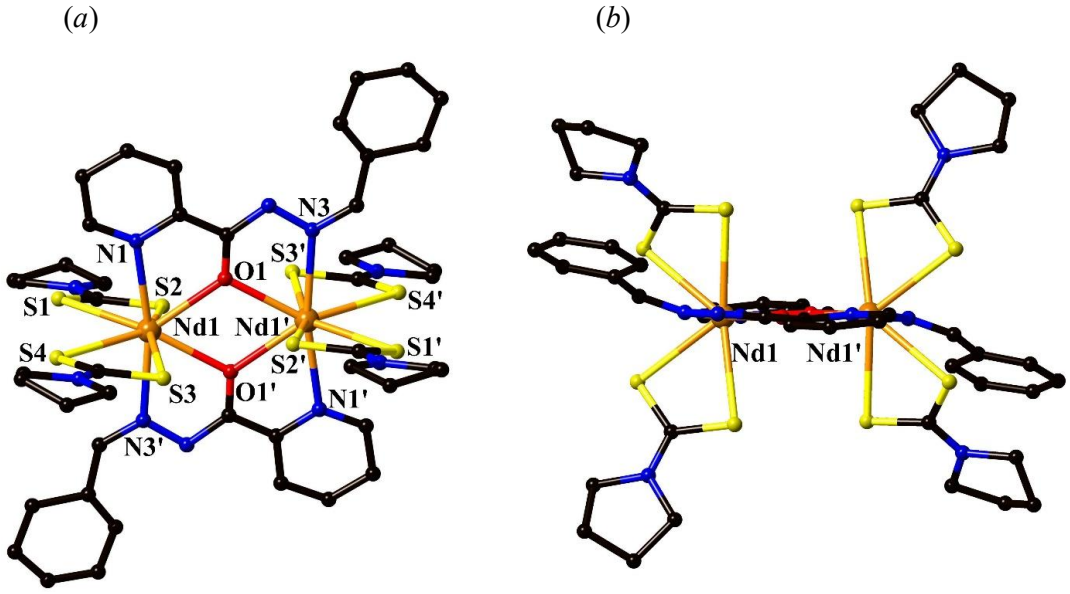

Figure 3.12. (*a*) A perspective view of molecular structures of [{Nd(pyrdtc)$_2$}$_2$(μ-bphz)$_2$] in **3b'** and (*b*) its perpendicular view of the pyrdtc planes to the Nd$_2$(bphz)$_2$ plane. Hydrogen atoms and lattice solvent molecules are omitted for clarity.

Spectroscopic Properties

FT-IR spectra

Figure 3.13 showed the FT-IR spectra of Hbphz and its complexes **3b** and **5b** as representative examples; other pyrdtc complexes of **1b**, **2b** and **4b** gave a similar spectral pattern. Also, the Me$_2$dtc complexes **1a–5a** showed similar IR spectra to one another. The ν(N–H) and ν(C=O) stretching bands appeared at 3212 cm^{-1} and 1664 cm^{-1}, respectively, in the spectrum of free Hbphz were disappeared in the spectra of the complexes, which indicated that the ligand has an anionic (i.e. bphz$^-$) and enolate character [22]. The ν(C=N)$_{imine}$ and ν(N–N) bands observed at 1522 and 1141 cm^{-1}, respectively, in the free Hbphz were shifted to higher wavenumber regions on complexation, suggesting the coordination of the imine-N donor to a Ln^{III} ion [1]. The ν(C–S) and ν(C–N) bands associated with the pyrdtc$^-$ ligand in the complexes appeared at 1007 and 1430 cm^{-1} in **3b** and 1005 and 1436 cm^{-1} in **5b**, respectively.

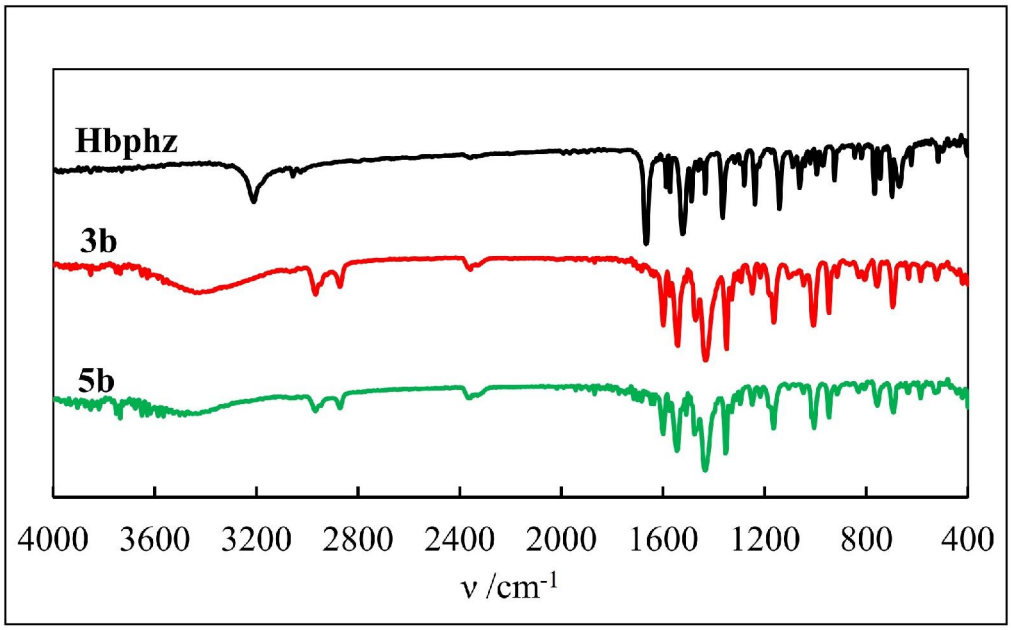

Figure 3.13. FT-IR spectra of Hbphz ligand and its Nd_2^{III} **3b** and Eu_2^{III} **5b**.

^{1}H NMR study

The ^{1}H NMR spectra of Hbphz and some Ln^{III} complexes in chloroform-*d* were measured. The ^{1}H NMR spectrum (Figure 3.14*a*) suggested that the isolated hydrazone was a single product of possible *E* and *Z* isomers. As representative examples, the spectra of free Hbphz and the Nd^{III}–pyrdtc complexes with 9:9- and 8:8-coordinate structures, [{Nd(pyrdtc)$_2$(EtOH)}$_2$(μ-bphz)$_2$] (**3b**) and [{Nd(pyrdtc)$_2$}$_2$(μ-bphz)$_2$] (**3b'**), which were obtained by recrystallization from dichloromethane/ethanol and dichloromethane/diethyl ether, respectively, are shown in Figure 3.14(*b*) and (*c*). In the spectrum of free Hbphz (bottom), the amide (NH) and imine (N=CH) proton resonances are observed at δ 10.99 and 8.58, respectively. In addition, multiplet resonances due to the aromatic (CH) protons are observed in the range of δ 7.31–8.42. The Nd^{III}_2 complexes gave relatively sharp resonances in the typical range (δ 10–0) for diamagnetic compounds (middle and top), although they contain Nd^{III} ions. In these spectra, the disappearance of the amide NH resonance indicates the deprotonation from

the hydrazone. The resonance for the imine (N=CH) proton is observed at δ 9.56, while those for the aromatic (CH) protons occurred in the range of δ 7.26–8.94. The methylene (CH_2) protons of pyrdtc$^-$ ligands gave two pseudo triplets around δ 3.8 and 1.3. In addition, in the spectrum of **3b** three sharp resonances due to free ethanol are observed [23]. These spectral features of **3b** and **3b'** suggest that the EtOH (or MeOH) molecule in the 9:9-coordinate complex dissociates in a chloroform solution to exist as an 8:8-coordinate dinuclear bphz-bridged complex.

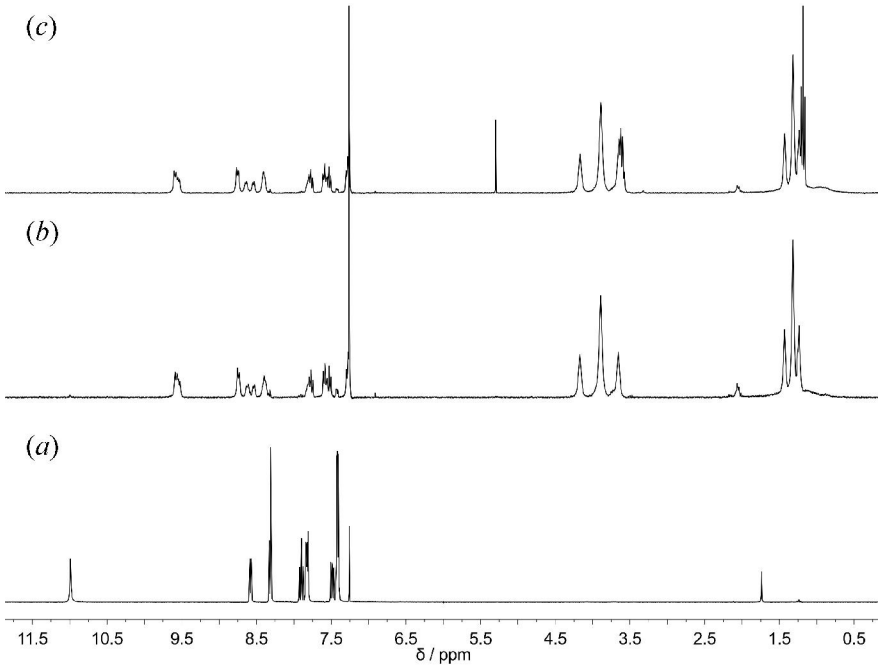

Figure 3.14. ^{1}H NMR (300 MHz, Chloroform-*d*) spectra of (*a*) Hbphz, (*b*) [{Nd(pyrdtc)$_2$}$_2$(μ-bphz)$_2$] and (*c*) [{Nd(pyrdtc)$_2$(EtOH)}$_2$(μ-bphz)$_2$].

UV-visible absorption and MCD spectra

The UV-visible absorption spectrum of Hbphz (Figure 3.15) measured in MeOH showed a characteristic intense band due to the π→π* transition centered at 306 nm. The UV-visible absorption and MCD spectra of the pyrdtc⁻ complexes, **1b**–**5b**, were measured in CH_2Cl_2 solutions. The complexes exhibited similar absorption spectral pattern in the UV region–as shown in Figure 3.16. The band at 340 nm was assigned to the intra-ligand charge transfer transition [24,25]. In the visible region, sharp but weak absorption bands and MCD signals characteristic of f–f transitions were observed in the complexes. The spectra are presented in Figures 3.17–3.20 and discussed below.

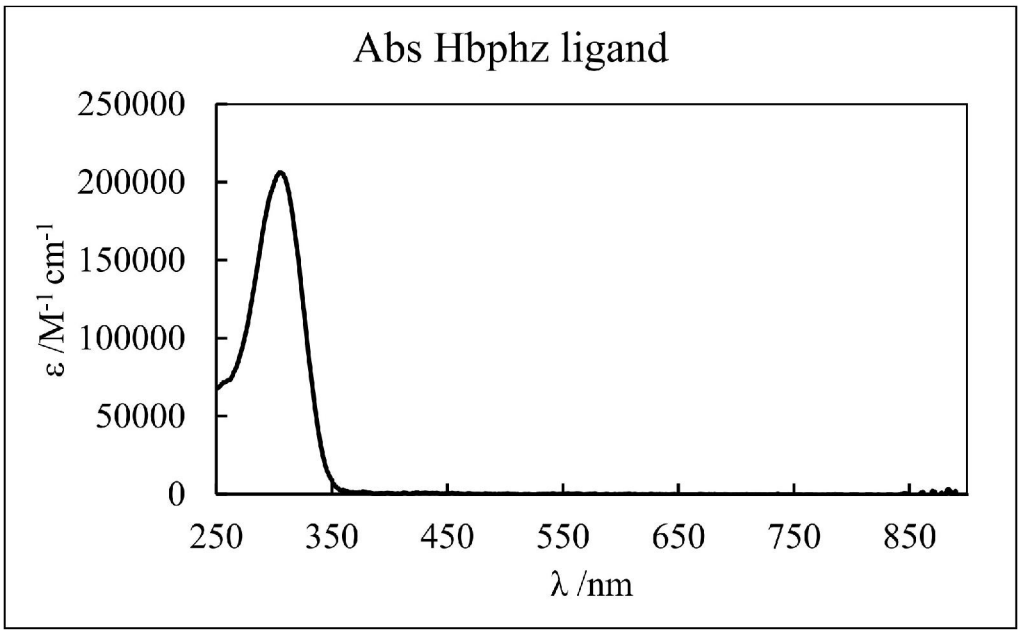

Figure 3.15. UV-visible absorption spectrum of Hbphz.

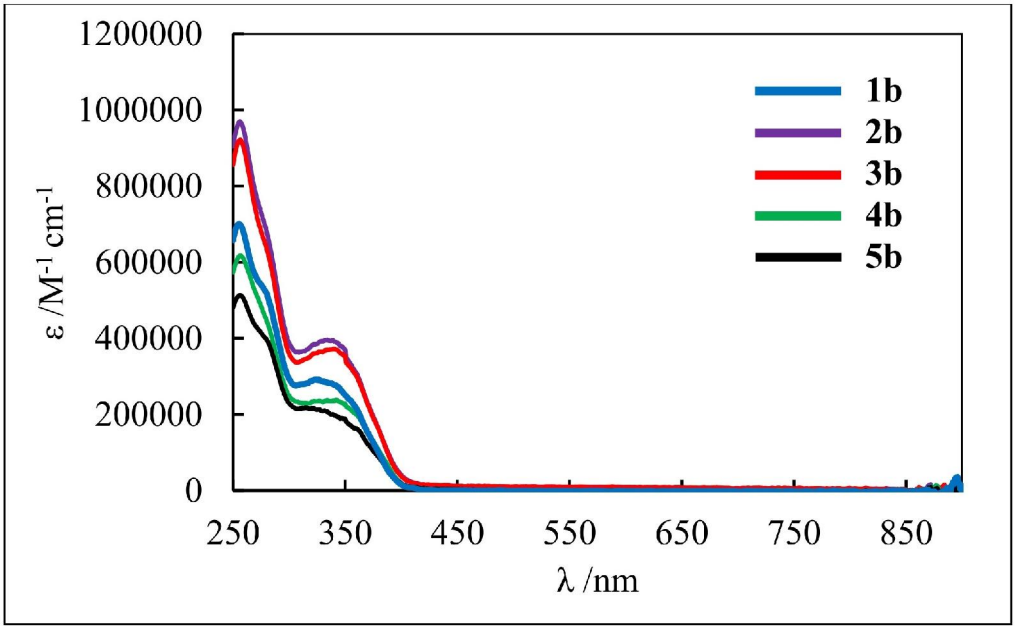

Figure 3.16. UV absorption spectra of complexes 1-**5**.

The absorption spectrum of **2b** (Figure 3.17, top) shows four sharp but weak bands at 16580, 20200, 20830 and 22050 cm^{-1}. These bands are due to the f–f transition from the ground state $^3H_4$ to the $^1D_2$, $^3P_0$, ($^3P_1$,$^1I_6$) and $^3P_2$ excited states, respectively, which are based on the reported signal assignments for an aqueous $Pr(NO_3)_3$ and $Pr(ClO_4)_3$ solutions [26]. In the MCD spectrum (bottom), the f–f transition bands are observed as characteristic positive *A*-term MCD signals at 16500 and 21930 cm^{-1}, while negative *A*- and *C*-term MCD signals at 20240 and 20830 cm^{-1}, respectively.

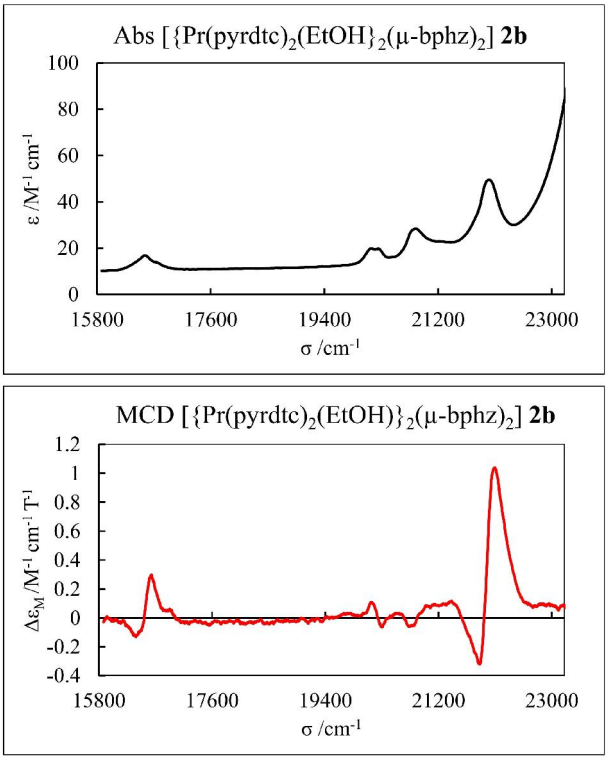

Figure 3.17. Absorption (top) and MCD (bottom) spectra of [{Pr(pyrdtc)$_2$(EtOH)}$_2$(μ-bphz)$_2$] **2b**.

The absorption spectrum (top) of complex **3b** (Figure 3.18) shows four sharp but weak f–f bands with maximum peaks at 12420, 13320, 17040 and 18800 cm^{-1}, which are assigned to the $^4I_{9/2} \rightarrow (^4F_{5/2}, {}^4H_{9/2})$, $(^4S_{3/2}, {}^4F_{7/2})$, $(^2G_{7/2}, {}^4G_{5/2})$ and $^4G_{7/2}$ transitions, respectively. The $^4I_{9/2} \rightarrow (^4F_{5/2}, {}^4H_{9/2})$, $(^4S_{3/2}, {}^4F_{7/2})$ and $(^2G_{7/2}, {}^4G_{5/2})$ transitions occurred at slightly lower in energies than those of a similar hydrazone-based Nd^{III} complex reported by Singh et al [27]. Compared to the related Nd^{III} complex with *N*-(furfuralidene)-*N*-isonicotinoylhydrazine [28], only the $^4I_{9/2} \rightarrow (^4F_{5/2}, {}^4H_{9/2})$ band was consistent, and the other transitions occurred at lower energies. In the MCD spectrum (bottom), the MCD signals were observed at 12380, 13290, 13500, 16910 and 17040 cm^{-1}. These signals are dominated by room temperature *C*-terms, except for the signal at 12380 cm^{-1} which appeared as a positive pseudo *A*-term [29].

The characteristic $^4I_{9/2} \rightarrow (^4G_{5/2},^2G_{7/2})$ hypersensitive transition exhibits splitting at 16910 and 17040 cm^{-1}. These crystal-field splitting was also observed in the second derivative absorption spectra of $Nd(C_2H_3O_2)_3H_2O$ **[**30] and neodymium complex with fleroxacin [31] at higher energies. The $^4I_{9/2} \rightarrow (^4G_{5/2}, ^2G_{7/2})$ hypersensitive transition *C*-term MCD signals are more clearly resolved in **3b** than those in previously reported mononuclear Nd^{III} analogues [29].

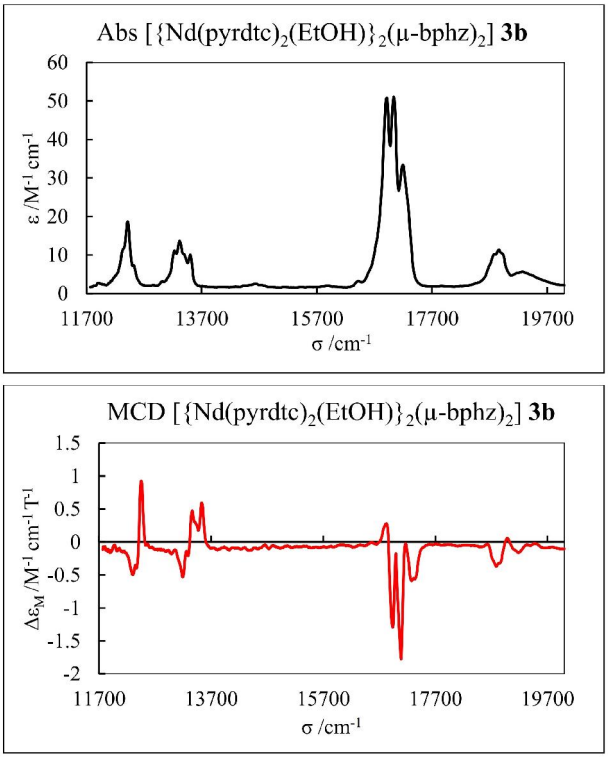

Figure 3.18. Absorption (top) and MCD (bottom) spectra of [{Nd(pyrdtc)$_2$(EtOH)}$_2$(μ-bphz)$_2$] **3b**.

In Figure 3.19 (top), no f–f bands were detected in the absorption spectrum for complex **4b** probably because they were overlapped or buried underneath the strong metal-ligand charge–transfer band around 24000 cm^{-1} [28, 32]. In the MCD spectrum (bottom), the structure of the MCD bands is very complicated due to the Zeeman splitting of the ground state and all the excited states [33]. Two characteristic MCD signals showing a positive *A*-term and a negative *C*-term occurred at 23510 and 21260 cm^{-1}, owing probably to the f–f transition from the $^{6}H_{6/2}$ ground state to the $^{6}P_{3/2}$ and $^{4}I_{13/2}$ excited states, respectively.

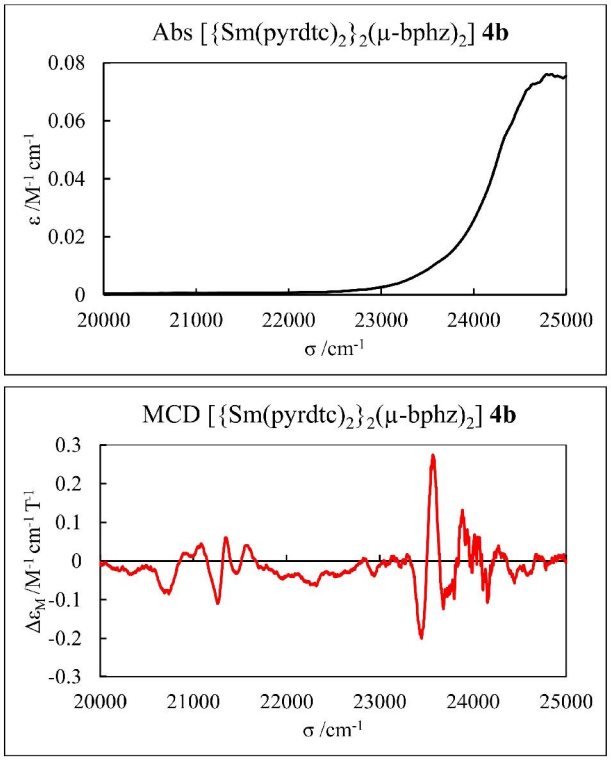

Figure 3.19. Absorption (top) and MCD (bottom) spectra of [{Sm(pyrdtc)$_2$}$_2$(μ-bphz)$_2$] **4b**.

In Figure 3.20 (top), complex **5b** exhibited two very weak bands at 21450 and 21460 cm^{-1} which are assigned to the $^7F_0 \rightarrow {}^5D_2$ transition. The positions of these bands are in good agreement, but the shapes are different from previously reported spectra of mononuclear [Eu(*RR'*dtc)$_3$(NN)] (*RR'* = dimethyl-, pyrrolidine- and *S*-prolinol-; NN = 1,10-phenanthroline or 2,2'-bipyridine) complexes [29]. In the MCD spectrum (bottom), a negative pseudo *A*-term MCD signal is observed at 21430 cm^{-1} and corresponds to the absorption bands. The shape of the negative pseudo *A*-term of **5b** is different from that of the negative *B*-term observed in the previously reported mononuclear Eu^{III} dithiocarbamato complexes [29]. The MCD results show that the coordination environment of the lanthanoid with a mixed N,O,S donor set gives a significant difference in the electronic structure from that of an N,S donor set. This finding shows that the sensitivity of the MCD technique [34] can be used as an effective tool to probe the electronic structure(s) and physical properties of Ln^{III} complexes in solution.

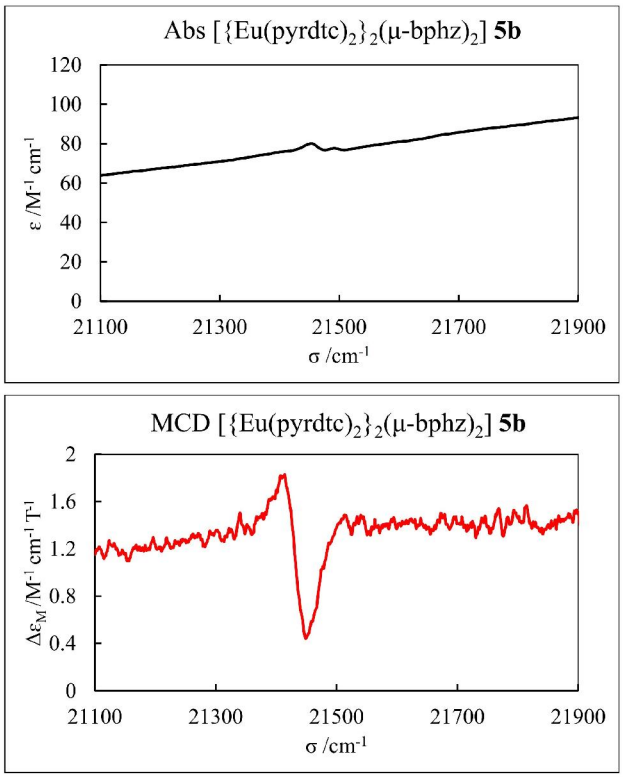

Figure 3.20. Absorption (top) and MCD (bottom) spectra of [{Eu(pyrdtc)$_2$}$_2$(μ-bphz)$_2$]

3.4 Conclusion

A series of novel hydrazonato-bridged homodinuclear Ln^{III}_2 dithiocarbamato complexes were prepared and their crystal and molecular structures and spectroscopic properties were investigated. The crystal structures revealed that the early Ln^{III} ions tend to crystallize as a 9:9-coordinate complex with the ninth position occupied by a solvent alcohol molecule, while the middle and late Ln^{III} ions deposit the crystals of only 8:8-coordinate complex. The coordination of a deprotonated monoanionic hydrazonato ligand was confirmed by the IR and ^{1}H NMR spectroscopy. Similar spectral patterns of ligand-centered and Laporte forbidden f–f transitions were observed in the UV-visible spectral region. The MCD parameters exhibited by the complexes demonstrate their potential in magneto-optical applications.

Table 3.1. Crystallographic data of Hbphz and the Ln^{III}_2 complexes

Compound	**Hbphz**	**1a**	**1b**	**2a**	**2b**
Molecular formula	$C_{13}H_{11}N_3O$	$C_{42}H_{54}N_{10}O_4La_2S_8$	$C_{50}H_{62}N_{10}O_4La_2S_8$	$C_{40}H_{48}Cl_4N_{10}Pr_2O_2S_8$	$C_{50}H_{62}N_{10}O_4Pr_2S_8$
Molecular weight	225.25	1297.24	1401.40	1380.99	1405.40
Temperature (K)	188	188	188	188	188
Crystal system	Orthorhombic	Monoclinic	Triclinic	Triclinic	Triclinic
Space group, Z	*Pbca*, 8	$P2_1/n$, 2	$P\bar{1}$, 1	$P\bar{1}$, 4	$P\bar{1}$, 1
a (Å)	12.0870(8)	10.5657(11)	10.8385(15)	16.3680(7)	10.8569(8)
b (Å)	7.5053(6)	22.305(2)	11.5016(15)	18.5418(9)	11.5007(8)
c (Å)	25.0504(18)	11.9039(13)	12.5627(13)	19.8671(9)	12.4732(8)
α (°)	90	90	79.953(4)	74.5353(18)	79.695(3)
β (°)	90	106.860(3)	87.714(4)	72.3561(15)	87.949(4)
γ (°)	90	90	73.948(5)	73.3711(19)	73.626(5)
V (Å^3)	2272.5(3)	2684.8(5)	1481.9(3)	5397.7(4)	1469.98(19)
D_{calcd} (g cm^{-3})	1.317	1.605	1.570	1.699	1.587
μ(Mo Kα) (cm^{-1})	0.872	19.226	17.481	23.297	19.672
F(000)	944	1300	706	2752	710
R_{int}	0.1066	0.1096	0.0896	0.0488	0.0509
$R1$ [$I > 2\sigma(I)$]	0.0638	0.0731	0.0882	0.0627	0.0526
$wR2$ [all data]	0.1410	0.2216	0.1923	0.2270	0.1601
GOF on F^2	1.035	1.112	1.035	1.061	1.121

Table 3.1. Continued

Compound	**3a**	**3b**	**3b'**	**4a**	**4b**
Molecular formula	$C_{41}H_{48}Cl_6N_{10}Nd_2O_3S_8$	$C_{50}H_{62}N_{10}Nd_2O_4S_8$	$C_{25}H_{30}N_5Cl_4NdOS_4$	$C_{38}H_{44}N_{10}Sm_2O_2S_8$	$C_{50}H_{56}N_{10}Cl_8Sm_2O_2S_8$
Molecular weight	1486.57	1412.06	830.84	1230.11	1669.96
Temperature (K)	188	188	188	188	188
Crystal system	Triclinic	Triclinic	Triclinic	Triclinic	Triclinic
Space group, Z	$P\bar{1}$, 2	$P\bar{1}$, 1	$P\bar{1}$, 2	$P\bar{1}$, 1	$P\bar{1}$, 1
a (Å)	11.4229(6)	10.8371(14)	9.91963	9.6035(13)	9.8617(11)
b (Å)	15.3318(5)	11.4378(12)	11.38027	11.6344(15)	11.4222(9)
c (Å)	19.2918(6)	12.4842(15)	15.19711	11.9327(18)	15.1507(14)
α (°)	67.8250(10)	79.633(3)	72.45700	112.088(4)	72.438(2)
β (°)	75.721(3)	87.700(3)	84.41900	100.897(4)	84.370(4)
γ (°)	69.064(3)	73.772(3)	89.79200	92.447(5)	89.843(4)
V (Å^3)	2897.7(2)	1461.4(3)	1627.43238	1203.6(3)	1618.6(3)
D_{calcd} (g cm^{-3})	1.704	1.604	1.695	1.697	1.713
μ(Mo Kα) (cm^{-1})	23.810	20.925	22.078	28.123	24.348
F(000)	1476	712	830	610	830
R_{int}	0.0466	0.0456	0.0409	0.0820	0.0373
$R1$ [$I > 2\sigma(I)$]	0.0630	0.0511	0.0554	0.0795	0.0396
$wR2$ [all data]	0.2109	0.1468	0.1599	0.2726	0.1195
GOF on F^2	1.111	1.110	1.061	1.104	1.068

Table 3.1. Continued

Compound	**5a**	**5b** ($\cdot 3CHCl_3$)
Molecular formula	$C_{38}H_{44}N_{10}Eu_2O_2S_8$	$C_{49}H_{55}N_{10}Cl_9Eu_2O_2S_8$
Molecular weight	1233.23	1695.52
Temperature (K)	188	188
Crystal system	Triclinic	Monoclinic
Space group, Z	$P\bar{1}$, 1	Cc, 4
a (Å)	9.6169(16)	35.816(3)
b (Å)	11.571(2)	9.9959(6)
c (Å)	11.920(2)	21.716(2)
α (°)	112.243(3)	90
β (°)	100.984(3)	122.602(3)
γ (°)	92.196(4)	90
V (Å^3)	1196.3(4)	6549.6(10)
D_{calcd} (g cm^{-3})	1.712	1.719
μ(Mo Kα) (cm^{-1})	29.851	25.613
F(000)	612	3368
R_{int}	0.0659	0.0454
$R1$ [$I > 2\sigma(I)$]	0.0488	0.0578
$wR2$ [all data]	0.1903	0.1512
GOF on F^2	1.191	1.047

Table 3.2. Selected parameters of Ln^{III}_2 complexes.[a]

parameters	1a	1b	2a	2b	3a(mol1)[b]	3a(mol2)[b,c]	3b	3b'	4a	4b	5a	5b
Bond Lengths (Å)												
Ln1─S1	3.002(3)	3.015(3)	2.906(4)	2.968(2)	2.920(3)	2.973(2)	2.990(2)	2.899(2)	2.856(5)	2.876(1)	2.853(3)	2.867(3)
Ln1─S2	3.031(3)	3.000(3)	2.921(3)	2.982(2)	2.895(3)	2.941(3)	2.992(2)	2.940(1)	2.863(6)	2.884(1)	2.844(3)	2.877(5)
Ln1─S3	3.032(3)	3.029(3)	2.919(3)	3.006(2)	2.898(3)	2.970(2)	2.963(2)	2.903(2)	2.893(6)	2.932(1)	2.857(3)	2.921(5)
Ln1─S4	3.052(3)	3.032(3)	2.889(4)	2.999(3)	2.889(2)	2.986(3)	2.952(2)	2.890(2)	2.870(5)	2.865(1)	2.870(3)	2.854(4)
Ln1─N1	2.695(8)	2.688(10)	2.658(9)	2.627(8)	2.629(7)	2.637(7)	2.620(7)	2.627(5)	2.620(13)	2.586(4)	2.589(7)	2.577(11)
Ln1─N3*	2.692(7)	2.702(10)	2.585(9)	2.639(7)	2.573(6)	2.624(7)	2.632(6)	2.589(6)	2.530(12)	2.560(4)	2.510(7)	2.498(10)
Ln1─O1	2.506(5)	2.520(6)	2.451(8)	2.480(4)	2.430(5)	2.456(5)	2.464(4)	2.409(5)	2.405(10)	2.375(3)	2.380(5)	2.390(7)
Ln1─O1*	2.518(6)	2.543(8)	2.488(10)	2.499(6)	2.432(5)	2.484(5)	2.483(5)	2.444(4)	2.410(8)	2.412(3)	2.398(6)	2.392(9)
Ln1─$O2_{EtOH}$	2.583(7)	2.586(7)	–	2.549(6)	–	2.525(9)[d]	2.533(5)	–	–	–	–	–
C6─O1	1.297(9)	1.310(14)	1.294(13)	1.311(10)	1.312(9)	1.307(9)	1.286(9)	1.309(7)	1.301(17)	1.303(5)	1.297(10)	1.332(15)
C6─N2	1.332(10)	1.355(13)	1.329(17)	1.332(9)	1.329(10)	1.281(10)	1.329(8)	1.295(9)	1.327(16)	1.298(6)	1.302(9)	1.300(14)
Bond angles (°)												
S1─Ln1─S2	58.43(9)	58.57(8)	61.32(12)	59.30(6)	61.30(7)	59.44(9)	59.27(7)	61.58(5)	62.04(15)	62.12(3)	62.48(9)	62.35(11)
S3─Ln1─S4	57.63(8)	58.30(9)	61.38(11)	58.94(7)	61.56(8)	59.69(6)	59.74(6)	62.11(5)	61.79(14)	61.90(4)	62.15(8)	62.02(10)
Ln1─O1─Ln1*	115.48(19)	114.7(3)	111.9(3)	115.7(2)	113.3(2)	116.11(19)	115.5(2)	113.1(2)	112.2(4)	113.6(1)	112.9(2)	113.5(3)
Average												
Bond length (Å)												
Ln─S	3.029(4)	3.019(4)	2.909(7)	2.989(5)	2.900(4)	2.967(4)	2.974(4)	2.908(3)	2.871(1)	2.889(3)	2.856(6)	2.8798(9)
Ln─N	2.694(11)	2.695(14)	2.622(13)	2.633(11)	2.601(10)	2.631(11)	2.626(9)	2.608(8)	2.575(18)	2.573(6)	2.510(10)	2.538(15)
Ln─O	2.512(8)	2.532(10)	2.470(13)	2.490(7)	2.431(7)	2.470(7)	2.474(6)	2.427(6)	2.408(13)	2.394(4)	2.389(8)	2.391(21)
Bond angles (°)												
S─Ln1─S	58.03(12)	58.44(12)	61.35(16)	59.12(9)	61.43(10)	59.57(11)	59.51(9)	61.85(7)	61.9(2)	62.01(5)	62.3(12)	62.17(15)

[a]The asterisk (*) indicates the symmetry-related atom. [b]Mol1 and mol2 have 8:8- and 9:9-coordinate structures, respectively. [c]Atom-numberings of mol2 is modified appropriately in Figure 3.5 ([d]Ln2–$O3_{MeOH}$).

Table 3.3. Dihedral angles of Ln^{III}_2 complexes.

	Dihedral angles *(°)*										
Planes	**1a**	**1b**	**2a**	**2b**	**3a**	**3b**	**3b'**	**4a**	**4b**	**5a**	**5b**
(dtc-1)[a] – (dtc-2)[a]	57.7(3)	81.5(3)	-	81.5(2)	-	81.19(9)	-	-	-	-	-
(dtc-1)[b] – (dtc-2)[b]	-	-	11.0(3)	-	11.73(4)	-	63.54(9)	20.7(6)	63.0(1)	21.3(4)	5.9(3)
(dtc-3)[a] – (dtc-4)[a]	-	-	-	-	92.60(9)	-	-	-	-	-	-
(py)[c] – (ph)[d]	8.3(4)	2.7(8)	19.1(5)	1.1(5)	3.80(6)	1.02(4)	27.77(7)	21.2(7)	27.7(2)	22.1(3)	20.0(5)
(py)[c] – (ph)[d]	-	-	-	-	11.29(7)	-	-	-	-	-	-

[a] Planes were defined by S_2CN atoms of the pseudo *cis*-positioned dtc ligand. [c] Planes were defined by the S_2CN atoms of the pseudo *trans*-positioned dtc ligands. [c] Plane was defined by all non-H atoms of the pyridyl moiety. [d] Plane was defined by all non-H atoms of the phenyl moiety.

References

1. R.S. Baligar, V.K. Revankar, *J. Serb. Chem. Soc.,* 71 (2006) 1301.
2. B. Moksharagni, K.H. Reddy. *Eur. J. Biom. Pharm. Sci.*, 5 (2018) 810.
3. B. Parmar, K.K. Bisht, P. Maiti, P. Paul, E. Suresh, *J. Chem. Sci.*, 126 (2014) 1373.
4. M. Chang, H. Horiki, K. Nakajima, A. Kobayashi, H.-C. Chang, M. Kato, *Bull*. *Chem*. *Soc*. *Jpn*., 83 (2010) 905.
5. A. Mori, T. Suzuki, Y. Sunatsuki, M. Kojima, *Bull*. *Chem*. *Soc*. *Jpn*., 88 (2015) 480.
6. S. Biswas, S. Das, G. Rogez, V. Chandrasekhar, *Eur. J. Inorg. Chem.*, (2016) 3322.
7. M.U. Anwar, S.S. Tandon, L.N. Dawe, F. Habib, M. Murugesu, L.K. Thompson, *Inorg. Chem.*, 51 (2012) 1028.
8. N.C. Anastasiadis, I. Mylonas-Margaritis, V. Psycharis, C.P. Raptopoulou, D.A. Kalofolias, C.J. Milios, N. Klouras, S.P. Perlepes, *Inorg. Chem. Comm.*, 51 (2015) 99.
9. L. Zhang, Q.-Y. Zhang, P. Zhang, L. Zhao, M. Guo, J. Tang, *Inorg. Chem.*, 56 (2017) 7882.
10. A. Gusev, R. Herchel, I. Nemec, V. Shul'gin, I.L. Eremenko, K.Lyssenko, W.Linert, Z. Trávníček, *Inorg. Chem.*, 55 (2016) 12470.
11. W.M. Faustino, O.L. Malta, E.E.S. Teotonio, H.F. Brito, A.M. Simas, G.F. de Sá, *J. Phys. Chem.,* A110 (2006) 2510.
12. P. Pitchaimani, K.M. Lo, K.P. Elango, *Polyhedron*, 93 (2015) 8.
13. A. Yakubu, T. Suzuki, M. Kita. *J. Chem*. *Educ*., 94 (2017) 1357.
14. (a) Rigaku Co. Ltd., Process−Auto, Akishima, Tokyo, 1998. (b) Rigaku Co., Ltd., CrystalClear, Akishima, Tokyo, 1998–2015.
15. Rigaku Co. Ltd., NUMABS, Akishima, Tokyo, 1999.
16. M.C. Burla, R. Caliandro, M. Camalli, B. Carrozzini, L.G. Cascarano, L. De Caro, C. Giacovazzo, G. Polidori, D. Siliqi, R. Spagna, SIR2008. *J. Appl. Cryst.*, 40 (2007) 609.

17. M.G. Sheldrick, SHELXT Version 2014/5. *Acta Cryst.*, A70 (2014) C1437.
18. M.G. Sheldrick, SHELXL Version 2014/7. *Acta Cryst.*, A64 (2008) 112.
19. Rigaku Co. Ltd., CrystalStructure 4.3, Akishima, Tokyo, 2000−2018.
20. A. Mori, T. Suzuki, Y. Sunatsuki, A. Kobayashi, M. Kato, M. Kojima, K. Nakajima, *Eur. J. Inorg. Chem.*, (2014) 186.
21. J. Qin, Q. Yin, S.-S. Zhao, J.-Z. Wang, S.-S. Qian, *Acta Chim. Slov.*, 63 (2016) 55.
22. V.C. Havanur, D.S. Badiger, S.G. Ligade, K.B. Gudasi, *Der Pharma Chemica*, 3 (2011) 292.
23. P. Pitchaimani, M.L. Lo, K.P. Elango, *J. Coord. Chem.*, 68 (2015) 2167.
24. M. Mahato, P.P. Jana, K. Harms, H.P. Nayek, *RSC Adv.*, 5 (2015) 62167.
25. V. Vrdoljak, G. Pavlovic, T. Hrenar, M. Rubci, P. Siega, R. Dreos, M. Cindri, *RSC Adv.,* 5 (2015) 104870.
26. C. Görller-Walrand, L. Fluyt, Magnetic circular dicroism of lanthanides, Handb. Phys. Chem. Rare Earths, 40 (2010) 1–107.
27. B. Singh, T.B. Singh, *Indian J. Chem.*, 38A (1999) 1286.
28. S.S. Devi, A.M. Singh, *J. Chem. Pharm. Res.*, 3 (2011) 399.
29. A. Yakubu, T. Suzuki, M. Kita, *Inorg. Chim. Acta*, 484 (2019) 394.
30. S.V.J. Lakshman, S. Buddhudu, *Proc. Indian natn. Sci. Acad.*, 47 A(6) (1981) 721.
31. N. Wang, W. Jiang, X. Xu, Z. Si, H. Bai, C. Tian, *Anal. Sci.*, 18 (2002) 591.
32. C. Su, M. Tan, N. Tang, X. Gan, W. Liu, X. Wang, *J. Coord. Chem., 38* (1996) 207
33. C. E. Secu, S. Polosan, M. Secu, *Journal of Luminescence,* 131 (2011) 1747.
34. K. Binnemans, *Coord. Chem. Rev.*, 295 (2015) 1.

General Conclusion

This thesis describes the syntheses, crystal structures and spectroscopic properties of mononuclear and homodinuclear lanthanoid(III) dithiocarbamato complexes. The mononuclear complexes presented in Chapter 1 were prepared using 1,10-phenanthroline and 2,2'-bipyridine as co-ligands. The novel homodinuclear lanthanoid(III) dithiocarbamato complexes discussed in Chapters 2 and 3 were prepared using 2,2'-bipyrimidine (bpm) and (*E*)-*N*-benzylidenepicolinohydrazonate ($bphz^{-}$), respectively, as the bridging ligands. The crystal structures of the complexes were solved by X-ray diffraction analysis, while the spectroscopic properties of the complexes were investigated, in particular by magnetic circular dichroism (MCD) spectral measurements. The summary of each chapter is presented below.

In Chapter 1, a series of mononuclear lanthanoid(III) adducts bearing achiral or chiral dithiocarbamato (dtc) ligands and 1,10-phenanthroline or 2,2'-bipyridine were prepared in a one-pot synthesis. The crystal structures of the complexes analyzed by X-ray diffraction method revealed each Ln^{III} (Nd^{III} or Eu^{III}) center was coordinated by three dithiocarbamato ligands through two S donor atoms and a phenanthroline or bipyridine ligand through two N donor atoms. The complexes possessed an 8-coordinate geometry around the Ln^{III} center with small structural deviations around the Ln center. The complexes exhibited similar spectral patterns in their absorption, natural CD and MCD spectra in solution. Weak but characteristic sharp f–f transition bands were observed in the absorption and MCD spectra, but no CD signals associated with these transitions were observed even in the *S*-proOHdtc complexes. This fact leads to the significant conclusion that the ligand-centered chirality does not transferred into the Ln center. The MCD spectral pattern suggests that the dithiocarbamato complexes of lanthanide(III) have a site (coordination) symmetry different from those of the related β-diketonato complexes.

Chapter 2 describes the preparation and characterization of four new novel homodinuclear lanthanoid(III) dithiocarbamato complexes using 2,2'-bipyrimidine (bpm) as the bridging unit. The complexes were prepared, and their crystal structures and spectroscopic properties were characterized. The structural and spectral comparison of the dithiocarbamato complexes with corresponding β-diketonato analogues were also investigated. Crystallographic studies revealed that all of the complexes possess a similar structural motif with an 8:8-coordination geometry, in which bpm bridges two Ln^{III} centers in the $\kappa^2N^{1,1'}$:$\kappa^2N^{3,3'}$ mode and three *RR'*dtc$^-$ ligands coordinate to each Ln^{III} center. For structural comparison, the crystal structures of the corresponding β-diketonato analogues were shown to have a similar coordination geometry with the dithiocarbamato complexes, differing in the planarity of the bridging bpm and the pseudo *trans*-positioned terminal ligand planes around the Ln^{III} center. The complexes exhibited weak but relatively sharp f–f transition bands in the absorption and magnetic circular dichroism (MCD) spectra recorded in the visible region. Comparison of the absorption and MCD spectra of the bpm-bridged dinuclear complexes to those of the mononuclear phen or bpy analogues revealed very similar spectral features. This suggests that there is no significant $Ln^{III}\cdots Ln^{III}$ electronic interaction in the dinuclear complexes, which may induce a different electronic structure or spectroscopic symmetry around the central Ln^{III} ion. However, the MCD spectral properties of the complexes revealed a distinctly different spectral feature of the dithiocarbamato complexes from their corresponding β-diketonato analogues, owing to the effect of the coordination environment on the electronic structure and spectroscopic symmetry around the central Ln^{III} ions in solution.

In Chapter 3, a series of novel hydrazonato-bridged homodinuclear Ln^{III}_2 dithiocarbamato complexes were prepared and their crystal and molecular structures and spectroscopic properties were investigated. (*E*)-*N*-Benzylidenepicolinohydrazide (Hbphz) was used as the bridging ligand to prepare the complexes. X-ray crystallographic studies revealed

that these complexes possessed a common head-to-tail type dinuclear structural motif in which two hydrazonato ligands bridged two Ln^{III} centers in the μ-1κ^2*N*(py),*O*:2κ^2*O*,*N*(imine) mode and two *RR'*dtc ligands are coordinated to each Ln^{III} center. The crystal structures revealed that the early Ln^{III} ions (i.e. La^{III}, Pr^{III} and Nd^{III}) tend to crystallize as a 9:9-coordinate complex with the ninth position occupied by a solvent alcohol molecule, while the middle and late Ln^{III} ions (i.e. Sm^{III} and Eu^{III}) deposit the crystals of only 8:8-coordinate complex. In the UV-visible absorption and magnetic circular dichroism (MCD) spectra of the complexes, similar spectral patterns for ligand-centered and Laporte forbidden f–f transitions were observed.

Finally, a series of mononuclear and homodinuclear lanthanoid(III) dithiocarbamato complexes have been prepared. The structural features of the complexes were thoroughly investigated and discussed. The spectroscopic properties of the complexes were also investigated particularly with magnetic circular dichroism (MCD) spectroscopic technique. The MCD spectral features of the Ln^{III} complexes, particularly those of the Eu^{III} complexes showed a distinct variation due to the different coordination environments around the Ln^{III} ions. (i.e. mixed N,O,S; N,S, and N,O donor sets). The MCD spectral studies also demonstrated a characteristic magneto-optical behavior of the lanthanoid(III) dithiocarbamato complexes and this property could be further investigated for potential magneto-optical applications. The complexes, particularly the dinuclear analogues could serve as significant precursors for the preparation of lanthanoid sulfide nanomaterials (e.g. nanocrystals, nanowires and nanorods). The catalytic activity of the complexes, for example, in cyanohydrin synthesis could also be evaluated. The 2,2'-bipyrimidine and hydrazonato-bridged dinuclear complexes, respectively, could also be interesting for investigation into their magnetic properties.

List of publications

1. A. Yakubu, T. Suzuki, M. Kita. (2017). Developing a Magnetic Circular Dichroism Apparatus Equipped with Neodymium Magnet for Students To Investigate the Electronic Structures of Transition Metals and Lanthanoids. *Journal of Chemical Educ*ation 94, 1357−1362.
2. A. Yakubu, T. Suzuki, M. Kita. (2019). Syntheses and crystal structures of neodymium(III) and europium(III) complexes bearing dimethyl-, pyrrolidine-, or S-prolinol-dithiocarbamato ligands and their natural and magnetic circular dichroism spectra. *Inorganica Chimica Acta*, 484, 394–401
3. A. Yakubu, T. Suzuki, M. Kita. (2019). Homodinuclear lanthanoid(III) dithiocarbamato complexes bridged by 2,2'-bipyrimidine: Syntheses, structures and spectroscopic properties. *Polyhedron*, 171, 515–522.
4. A. Yakubu, T. Suzuki, M. Kita. (2019). Dinuclear lanthanoid(III) dithiocarbamato complexes bridged by (*E*)-*N*-benzylidenepicolinohydrazonate: Syntheses, crystal structures and spectroscopic properties. *Inorganica Chimica Acta*, 498, Article 119124.

Acknowledgements

All Praise and Thanks be to Almighty Allah, Lord of the Worlds. Allah accorded us the earth and whatever is in it that we might proceed upon it in obedience and servitude to Him. For that, my living, acts of worship, accomplishments and recall are subservient to His divine Will.

I wish to express my profoundest thankfulness to my supervisor, Prof. Takayoshi Suzuki for his guidance, insightful discussions, support, patience and excellent mentorship. I am grateful for his understanding and all the support he gave me throughout my studies under him. I am also profoundly grateful to Prof. Masakazu Kita, who assiduously facilitated all processes to get me enrolled into Okayama University and being my mentor as well. I am grateful to him for this golden opportunity.

I equally express my gratitude to Dr. Yukinari Sunatsuki for his assistance during the conduct of my research. I appreciate the support and assistance accorded me in the conduct of my research by all past and present members of the Coordination Chemistry Laboratory. Let the candlelight continue to illuminate the Lab with the team spirit of cooperation and togetherness.

I also wish to extend my gratitude to all family and friends who encouraged, prayed, and morally supported me throughout my educational life.

Finally, I express my gratitude to the Government of Japan, through the Ministry of Education, Culture, Sports, Science, and Technology for supporting my research project with a Grant-in-Aid for Scientific Research No. 18K05146.

March 2020

DEDICATION

This thesis is dedicated to my wife and daughters for their immeasurable sacrifice and patience. The most beautiful blessing that I ever had was to have you in my life.